SILICA NANOPOROUS MEMBRANES AND THEIR APPLICATIONS

by

Amir Khabibullin

A dissertation submitted to the faculty of
The University of Utah
in partial fulfillment of the requirements for a degree of

Doctor of Philosophy

Department of Chemistry

The University of Utah

December 2014

The University of Utah Graduate School

STATEMENT OF DISSERTATION APPROVAL

The dissertation of **Amir Khabibullin**

has been approved by the following supervisory committee members:

Ilya Y. Zharov	, Chair	**05/20/2014** Date Approved
Valeria Molinero	, Member	**05/20/2014** Date Approved
Michael H. Bartl	, Member	**05/20/2014** Date Approved
Shelley D. Minteer	, Member	**05/20/2014** Date Approved
Dmitro Bedrov	, Member	**05/20/2014** Date Approved

and by **Cynthia J. Burrows**, Chair/Dean of

the Department/College/School of **Chemistry**

and by David B. Kieda, Dean of The Graduate School.

ABSTRACT

This thesis describes the development of novel silica and hybrid nanoporous membranes. Nanoporous membranes are widely used in various applications. This thesis focuses on their potential applications in the energy area, such as fuel cells and lithium batteries, and in separations and ultrafiltration. We use silica colloidal spheres and polymer-modified silica spheres to prepare the membranes in a time-, cost- and material-efficient manner.

First, we prepared novel silica nanoporous membranes by pressing silica colloidal spheres followed by sintering. The pore size, the thickness, and the area of the membrane are precisely controlled by experiment parameters. The resulting membranes are mechanically and thermally durable, crack-free, and capable of size-selective transport.

Next, to demonstrate the utility of the pressed membranes, described above, the proton-conductive pore-filled silica colloidal membranes were prepared and the fuel cells were constructed using these membranes. We modified these membranes by filling the membrane pores with surface-attached proton-conductive polymer brushes and prepared membrane-electrode assemblies to test fuel cell performance. We studied the proton conductivity and fuel cell performance as a function of the amount of sulfonic groups in the membrane.

We also prepared and characterized reversible hybrid nanoporous membranes, self-assembled from solution containing polymer-modified silica colloidal spheres. Here

we applied the new concept of noncovalent membranes, where the material is held together via noncovalent interactions of polymer brushes. This enables so-called reversible assembly of the membranes, in which membrane can be assembled in one solvent and dissolved in other. This approach provides advantages in recycling and reusing of the material. This work is one of the first of its kind and it opens a whole new area of research on reversible membranes made of polymer-modified nanoparticles.

Finally, we applied our approach for preparation of both pore-filled and reversible self-assembled silica membranes to develop new SPE material for lithium rechargeable batteries. We successfully prepared ion-conductive SPE from each of the materials and demonstrated the proof-of-concept for these approaches.

Overall, in this thesis, we introduce unique approaches where we combine simple materials with novel yet easy preparation and modification methods to obtain new functional nanoporous membranes with desired properties.

TABLE OF CONTENTS

LIST OF FIGURES

LIST OF TABLES

LIST OF SCHEMES

LIST OF ABBREVIATIONS

2-BIB	2-Bromoisobutyrylbromide
3-APTES	3-(Aminopropyl)triethoxysilane
3D	Three Dimension
A	Surface Area
AC	Alternating Current
AEMFC	Anion Exchange Membrane Fuel Cells
Al_2O_3	Aluminum Oxide
atm	Atmosphere
ATRP	Atom Transfer Radical Polymerization
AuNP	Gold Nanoparticles
b	Beam Width
bipy	2-,2'-Dipyridine
CuCl	Copper (I) Chloride
$CuCl_2$	Copper (II) Chloride
d	Beam Thickness
DCM	Dichloromethane
Dcolloid, Dmembr	Diffusivity of the Molecules in Membrane
DLS	Dynamic Light Scattering
DMAEMA	N,N-Dimethylaminoethoxy methacrylate
DMAP	4-Dimethylaminopyridine
DMF	N,N-Dimethylformamide
DMFC	Direct Methanol Fuel Cells
DNA	Deoxyribonucleic Acid
DS	Degree of Sulfonation
Dsol	Diffusivity of the Molecules in Solution
EEMA	2-Ethoxyethyl methacrylate
EIS	Electrochemical Impedance Spectroscopy
F	Rupture Force
fcc	Face-Centered Cubic
g	Gravitational Acceleration
GPC	Gel Permeation Chromatography
gpm	Gallon per Minute
h	Hour

H_2O	Water
HCl	Hydrochloric acid
HEMA	Hydroxyethyl methacrylate
Jfcc, Jmembr	Molecular Flux through the Membrane
l	Distance Between Electrodes
L	Thickness of the Membrane
l	Support Length
lb	Pound
$LiPF_6$	Lithium Hexafluorophosphate
MEA	Membrane Electrode Assembly
MeOH, CH_3OH	Methanol
mg, g	Milligram, Gram
min	Minute
mL, L	Milliliter, Liter
mM, M	Millimolar, Molar
MMA	Methyl methacrylate
mmol, mol	Millimole, Mole
MPa, Pa	MegaPascal, Pascal
mV, V	Millivolt, Volt
NH_3	Ammonia
NH_4OH	Ammonium Hydroxide
NMR	Nuclear Magnetic Resonance
ºC	Celsius Degree
OCV	Open Circuit Voltage
PAFC	Phosphoric Acid Fuel Cells
PAMAM	Poly(amidoamine) Dendrimers
PDMAEMA	Poly(N,N-dimethylaminoethoxy methacrylate)
PEEMA	Poly(2-ethoxyethyl methacrylate)
PEG	Polyethylene glycol
PEGMA	Poly(ethylene glycol) ether methacrylate
PEM	Polymer Electrolyte Membranes
PEMFC	Proton Exchange Membrane Fuel Cells
PEO	Polyethylene oxide
pH	Negative Logarith of Hydrogen Ion Concentration
PHEMA	Poly(hydroxyethyl methacrylate)
PMDETA	N,N,N′,N′,N″-pentamethyldiethylenetriamine
PMMA	Poly(methyl methacrylate)
PNIPAAm	Poly(N-isopropylacrylamide)
PS	Polystyrene
psi	Pound per Square Inch

PSPM	Poly(3-sulfopropyl methacrylate)
PSSA	Poly(styrene sulfonic acid)
Pt	Platinum
PTFE	Polytetrafluoroethylene
R	Ohmic Resistance
RD	Diffusion Rate
RH	Relative Humidity
rpm	Revolution per minute
S	Surface Area
s, sec	Second
S/cm	Siemens per Centimeter
SEM	Scanning Electron Microscopy
SI-ATRP	Surface-Initiated Atom Transfer Radical Polymerization
SiO_2	Silica
SOFC	Solid Oxide Fuel Cells
SPE	Solid Polymer Electrolyte
SPM	3-Sulfopropyl methacrylate
T	Temperature
TEM	Transmission Electron Microscopy
TEOS	Tetraethylorthosilicate
TGA	Thermogravimetric Analysis
THF	Tetrahydrofuran
TiO_2	Titanium Oxide
UV/vis	Ultraviolet/Visible
W_{dry}	Dry Weigth of the Membrane
W_{MeOH}	Weigth of the Membrane after Soaking in Methanol
wt %	Weight Percent
ΔC	Concetration Gradient
ε	Void Fraction
μA	MicroAmper
μm, nm, mm, cm, m	Micrometer, Nanometer, Millimeter, Centimeter, Meter
σ	Proton Conductivity
σ	Flexural Strength
τ	Tortuosity

ACKNOWLEDGEMENTS

First, I would like thank my advisor Prof. Ilya Zharov for his generous support, guidance, and patience. He is the person who helped me the most in my work, who answered my questions and provided both challenges and help in resolving them. I appreciate his mentoring and research philosophy, and the freedom in the lab he provided me. I also appreciate his help and advice beyond the research as well as his sense of humor, which is essential in science. It has been my honor and pleasure working with him.

I would also like to thank the Fulbright Foundation for the provided opportunity to work and study at the University of Utah.

I would like to thank the Department of Chemistry at the University of Utah and my graduate committee members for their support, suggestions, and criticism. I would especially like to thank Jo Hoovey, Prof. Shelley Minteer, Prof. Michael Bartl, Prof. Peter Flynn, Prof. Henry Kopecek (School of Pharmacy), and the members of their research groups for the help they provided me.

I would also like to thank past and present members of Prof. Zharov's research group, Dr. Patricia Ignacio-DeLeon, Dr. Zhe Gao, Dr. Nathan Walton, Robert Haynes, Patrick Kolbay, Erica Green, Emily Fullwood, Joe Glasing, and Megan Facer for their support and the good times we had together.

Finally, I am thankful to my family and friends, especially to my mother and first chemistry teacher Alfiya, my father Asgat, my brother Azat, my loving wife Gulnaz, and my lovely daughter Aliya. They mean everything to me.

CHAPTER 1

SILICA NANOPOROUS MEMBRANES

1.1 Introduction

A membrane is a selective barrier whose primary role is to permit the passage of certain components and retain certain other components of the mixture.[1,2] Biological membranes act as a selectively permeable barrier within cells, while synthetic nanoporous membranes, containing both single and multiple nanopores (pore size in 1-100 nm range), have attracted attention in fundamental research[3,4,5] (e.g., for studying the transport of small molecules and macromolecules through nanopores[6-8]), and in various applications, including separation of biomacromolecules[9] and pharmaceuticals,[10] sensing,[11] and novel medical devices, such as controlled release[12-15] and drug delivery systems.[16-18] Most commonly used nanoporous membrane materials are based on polymers,[19,20,21] which have the advantage of good mechanical properties, flexibility, and processability. However, the nanostructure of polymeric membranes is often not well defined and well controlled, and their surface is hard to modify. Therefore, inorganic nanoporous materials, such as zeolites,[22,23,24] silicon nitride,[25,26] silicon,[27] silica,[28,29] alumina[30,31] and nanotubes,[32,33] are attractive alternatives for polymeric nanoporous membranes. Despite the impressive advances in the field of inorganic nanoporous membrane materials, several problems remain unsolved. Many of the inorganic nanoporous membranes possess low pore density, which results in low molecular fluxes

through these membranes, limiting their usefulness. Secondly, it is difficult to control the pore size in a broad range in these materials. In addition, many of these membranes require specialized methods and equipment for their preparation.

1.2 Silica Colloidal Membranes

Silica colloidal membranes, developed in our group in the past several years, provide a simple and powerful approach to self-assembled nanoporous membranes with high molecular flux, easily controllable nanopore size in the 5-100 nm range, and, most importantly, with facile surface chemistry allowing to achieve controlled ionic and molecular transport and ultrafiltration.[3,4,5] Historically, silica colloidal crystals have been developed as templates for preparing photonic materials,[34,35] energy storage media,[36] magnetic materials,[37] macroporous polymer membranes,[38,39] and sensors.[40] Silica colloidal crystals comprise a close-packed face-centered cubic (fcc) lattice of amorphous nonporous silica spheres of a sub-micrometer diameter (Figure 1.1) with ordered arrays of interconnected three-dimensional nanoscale voids.[41] The preparation of silica spheres (Scheme 1.1) is straightforward,[42] self-assembly of the spheres is well developed,[43] and pore size in the crystals can be readily controlled by selecting the sphere size. The distance from the center of the nanopore projection to the nearest silica sphere surface is ca. 15% of the sphere radius. Because of the three-dimensional nature of the pores, we use this projection (Figure 1.1A) as a simplified description of the pore geometry, and the distance described above as the nanopore "radius."

The surface silanol groups in colloidal membranes can be directly modified by nucleophilic silylation to introduce a variety of functional groups.[44] Alternatively, silica surface can be first modified with 3-aminopropyltriethoxysilane, followed by treatment

with organic molecules carrying electrophilic moieties such as acyl chloride, isocyanate, isothiocyanate, carboxylic acid, sulfonyl chloride,[45] or succinimidyl ester.[46]

3-Aminopropyltriethoxysilane-treated silica can also be modified with 2-bromoisobutyrylbromide,[47] which can serve as atom transfer radical polymerization (ATRP) initiator.[48] This provides the possibility of growing various polymer brushes on the silica surface.[49-52]

An important advantage of colloidal crystals as nanoporous membranes is their highly ordered structure, which allows using accurate mathematical descriptions of the molecular transport.[53-57] The effective diffusion coefficient of molecules in the fcc lattice, $D_{colloid}$, can be expressed as $(\varepsilon/\tau)D_{sol}$, where D_{sol} is the diffusivity of molecules in free solution, and the void fraction ε (0.26) and the tortuosity τ (~3.0) are intrinsic geometrical parameters independent of the size of the silica spheres used to prepare the colloidal crystal. An estimate of the molecular flux J_{fcc} can be obtained using eq 1.1,[53] where ΔC is the concentration gradient and L is the thickness of the membrane:

$$J_{colloid} = (\Delta C/L) \times (\varepsilon/\tau)D_{sol} \quad (1.1)$$

Importantly, the diffusive flux of small molecules normal to the (111) plane of a semi-infinite colloidal crystal is only ca. 10 times smaller relative to the free solution value, independent of the size of the spheres used to assemble the crystal.[55] Thus, the rate of molecular transport remains significant, even when the pore size is reduced to the nanoscale to impart molecular transport selectivity. For a typical D_{sol} of 10^{-5} $cm^2 \cdot s^{-1}$, L of 100 μm, and ΔC of 100 mM, $J_{colloid}$ is ~10^{-8} $mol/cm^2 \cdot s$.

Previously, the Zharov group reported permselective silica colloidal nanoporous membranes in the form of pH-responsive amine-modified colloidal films with controlled

transport of positively charged species[58,59] as well as membranes modified with sulfonic acids[60,61] and spiropyran moieties.[62] Silica colloidal films modified with chiral selector moieties and possessing chiral permselectivity were also reported.[63,64] Several methods for the preparation of silica colloidal membranes, including supported films,[57,58] suspended colloidal membranes,[65,66] and mechanically robust free-standing silica membranes[67] were developed. Methods were developed to modify the colloidal nanopores with polmyers, such as acrylamide,[68] temperature-responsive poly(*N*-isopropylacryl amide), PNIPAAM,[69] pH- and ion-responsive poly(2-(dimethylamino)ethyl methacrylate), PDMAEMA,[70,71] temperature-responsive poly(L-alanine),[72] and a small molecule-responsive aptamer.[73] Finally, proton-conducting silica colloidal membranes were prepared by modifying the surface of the nanopores with sulfonic groups[61] and sulfonated polymers.[74]

1.3 Free-standing Silica Colloidal Membranes

Free-standing silica colloidal crystals are generally more practical than supported thin films. Earlier Zharov group prepared free-standing silica colloidal crystals by vertical deposition from colloidal solution of silica spheres in ethanol.[67] The resulting crystals were sintered in an oven at 1050 ºC for 12 hours. The silica spheres flow at the surface at this temperature and after cooling down, they are physically bonded to each other. Free-standing silica colloidal membranes are capable of size-selective transport.[75] The average membrane thickness can be controlled by silica concentration. The silica spheres in the resulting membranes remain highly-ordered in fcc lattice after thermal treatment (Figure 1.2) and the membranes are robust and possess large area (Figure 1.3).

Free-standing colloidal membranes were also prepared using gold-coated silica

nanospheres, their surface was modified with pH-responsive *L*-cysteine and methacrylic acid, and studies of the ionic and molecular transport through these membranes were carried out.[76]

Free-standing highly-ordered silica colloidal membrane possess several advantages; however, there are a few challenges that limit practical applications of silica membranes. Controlled area and thickness are desired for some applications.[77] Ordered silica membranes prepared via vertical deposition do not possess uniform thickness throughout the membrane: they usually have smaller thickness at the top side of the membrane (the side that was on top of the glass slide during the vertical deposition process) and the larger thickness at the other side. This problem, which is common for vertical deposition, arises from sedimentation of silica spheres during solvent evaporation in the vertical deposition process. Sometimes the thicknesses at the top and the bottom sides of the membrane differ by a factor of 2. It is also hard to control the area of the membrane, since the vertically deposited silica colloidal membranes are prone to cracking before the sintering step. This thesis will discuss the development of close-packed silica colloidal membranes with uniform controlled thickness and area. The membranes are prepared by pressing the silica spheres in a die set with further sintering in the oven. The resulting membranes are chemically and thermally stable, mechanically robust, and are capable of size-selective transport and further modification of pore surface with functional polymer brushes.

1.4 Fuel Cells Membranes

A fuel cell is a device that converts chemical energy, released from fuel oxidation, directly into electrical energy.

Fuel cells attract increased attention as a promising energy solution for several reasons.

They are generally more efficient compared to combustion engines, have lower emission (only water and carbon dioxide), they have a simple design due to the absence of any moving parts, are quiet compared to combustion engines, and have a wide variety of applications in portable devices, cars, submarines, etc.

Different types of fuel cells include proton exchange membrane fuel cells (PEMFC), anion exchange membrane fuel cells (AEMFC), solid oxide fuel cells (SOFC), and phosphoric acid fuel cells (PAFC), each of them having their advantages, limitations and potential applications.[78,79] Although each fuel cell type operates differently, they are all made of similar components such as an anode, cathode, and electrolyte media.

The electrolyte membrane that transports positive or negative ions form one electrode to another is a key component to complete the circuit in a fuel cell. PEMFCs use proton exchange membranes that transfer protons from the anode, where the fuel is oxidized, to the cathode, where oxygen is reduced. The types of PEMFCs vary depending on used fuel; the two major types are hydrogen fuel cells and direct methanol fuel cells (DMFC). One of the roles of the membrane is to prevent mixing of fuel and oxidant. Another role is to transport ions, while preventing conduction of electrons, thus the membrane should possess high ionic conductivity and no electric conductivity. The proton conductivity of the membrane depends on temperature, pressure, type, and concentration of ions present in the system. [80] The conductivity highly depends on degree of hydration.[81,82] Thus, it is important for the fuel cell membrane to remain hydrated at elevated temperatures (>90 ºC). The membrane should also be mechanically and

thermally stable.

Proton conductivity is one of the most important parameters of proton exchange membrane. As a relatively easy and fast experiment, proton conductivity measurements are usually performed to estimate membrane's potential prior to more complicated fuel cell experiments.[78] The proton conductivity is usually measured using electrochemical impedance spectroscopy (EIS). Impedance is a measure of the ability of the system to resist current, taking into account resistance, capacitance, and inductance, the latter two being dependent on frequency. In this experiment, AC voltage is applied at variable frequencies and the complex impedance of the system is measured. After a few mathematical operations, the bulk resistance R (Ohmic resistance) of the membrane is calculated. The proton conductivity of the membrane is calculated as shown in eq 1.2.

$$\sigma = \frac{l}{R\,A} \tag{1.2}$$

where σ is conductivity (S/cm), l is distance between the two electrodes (cm), and A is the cross-sectional area of the membrane (cm^2).

Open-circuit voltage and polarization are key parameters of a fuel cell. To measure these parameters, a working fuel cell with cathode, anode, and proton-conducting membrane is needed. Thus, the membrane-electrode assembly (MEA) is constructed, where both electrodes are modified with catalysts (usually Pt or Pt-alloys for DMFCs). The fuel and oxidant are then supplied to the system and the equilibrated voltage is recorded. The polarization curves are obtained by scanning the potential starting from equilibrated open-circuit voltage value and recording the resulting current.

1.5 Polymer Electrolyte Membranes

The most commonly used proton-conducting materials are polymer electrolyte membranes (PEMs).[78,83] The industrial standard for PEMs is Nafion® – a material developed by DuPont in the 1960s. Nafion consists of perfluorinated backbone with side chains having sulfonic end groups (Figure 1.4).

The advantages of Nafion are high proton conductivity, chemical stability, and relative mechanical stability. However, Nafion also has some important disadvantages, such as significant swelling in water, which creates difficulties in fuel cell design and performance, as well as lower proton conductivity at high temperatures (> 90 ºC) due to water loss, and poor mechanical properties at elevated temperatures. [84,85,86] Many analogs of Nafion were developed based on perfluorinated polymers containing sulfonic groups, such as sulfonated polystyrenes, sulfonated polyarelene ethers, etc. [87]

Polymer electrolyte membranes, just as other membranes in PEMFCs, only possess high proton conductivity when they are heavily hydrated. Since most fuel cells operate better at high temperatures, the membrane should retain water upon heating. Also, polymer membranes in DMFCs swell in presence of methanol and water, which can distort the fuel cell assembly. Finally, methanol permeability becomes an issue in DMFCs that use polymer membranes.[88] Thus, nonswelling membranes with reduced methanol permeability and high proton conductivity are desirable.

Hybrid organic-inorganic composite membranes may meet these requirements. [89,90,91] One way to make them is to incorporate inorganic oxide nanoparticles into polymer membranes. Hydrophilic nanoparticles help to keep water in the membrane at elevated temperature, reduce the methanol permeability,[92,93] and add mechanical and

thermal stability to the material.[91,94] The most commonly used inorganic particles are oxides, such as SiO_2, Al_2O_3, TiO_2,[93,95,96] as well as clays[97] and zeolites.[98,99]

1.6 Pore-filled Silica Colloidal Membranes for Fuel Cells

Another approach is to develop a rigid porous scaffold filled with a proton-conducting material (polymer electrolyte), resulting in formation of proton-conductive pathways.[100] The resulting pore-filled hybrid organic-inorganic membranes meet and exceed many performance requirements due to their better mechanical stability and non-swelling properties.[90,91] The porous scaffolds in pore-filled membranes can be made of polymers[101,102,103,104] or inorganic materials.[105,106,107,108] The porous substrate is then filled by impregnation with ion-conductive polymers, usually containing sulfonic groups.[101-106] However, in this assembly, the polymer can be washed out from the scaffold, causing membrane instability and proton conductivity loss in long term. To stabilize the pore-filled structures, polymers can be cross-linked,[108] but linking the polymer to the surface of scaffold is more reliable.

In the Zharov group, this approach was used earlier to prepare pore-filled silica colloidal membranes, where the highly-ordered silica colloidal crystal containing a continuous network of interconnected mesopores provides a rigid scaffold. The silica colloidal membranes were prepared by vertical deposition from colloidal solution containing dispersed silica colloidal spheres in ethanol with further sintering at 1050 ºC for 12 hours. The resulting membranes are chemically inert, mechanically durable, and thermally stable. They provide better water retaining properties due to hydrophilic nature of silica. The pore size is controlled and easily varied by changing the silica sphere size.

The proton-conducting polymer brushes, containing sulfonic groups: poly(3-

sulfopropylmethacrylate) (pSPM) or poly(stryrenesulfonic acid) (pSSA) were grown from the surface of silica via surface-initiated atom transfer radical polymerization (SI-ATRP) (Scheme 1.2).[74] This polymerization method guarantees that polymers will not leach out of the nanopores. According to the thermogravimetric analysis (TGA) data, the polymer brushes fill the pores completely.[74] The resulting pore-filled colloidal membranes were modified with silver electrodes and the proton conductivity was measured using EIS method inside the home-made humidity- and temperature-controlled chamber.[74]

It was found that the proton conductivity of pore-filled silica colloidal membranes is comparable to that of Nafion™ and generally increases with increasing temperature (until temperature reaches 90 ºC) and relative humidity.[74] While the proton conductivity observed for this material was quite high, it is still lower than expected based on continuous interconnected nanochannels. To further study the proton conductivity in pore-filled membranes is important for both the fundamental understanding of proton conductivity mechanisms and for the improvement of fuel cell design and performance. The silica pore-filled colloidal membranes provide a good model for these studies. The rigid silica scaffold does not swell or dissolve in water and methanol, which is a typical problem for most highly-sulfonated polymer proton-conductive membranes. At the same time, well-established silica surface chemistry allows controlled growing of various polymer structures inside the pores to study structure-property relationship for the membranes and fuel cells.

This dissertation will describe the dependence of proton conductivity of the PEM membrane and the performance of methanol fuel cell on the degree of sulfonation of the

polymer brushes inside the silica pores. The research on how the proton conductivity depends on the amount of sulfonic groups in the system is essential for the fundamental understanding of proton conductivity mechanisms and for optimizing the fuel cell design. Both highly-ordered and pressed silica colloidal membranes served as rigid matrix for further pore-filling with conductive polymer brushes containing various amounts of sulfonic groups.

1.7 Lithium Batteries

Lithium rechargeable batteries are used in a wide variety of demanding applications, such as electric vehicles, start-light ignition, portable electronics, and personal communication. The key components of lithium batteries are the positive electrode, the negative electrode, and the electrolyte. The electrolyte is a medium with good lithium ion conductivity.[109] Usually it is a lithium salt, dissolved in an organic solvent. However, currently used liquid electrolyte batteries have a number of serious disadvantages, such as lack of chemical and electrochemical stability, as well as lack of reliability and environmental safety due to possible leaks.[110] Therefore, the solid polymer electrolyte (SPE) has been recognized as a promising material for the production of lithium batteries.[111,112] The required parameters for a successful SPE are high ionic conductivity, high transport number for lithium cation, and good mechanical stability.[113] Most commonly used SPEs are based on complexes formed between polyethylene oxide (PEO) and various lithium salts, usually having noncoordination anion, such as perchlorate, tetrafluoroborate, hexafluorophosphate, etc.[114,115] These systems possess good mechanical properties, large redox stability windows, good compatibility with cathodes and lithium anode, a very high solvating power, and chain flexibility at elevated

temperatures.[116] However, they possess low conductivity at ambient temperature, very low cation transference numbers, and high crystallinity.[117] There are several approaches to increase the lithium conductivity at room temperatures by variation of polymer composition, structure, and geometry.[118-122] Other approaches propose adding inorganic materials or introducing a second phase to the SPE.[123-128] The challenge is to optimize both lithium ion conductivity and mechanical properties of the SPE simultaneously.

The ionic conductivity is one of the key parameters of SPE and it can be measured using electrochemical impedance spectroscopy (EIS), as was discussed above for fuel cell membranes. The silver mesh is attached to the membrane and serves as electrodes. The complex impedance of the membrane is measured, and the ionic conductivity is calculated taking into account membrane thickness and area.

In this dissertation, we will describe a new approach to the preparation of SPEs for lithium batteries, where a rigid silica porous scaffold serves as a matrix, while pore-filling polymer brushes impregnated with a lithium salt are grafted to silica surface and are responsible for the ionic conductivity of the SPE.

1.8 Reversible Membranes

As was discussed above, nanoporous membranes are most commonly made of polymers, zeolites, inorganic oxides, etc. However, regardless of the material, these membranes are formed via irreversible covalent bonds.[129] Once the membrane is formed, it cannot be dissolved or disassembled into initial components. Thus, if the membrane clogs due to pore blocking or surface fouling, it requires a time- and money-consuming cleaning and regeneration process. Membranes formed by noncovalent reversible assembly of molecular or nanoscale building blocks may address this challenge, which

will be useful for membrane fabrication, processing, cleaning, recycling, and reusing.[129]

Recently, the assembly of nanoporous membranes using molecular building blocks allowing for the preparation of thin supported materials suitable for ultrafiltration of nanoparticles was reported.[129] These membranes, made by reversible self-assembly of perylene diimide-based organic molecules, contained a continuous three-dimensional network, formed in water/THF, could be dissolved in water/ethanol and possessed a cut-off of 5 nm. The membrane preparation process was fast and easy, the material could be easily recycled and reused, however, the pore size of such membranes is defined by the structure of the molecular building block and thus cannot be easily varied in a broad range.

Self-assembly of colloidal particles into nanoporous membranes would allow combining the advantages of the reversible assembly with easy pore size tunability and cheap building blocks. The challenge in this case is to develop a system that is held together by noncovalent interactions strong enough to provide materials that can withstand the ultrafiltration conditions.

Only gold nanoparticles were used so far to form self-assembled nanoporous membranes, either by chemically directed assembly of AuNPs and polyamidoamine dendrimers (PAMAM), in which the pore size was controlled by varying the dendrimer generation,[130] or by self-assembly of dodecanethiole-ligated Au nanocrystals,[131,132] where the pore size was controlled by the gold nanoparticles size. The free-standing AuNP/dendrimer membranes were relatively easy to prepare, they were durable and capable of size-selective separations and filtration, however, their application is limited by high cost and small size of gold nanoparticles.

The silica colloidal spheres, discussed above, could provide a cheap alternative to gold nanoparticles. However, only sintered silica colloidal membranes were prepared, where silica spheres were attached to each other by covalent bond. The formation of these membranes is not reversible. We decided to develop a membrane where silica spheres will be held together by other interactions, such as van der Waals and coulombic interactions of polymer brushes, grafted on the surface of silica spheres.

In this thesis, the reversible formation of two types of nanoporous membranes via the self-assembly of silica nanospheres modified with polymer brushes is described. The interactions between entangled polymer brushes of neighboring silica spheres are responsible for holding the silica spheres together in the membrane. We developed two types of membranes: the first type is stable in organic solvents and can be dissolved in water, while the second type is practical in water and can be disassembled in organic solvents. In general, this approach allows for the preparation of stable and durable reversible nanoporous membranes with controlled pore size. The membranes could be both supported and free-standing. The resulting membranes are capable of size-selective transport.

1.9 Thesis Overview

This thesis focuses on the preparation of novel silica and hybrid nanoporous membranes and demonstration of some of their application. Chapter 2 describes the preparation of silica nanoporous membranes with controlled thickness, area, and pore size by pressing silica colloidal spheres followed by thermal sintering. The resulting membranes are capable of size-selective transport. Chapter 3 describes the preparation of proton-conductive pore-filled silica colloidal membranes and the fuel cells prepared using

these membranes. We discuss how the proton conductivity and fuel cell performance depends on the number of sulfonic groups in the pore-filling polymer brushes. Chapter 4 describes the preparation and characterization of reversible nanoporous membranes, comprised of polymer-modified silica colloidal spheres. In Chapter 5, our progress in development of solid polymer electrolyte material for lithium ion batteries is described. Finally, Chapter 6 summarizes the results and outlines the future work.

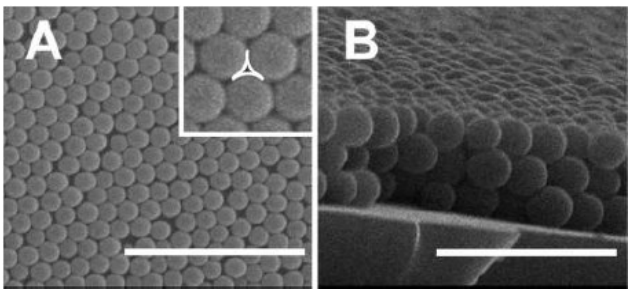

Figure 1.1. SEM images of silica colloidal films prepared on glass from 440 nm diameter silica spheres deposited (a) top view (size bar 4 μm); and (b) side view (size bar 2 μm). The geometric projection of a pore observed from the (111) plane is outlined in the inset in (a).[58]

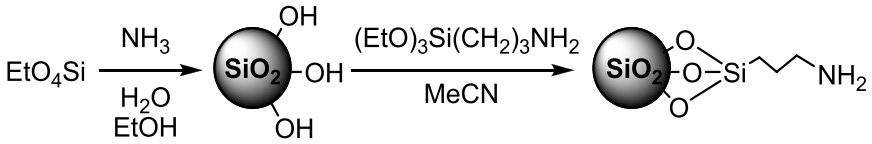

Scheme 1.1 Preparation and surface amination of silica spheres.

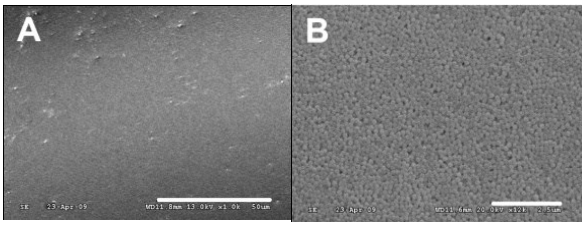

Figure 1.2. SEM images of sintered colloidal crystals comprised of 180 nm silica spheres: (a). SEM image showing no major cracks over a large area (size bar = 50 μm); (b) Magnified image displaying the close-packed fcc lattice (size bar = 2.5 μm).

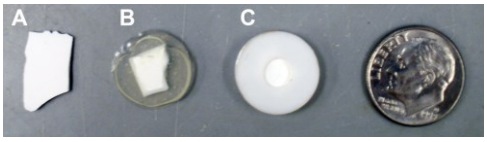

Figure 1.3. Photographs of sintered silica colloidal membranes. (a) as-sintered; (b) without PTFE washers showing the sintered colloidal membrane in the epoxy; (c) with PTFE washers.

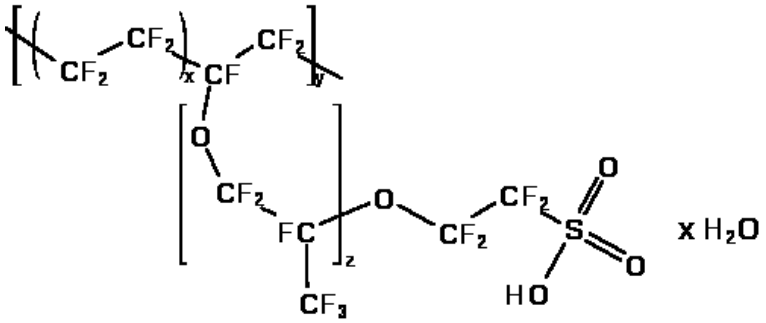

Figure 1.4. Chemical structure of Nafion® 117

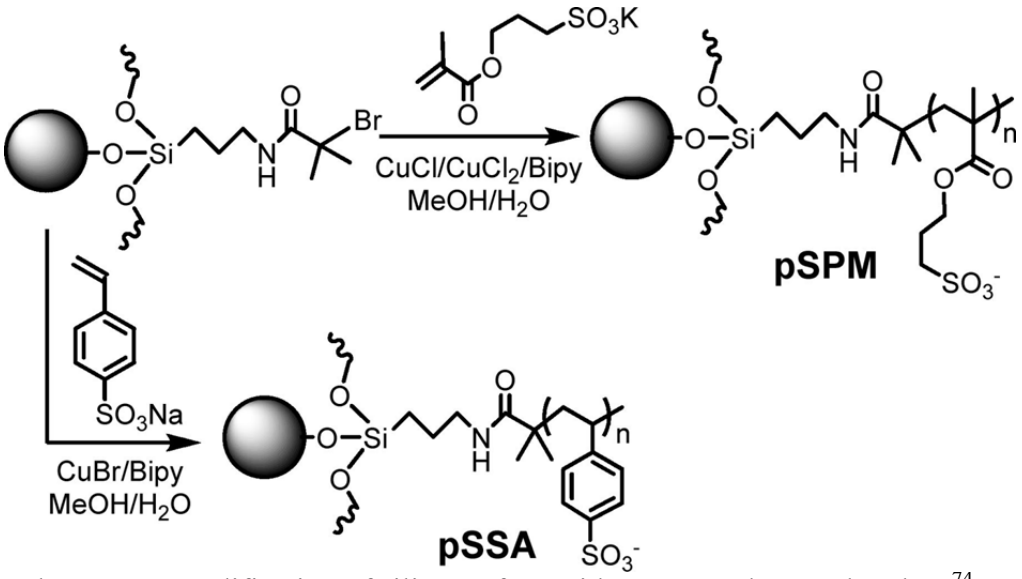

Scheme 1.2. Modification of silica surface with pSPM and pSSA brushes.[74]

1.10 References

[1] Cheryan, M. *Microfiltration and Ultrafiltration Handbook*, CRC Press: Boca Raton, FL, 1998, pp. 1-28.

[2] Zeman, L.; Zydney, A. *Microfiltration and Ultrafiltration. Principles and Applications*, Marcel Dekker: New York, 1996, pp. 1-20.

[3] Zharov, I.; Khabibullin, A. Surface-Modified Silica Colloidal Crystals: Nanoporous Films and Membranes with Controlled Ionic and Molecular Transport. *Acc. Chem. Res.*, **2014**, *47*, 440–449.

[4] Khabibullin, A.; Zharov, I. Responsive Nanoporous Silica Colloidal Films and Membranes. In *Intelligent Stimuli Responsive Materials: From Well-Defined Nanostructures to Applications*, Li, Q, Ed. John Wiley & Sons, Inc.: Hoboken, New Jersey, 2013, pp. 265-292.

[5] Khabibullin, A.; Zharov, I. Silica Colloidal Nanoporous Membranes. In *Encyclopedia of Membrane Science and Technology*, *Part II. Membrane Materials, Characterization, and Module Design*. Hoek, E. M. V., Volodymyr V. Tarabara, V. V., Eds. John Wiley & Sons, Inc.: Hoboken, New Jersey, 2013, pp. 797-828.

[6] Tanev, P. T.; Butruille, J.-R.; Pinnavaia, T. J. Nanoporous Materials. In *Chemistry of Advanced Materials: An Overview*, Interrante, L. V.; Hampden-Smith, M. J., Eds. Wiley-VCH: New York, N. Y, 1998, pp. 328-388.

[7] Davis, M. E. Ordered Porous Materials for Emerging Applications. *Nature* **2002**, *417*, 813–821.

[8] Bayley, H.; Martin, C. R. Resistive-Pulse Sensing-From Microbes to Molecules. *Chem. Rev.* **2000**, *100*, 2575–2594.

[9] van Reis, R.; Zydney, A. Bioprocess Membrane Technology. *J. Membr. Sci.* **2007**, *297*, 16–50.

[10] Afonso, C. A. M.; Crespo J. G. Recent Advances in Chiral Resolution through Membrane-Based Approaches. *Angew. Chem. Int. Ed.* **2004**, *43*, 5293–5295.

[11] Piruska, A.; Gong, M.; Sweedler, J. V.; Bohn, P. W. Nanofluidics in Chemical Analysis. *Chem. Soc. Rev.* **2010**, *39*, 1060–1072.

[12] Martina, F.; Walczaka, R.; Boiarskia, A.; Cohena, M.; Westa, T.; Cosentinob, C.; Ferrari, M. Tailoring Width of Microfabricated Nanochannels to Solute Size Can Be Used to Control Diffusion Kinetics. *J. Control. Release* **2005**, *102*, 123–133.

[13] Orosz, K. E.; Gupta, S.; Hassink, M.; Abdel-Rahman, M.; Moldovan, L.; Davidorf, F. H.; Moldovan, N. I. Delivery of Antiangiogenic and Antioxidant Drugs of Ophthalmic Interest through a Nanoporous Inorganic Filter. *Mol. Vision* **2004**, *10*, 555–65.

[14] Kipke, S.; Schmid, G. Nanoporous Alumina Membranes as Diffusion Controlling Systems. *Adv. Funct. Mater.* **2004**, *14*, 1184–1188.

[15] Gong, D.; Yadavalli, V.; Paulose, M.; Pishko, M.; Grimes, C. A. Controlled Molecular Release Using Nanoporous Alumina Capsules. *Biomed. Microdev.* **2003**, *5*, 75–80.

[16] Ziaiea, B.; Baldia, A.; Leia, M.; Guc, Y.; Siegel, R. A. Hard and Soft Micromachining for BioMEMS: Review of Techniques and Examples of Applications in Microfluidics and Drug Delivery. *Adv. Drug Delivery Rev.* **2004**, *56*, 145–172.

[17] Santini, J. T., Jr.; Cima, M. J.; Langer, R. A Controlled-Release Microchip. *Nature* **1999**, *397*, 335–338.

[18] Grayson, A. C. R.; Choi, I. S.; Tyler, B. M.;. Wang, P. P.; Brem, H.; Cima, M. J.; Langer, R. Multi-Pulse Drug Delivery from a Resorbable Polymeric Microchip Device. *Nature Mat.* **2003**, *2*, 767–772.

[19] Ulbricht, M. Advanced Functional Polymer Membranes. *Polymer* **2006**, *47*, 2217–2262.

[20] Lee, S. B.; Mitchell, D. T.; Trofin, L.; Nevanen, T. K.; Söderlund, H.; Martin, C. R. Antibody-Based Bio-Nanotube Membranes for Enantiomeric Drug Separations. *Science* **2002**, *296*, 2198–2201.

[21] Mansourpanah, Y.; Gheshlaghi, A. Effects of Adding Different Ethanol Amines During Membrane Preparation on the Performance and Morphology of Nanoporous PES Membranes. *J Polym Res*. **2012**, *19*, 1–7.

[22] Kallus, S.; Condre, J.-M.; Hahn, A.; Golemme, G.; Algieri, C.; Dieudonne, P.; Timmins, P.; Ramsay, J. D. F. Colloidal Zeolites and Zeolite Membranes. *J. Mat. Chem.* **2002**, *12*, 3343–3350.

[23] Chiang, A. S. T.; Chao, K.-J. Membranes and Films of Zeolite and Zeolite-Like Materials. *J. Phys. Chem. Solids* **2001**, *62*, 1899–1910.

[24] Chong Lua. A.; Shen, Y. Influence of Inorganic Fillers on the Structural and Transport Properties of Mixed Matrix Membranes. *J. Appl. Polym. Sci.* **2013**, *128*, 4058–4066.

[25] Yen, B. K.; White, R. L.; Waltman, R. J.; Dai, Q.; Miller, D. C.; Kellock, A. J.; Marchon, B.; Kasai, P.H.; Toney, M. F.; York, B. R.; Deng, H.; Xiao, Q.-F.; Raman, V. Microstructure and Properties of Ultrathin Amorphous Silicon Nitride Protective Coating. *J. Vac. Sci. Tech.* **2003***, A21*, 1895–1904.

[26] Tong, H. D.; Jansen, H. V.; Gadgil, V. J.; Bostan, C. G.; Berenschot, C. G. E.; van Rijn, C. J. M.; Elwenspoek, M. Silicon Nitride Nanosieve Membrane. *Nano Lett*. **2004**, *4*, 283-287.

[27] Striemer, C. C.; Thomas R.; Gaborski, T. R.; McGrath, J. L.; Fauchet, P. M. Charge- and Size-Based Separation of Macromolecules Using Ultrathin Silicon Membranes. *Nature* **2007**, *445*, 749–753.

[28] Liu, N. G.; Dunphy, D. R.; Atanassov, P.; Bunge, S. D.; Chen, Z.; Lopez, G. P.; Boyle, T. J.; Brinker, C. J. Photoregulation of Mass Transport through a

Photoresponsive Azobenzene-Modified Nanoporous Membrane. *Nano Lett*. **2004**, *4*, 551–554.

[29] Nicole, L.; Boissiere, C.; Grosso, D.; Quach, A.; Sanchez, C. Mesostructured Hybrid Organic–Inorganic Thin Films. *J. Mater. Chem.* **2005**, *15*, 3598–3627.

[30] Toh, C.-S.; Kayes, B. M.; Nemanick, E. J.; Lewis, N. S. Fabrication of Free-Standing Nanoscale Alumina Membranes with Controllable Pore Aspect Ratios. *Nano Lett*. **2004**, *4*, 767–770.

[31] Yamaguchi, A.; Uejo, F.; Yoda, T.; Uchida, T.; Tanamura, Y.; Yamashita, T.; Teramae, N. Self-Assembly of a Silica-Surfactant Nanocomposite in a Porous Alumina Membrane. *Nature Mat.* **2004**, *3*, 337–341.

[32] Hinds, B. J.; Chopra, N.; Rantell, T.; Andrews, R.; Gavalas, V.; Bachas, L. G. Aligned Multiwalled Carbon Nanotube Membranes. *Science* **2004**, *303*, 62–65.

[33] Miller, S. A.; Martin, C. R. Redox Modulation of Electroosmotic Flow in a Carbon Nanotube Membrane. *J. Am. Chem. Soc*. **2004**, *126*, 6226–6227.

[34] Blanco, A.; Chomski, E.; Grabtchak, S.; Ibisate, M.; John, S.; Leonard, S. W.; Lopez, C.; Mesequer, F.; Miguez, H.; Mondla, J. P.; Ozin, G. A.; Toader, O.; Van Driel, H. M. Large-Scale Synthesis of a Silicon Photonic Crystal with a Complete Three-Dimensional Bandgap Near 1.5 Micrometres. *Nature* **2000**, *405*, 437–440.

[35] Kubo, S.; Gu, Z.-Z.; Takahashi, K.; Fujishima, A.; Segawa, H.; Sato, O. Tunable Photonic Band Gap Crystals Based on a Liquid Crystal-Infiltrated Inverse Opal Structure. *J. Am. Chem. Soc.* **2004**, *126*, 8314–8319.

[36] Stein, A. Advances in Microporous and Mesoporous Solids – Highlights of Recent Progress. *Adv. Mater.* **2003**, *15*, 763–775.

[37] Bartlett, P. N.; Ghanem, M. A.; Hallag, E.; De Groot, P.; Zhukov, A. Electrochemical Deposition of Macroporous Magnetic Networks Using Colloidal Templates. *J. Mater. Chem.* **2003**, *13*, 2596–2602.

[38] Jiang, P.; Hwang, K. S.; Mittleman, D. M.; Bertone, J. F.; Colvin, V. L. Template-Directed Preparation of Macroporous Polymers with Oriented and Crystalline Arrays of Voids. *J. Am. Chem. Soc.* **1999**, *121*, 11630-11637.

[39] Park, S. H.; Xia, Y. Macroporous Membranes with Highly Ordered and Three-Dimensionally Interconnected Spherical Pores. *Adv. Mat.* **1999**, *10*, 1045–1048.

[40] Cassagneau, S.; Caruso, F. Semiconducting Polymer Inverse Opals Prepared by Electropolymerization. *Adv. Mater.* **2002**, *14*, 34–38.

[41] Wong, S.; Kitaev, V.; Ozin, G. A. Colloidal Crystal Films: Advances in Universality and Perfection. *J. Am. Chem. Soc.* **2003**, *125*, 15589–15598.

[42] Stöber, W.; Fink, A.; Bohn, E. Controlled Growth of Monodispersed Spheres in the Micron Size Range. *J. Colloid Interface Sci.* **1968**, *26*, 62–69.

[43] Jiang, P.; Bertone, J. F.; Hwang, K. S.; Colvin, V. L. Single-Crystal Colloidal Multilayers of Controlled Thickness. *Chem. Mater.* **1999**, *11*, 2132–2140.

[44] Onclin, S.; Ravoo, B. J.; Reinhoudt, D. N. Engineering Silicon Oxide Surfaces Using Self-Assembled Monolayers. *Angew Chem Int Ed.* **2005**, *44*, 6282–6304.

[45] Flink, S.; van Veggel, F. C. J. M.; Reinhoudt, D. N. Functionalization of Self-Assembled Monolayers on Glass and Oxidized Silicon Wafers by Surface Reactions. *J. Phys. Org. Chem.* **2001**, *14*, 407–415.

[46] Kanoh, N.; Kumashiro, S.; Simizu, S.; Kandoh, Y.; Hatakeyama, S.; Tashiro, H.; Osada, H. Immobilization of Natural Products on Glass Slides by Using a Photoaffinity Reaction and the Detection of Protein–Small-Molecule Interactions. *Angew. Chem. Int. Ed.* **2003**, *42*, 5584–5587.

[47] Matyjaszewski, K.; Xia, J. Atom Transfer Radical Polymerization. *Chem. Rev.* **2001**, *101*, 2921–2990.

[48] Wang, J.-S.; Matyjaszewski, K. Controlled/"Living" Radical Polymerization. Halogen Atom Transfer Radical Polymerization Promoted by a Cu(I)/Cu(II) Redox Process. *Macromolecules* **1995**, *28*, 7901–7910.

[49] Kong, X.; Kawai, T.; Abe J.; Iyoda, T. Amphiphilic Polymer Brushes Grown From The Silicon Surface By Atom Transfer Radical Polymerization. *Macromolecules* **2001**, *34*, 1837–1844.

[50] Minko, S.; Usov, D.; Goreshnik, E.; Stamm, M. Environment-Adopting Surfaces with Reversibly Switchable Morphology. Macromol. *Rapid. Commun.* **2001**, *22*, 206–211.

[51] Tran, Y.; Auroy, P.; Lee, L.-T. Determination of the Structure of Polyelectrolyte Brushes. *Macromolecules* **1999**, *32*, 8952–8964.

[52] Biesalski, M.; Johannsmann, D.; Ruhe, J. Synthesis and Swelling Behavior of a Weak Polyacid Brush. *J. Chem. Phys.* **2002**, *117*, 4988–4994.

[53] Cussler, E. L. *Diffusion. Mass Transfer in Fluid Systems,* 2nd ed.; Cambridge University Press, Cambridge, UK, 1997, pp. 169.

[54] Crank, J. *The Mathematics of Diffusion*, 2nd ed.; Oxford University Press: New York, 1975.

[55] Brenner, H.; Edwards, D. A. *Macrotransport Processes*, Butterworth-Heinemann: Boston, 1993.

[56] Maxwell, J. C. *Treatise on Electrochemistry and Magnetism*, Vol. 1, 3rd ed.; Oxford University Press, Oxford, UK, 1892, pp. 435-449.

[57] Newton, M. R.; Morey, K. A.; Zhang, Y.; Snow, R. J.; Diwekar, M.; Shi, J.; White, H. S. Anisotropic Diffusion in Face-Centered Cubic Opals. *Nano Lett.* **2004**, *4*, 875–880.

[58] Newton, M. R.; Bohaty, A. K.; White, H. S.; Zharov, I. Chemically Modified Opals as Thin Permselective Nanoporous Membranes. *J. Am. Chem. Soc*. **2005**, *127*, 7268–7269.

[59] Newton, M. R.; Bohaty, A. K.; Zhang, Y.; White, H. S.; Zharov, I. pH and Ionic Strength Controlled Cation Permselectivity in Amine-Modified Nanoporous Opal Films. *Langmuir* **2006**, *22*, 4429–4432.

[60] Smith, J. J.; Zharov, I. Ion Transport in Sulfonated Nanoporous Colloidal Films. *Langmuir* **2008**, *24*, 2650–2654.

[61] Smith, J. J.; Abbaraju, R, R.; Zharov, I. Proton Transport in Assemblies of Silica Colloidal Spheres. *J. Mater. Chem.* **2008**, *18*, 5335–5338.

[62] Bohaty, A. K.; Newton, M. R.; Zharov, I. Light-Controlled Ion Transport through Spiropyran-Modified Nanoporous Silica Colloidal Films. *J. Porous Mater.* **2010**, *17*, 465–473.

[63] Cichelli, J.; Zharov, I. Chiral Selectivity in Surface-Modified Porous Colloidal Films. *J. Am. Chem. Soc.* **2006**, *128*, 8130–8131.

[64] Cichelli, J.; Zharov, I. Chiral Permselectivity in Nanoporous Opal Films Surface-Modified with Chiral Selector Moieties. *J. Mater. Chem.* **2007**, *17*, 1870–1875.

[65] Bohaty, A. K.; Zharov, I. Suspended Self-Assembled Opal Membranes. *Langmuir* **2006**, *22*, 5533–5536.

[66] Bohaty, A.; Abelow, A. E.; Zharov, I. Nanoporous Silica Colloidal Membranes Suspended in Glass. *J. Porous Mater.* **2011**, *18*, 297–304.

[67] Bohaty, A. K.; Smith, J. J.; Zharov, I. Free-Standing Silica Colloidal Nanoporous Membranes. *Langmuir* **2009**, *25*, 3096–3101.

[68] Schepelina, O.; Zharov, I. Polymer-Modified Opal Nanopores. *Langmuir* **2006**, *22*, 10523–10527.

[69] Schepelina, O.; Zharov, I. Poly(*N*-isopropylacrylamide)-Modified Nanoporous Opals. *Polym. Prepr.* **2007**, *48*, 455–456.

[70] Schepelina, O.; Zharov, I. Poly(2-(dimethylamino)ethyl methacrylate)-Modified Nanoporous Colloidal Films with pH and Ion Response. *Langmuir* **2008**, *24*, 14188–14194.

[71] Schepelina, O.; Poth, N.; Zharov, I. pH-Responsive Nanoporous Silica Colloidal Membranes. *Adv. Funct. Mater.* **2010**, *20*, 1962–1969.

[72] Abelow, A. E.; Zharov, I. Poly(L-alanine)-Modified Nanoporous Colloidal Films. *Soft Matter* **2009**, *5*, 457–462.

[73] Abelow, A. E.; White, R. J.; Plaxco, K. W.; Zharov, I. Nanoporous Silica Colloidal Films with Molecular Transport Gated by Aptamers Responsive to Small Molecules. *Coll. Czech Chem. Commun.* **2011**, *76*, 683–694.

[74] Smith, J. J.; Zharov, I. Preparation and Proton Conductivity of Self-Assembled Sulfonated Polymer-Modified Silica Colloidal Crystals. *Chem. Mater.* **2009**, *21*, 2013–2019.

[75] Ignacio-de Leon, P. A.; Zharov. I. Size-Selective Transport in Colloidal Nano-Frits. *Chem. Commun.* **2011**, *47*, 553–555.

[76] Ignacio-de Leon, P. A.; Zharov. I. SiO_2@Au Core-Shell Nanospheres Self-Assemble to Form Colloidal Crystals That Can Be Sintered and Surface Modified to Produce pH-Controlled Membranes. *Langmuir* **2013**, 29, 3749–3756.

[77] Birnbaum, A. J.; Zalalutdinov, M. K.; Wahl, K. J.; Pique, A. Fabrication and Response of Laser-Printed Cavity-Sealing Membranes. *J. Microelectromech. Syst.* **2011**, *20*, 436-440.

[78] Smith, J. J. Sulfonated Nanoporous Colloidal Films and Membranes Ph.D. Thesis, University of Utah, Salt Lake City, Utah, USA, 2009.

[79] Winter, M.; Brodd, R.J. What Are Batteries, Fuel Cells, and Supercapacitors? *Chem. Rev*. **2004**, *104*, 4245–4269.

[80] Kreuer, K.; Paddison S;, Spohr E.; Schuster M. Transport in Proton Conductors for Fuel Cell Applications: Simulations, Elementary Reactions, and Phenomenology. *Chem. Rev.*, **2004**, *104*, 4637–4678.

[81] Hickner, M. A.; Ghassemi, H.; Kim, Y. S.; Einsla, B. R.; McGrath, J. E. Alternative Polymer Systems for Proton Exchange Membranes (PEMs). *Chem. Re*v. **2004**, *104*, 4587–4611.

[82] Li, Q.; He, R.; Jensen, J. O.; Bjerrum, N. J. Approaches and Recent Development of Polymer Electrolyte Membranes for Fuel Cells Operating above 100 °C. *Chem. Mater.* **2003**, *15*, 4896–4915.

[83] Gary, F. M. *Polymer Electrolytes*, Royal Society of Chemistry, Cambridge, 1997.

[84] Yang, Y.; Holdcroft, S. Synthetic Strategies for Controlling the Morphology of Proton Conducting Polymer. *Fuel Cells* **2005**, *5*, 171–185.

[85] Kerres, J. A. Blended and Cross-Linked Ionomer Membranes for Application in Membrane Fuel Cells. *Fuel Cells* **2005**, *5*, 230–247.

[86] Hogarth, W. H.; Diniz da Costa, J. C.; Lu, G. Q. Solid Acid Membranes for High Temperature (140 °C) Proton Exchange Membrane Fuel Cells. *J. Power Sources* **2005**, *142*, 223–237.

[87] Hickner, M. A.; Pivovar, B. S. The Chemical and Structural Nature of Proton Exchange Membrane Fuel Cell Properties. *Fuel Cells* **2005**, *5*, 213–229.

[88] Yeo, S. C.; Eisenberg, A. Physical Properties and Supermolecular Structure of Perfluorinated Ion-Containing (Nafion) Polymers. *J. Appl. Polym. Sci.* **1977**, 21, 875–898.

[89] Tripathi, B.; Shahi, K. Recent Progress on Organic-Inorganic Nanocomposite Polymer Electrolyte Membranes for Fuel Cell Applications. *Prog. Polym. Sci.*, **2011**, 36, 945–979.

[90] Valle, K.; Belleville, P.; Pereira, F.; Sanchez, C. Hierarchically Structured Transparent Hybrid Membranes by in Situ Growth of Mesostructured Organosilica in Host Polymer. *Nat. Mater*. **2006**, *5*, 107–111.

[91] Bhattacharyya, A. J.; Maier, J. Second Phase Effects on the Conductivity of Non-Aqueous Salt Solutions: “Soggy Sand Electrolytes”. *Adv. Mater.* **2004**, *16*, 811–814.

[92] Navarra, M.; Materazzi, S.; Panero, S.; Scrosati, B. PVdF-Based Membranes for DMFC Applications. *J. Electrochem. Soc.* **2003**, *150*, A1528–A1532.

[93] Satolli, D.; Navarra, M. A.; Panero, S.; Scrosati. B.; Ostrovski, D.; Jacobsson, P.; Albinsson, I.; Mellander, B.-E. Macro- and Microscopic Properties of Nonaqueous Proton Conducting Membranes Based on PAN. *J. Electrochem. Soc.* **2003**, *150*, A267–A273.

[94] Beyazyildirim, S.; Kreuer, K. D.; Schuster, M.; Bhattacharyya, A. J.; Maier, J. Heterogeneous Doping of a Weak Covalent Electrolyte: Proton Conductivity Enhancement of Imidazole by Admixture of Oxide Particles. *Adv.Mater.* **2008**, *20*, 1274–1278.

[95] Watanabe, M.; Uchida, H.; Igarashi, H.; Effects of Polymer Electrolyte Membrane's Property on Fuel Cell Performances. *Macromol. Symp.* **2000**, *156*, 223–230.

[96] Hamoudi, S.; Kaliaguine, S. Sulfonic Acid-Functionalized Periodic Mesoporous Organosilica. *Microporous Mesoporous Mater.* **2003**, *59*, 223–230.

[97] Wang, J.; Merino, J.; Aranda, P.; Galvan, J.-C.; Hitzky-Ruiz, E. Reactive Nanocomposites Based on Pillared Clays. *J. Mater. Chem.* **1999**, 161–167.

[98] Kwak, S.-H.; Yang, T.-H.; Kim, C.-S.; Yoon, K. H. Polymer composite membrane incorporated with a hygroscopic material for high-temperature PEMFC. *Electrochim. Acta* **2004**, *50*, 653–657.

[99] Tricoli, V.; Nannetti, F. Zeolite–Nafion composites as ion conducting membrane materials. *Electrochim. Acta* **2003**, *48*, 2625–2633.

[100] Soler-Illia, G. J. A. A.; Azzaroni, O. Multifunctional Hybrids by Combining Ordered Mesoporous Materials and Macromolecular Building Blocks. *Chem. Soc. Rev.*, **2011**, *40*, 1107–1150.

[101] Zhang, H.; Ohashi, H.; Tamaki, T.; Yamaguchi, T. Water Movement in a Solid-State Alkaline Fuel Cell Affected by the Anion-Exchange Pore-Filling Membrane Properties. *J. Phys. Chem. C*, **2013**, *117*, 16791−16801.

[102] Park, S.-H.; Choi, Y.-W.; Park, J.-S. Characterization of Sulfonated Poly(Styrene-Co-Pyrrolidone) Pore-Filling Membranes for Fuel Cell Applications. *J. Appl. Electrochem.*, **2011**, *41*, 849–857.

[103] Jung, H.; Ohashi, H.; Tamak, T.; Yamaguchi, T. Improvement of Thermal-Stability of Anion Exchange Membranes for Fuel Cell Applications by Controlling Water State. *Chem. Lett.*, **2013**, *42*, 14–16.

[104] Yamamoto, D.; Munakata, H.; Kanamura, K. Synthesis and Characterization of Composite Membrane with Three-Dimensionally Ordered Macroporous Polyimide Matrix for DMFC. *J. Electrochem. Soc.*, **2008**, *155*, B303–B308.

[105] Gohil, J. M.; Karamanev, D. G. Novel Pore-Filled Polyelectrolyte Composite Membranes for Cathodic Microbial Fuel Cell Application. *J. Power Sources*, **2013**, *243*, 603–610.

[106] Kanamura, K.; Mitsui, T.; Munakata, H. Preparation of Composite Membrane between a Uniform Porous Silica Matrix and Injected Proton Conductive Gel Polymer. *Chem. Mater.*, **2005**, *17*, 4845–4851.

[107] Yameen, B.; Kaltbeitzel, A.; Langer, A.; Müller, F.; Gösele, U.; Knoll, W.; Azzaroni, O. Highly Proton-Conducting Self-Humidifying Microchannels Generated by Copolymer Brushes on a Scaffold. *Angew. Chem. Int. Ed.*, **2009**, *48*, 3124–3128.

[108] Yang, Q.; Adrus, N.; Tomicki, F.; Ulbricht, M. Composites of Functional Polymeric Hydrogels and Porous Membranes. *J. Mater. Chem*., **2011**, *21*, 2783–2811.

[109] Julien, C. Solid State Batteries. In *CRC Handbook of Solid State Electrochemistry*; Gellings, P. J.; Bouwmeester, H. J. M., Eds.; CRC: Boca Raton, 1997; Chapter 11, pp. 371–406.

[110] Wakihara, M.; Yamamoto, O., Eds. *Lithium Batteries*, Wiley-VCH: Berlin, New York, Chichester, Brisbane, Singapore, Toronto, 1998.

[111] Einset, A. G.; Wnek, G. E. Polymer Electrolyte Review. In *Handbook of Solid State Batteries & Capacitors*; Munshi, M. Z. A., Ed.; World Scientific: Singapore, New Jersey, London, Hong Kong, 1995; Chapter 15, pp. 289–310.

[112] Wright, P. V. Polymer Electrolytes - the Early Days. *Electrochim. Acta* **1998**, *43*, 1137–1143.

[113] Fauteux, D.; Massucco, A.; McLin, M.; van Buren, M.; Shi, J. Lithium Polymer Electrolyte Rechargeable Battery. *Electrochim. Acta* **1995**, *40*, 2185–2190.

[114] Fenton, B. E.; Parker, J. M.; Wright, P. V. Complexes of Alkali Metal Ions with Poly(Ethylene Oxide). *Polymer* **1973**, *14*, 589.

[115] Armand, M. B. Polymer Electrolytes. *Annu. Rev. Mater. Sci.* **1986**, *16*, 245–261.

[116] Stainer, M.; Hardy, L. C.; Whitmore, D. H.; Schriver, D. F. Stoichiometry of Formation and Conductivity Response of Amorphous and Crystalline Complexes Formed Between Poly(ethylene oxide) and Ammonium Salts: PEO_x• NH_4SCN and PEO_x• $NH_4SO_3CF_3$. *J. Electrochem. Soc.* **1984**, *131*, 784–790.

[117] Quartarone, E.; Mustarelli, P.; Magistris, A. PEO-Based Composite Polymer Electrolytes. *Solid State Ionics* **1998**, *110*, 1–14.

[118] Giles, J. R. M. Electrolytic Conduction in Amorphous Salt Complexed Polyethers. *Solid State Ionics* **1987**, *24*, 155–167.

[119] Giles, J. R. M.; Gray, F. M.; McCallum, J. R.; Vincent, C. A. Synthesis and Characterization of ABA Block Copolymer-Based Polymer Electrolytes. *Polymer* **1987**, *28*, 1977–1981.

[120] Sun, J.; McFarlane, D. R.; Forsyth, M. Mechanical Properties of Polyether-Plasticiser-Salt Systems as Polymer Electrolytes. *Solid State Ionics* **1996**, *85*, 137–141.

[121] Giles, J. R. M.; Greenhall, M. P. Ionic Conduction in Phosphate Ester-Crosslinked Polyethylene Glycols Complexed with Lithium Trifluoromethanesulfonate *Polymer Comm.* **1986**, *27*, 360-362.

[122] Rawsky, G. C.; Fujinami, T.; Shriver, D. F. Aluminosilicate/Polyethylene Glycol Copolymers: a New Class of Polyelectrolytes *Polym. Mater. Sci. Eng.* **1994**, *71*, 523-527.

[123] Meyer, W. H. Polymer Electrolytes for Lithium-Ion Batteries. *Adv. Mater.* **1998**, *10*, 439–448.

[124] Scrosati, B. Conducting Polymers: Advanced Materials for New Design, Rechargeable Lithium Batteries. *Polym. Int.* **1998**, *47*, 50–55.

[125] Angell, C. A.; Xu, K.; Zhang, S.-S.; Videa, M. Variations on the Salt-Polymer Electrolyte Theme for Flexible Solid Electrolytes. *Solid State Ionics* **1996**, *86-88*, 17–28.

[126] Ogata, N.; Sanui, K.; Rikukawa, M.; Yamada, W.; Watanabe, M. Super Ion Conducting Polymers For Solid Polymer Electrolytes. *Synth. Met.* **1995**, *69*, 521–524.

[127] Ardel, G.; Golodnitsky, D.; Peled, E.; Wang, Y.; Bajue, S.; Greenbaum, S. Bulk and Interfacial Ionic Conduction in LiI/Al_2O_3 Mixtures. *Solid State Ionics* **1998**, *113-115*, 477–485.

[128] Dudney, N. J. Composite Electrolites. In *Handbook of Solid State Batteries & Capacitors*; Munshi, M. Z. A., Ed.; World Scientific: Singapore, New Jersey, London, Hong Kong, 1995; Chapter 12, pp. 231–246.

[129] Krieg, E.; Weissman, H.; Shirman, E.; Shimoni, E.; Rybtchinski B. A Recyclable Supramolecular Membrane for Size-Selective Separation of Nanoparticles. *Nat. Nanotechnol.* **2011**, *6*, 141–146.

[130] Park, M.-H.; Subramani, C.; Rana, S.; Rotello, V. M. Chemoselective Nanoporous Membranes via Chemically Directed Assembly of Nanoparticles and Dendrimers. *Adv. Mater*. **2012**, *24*, 5862–5866.

[131] Mueggenburg, K. E.; Lin, X.-M.; Goldsmith, R. H.; Jaeger, H. M. Elastic Membranes of Close-Packed Nanoparticle Arrays. *Nat. Mater.,* **2007***, 6*, 656–660.

[132] He, J.; Lin, X.-M.; Chan, H.; Vukovic, L.; Kral, P.; Jaeger H. M. Diffusion and Filtration Properties of Self-Assembled Gold Nanocrystal Membranes. *Nano Lett.* **2011**, *11*, 2430–2435.

CHAPTER 2

NANOPOROUS MEMBRANES WITH TUNABLE PORE SIZE BY PRESSING/SINTERING SILICA COLLOIDAL SPHERES

2.1 Introduction

Over the past decade, nanoporous membranes attracted increasing attention due to their potential applications in molecular sorting, separations, and sensing.[1-3] Several methods have been developed for the preparation of nanoporous membranes, including lithography,[4] anodic oxidation of aluminum films,[5] track etching of polymers,[6] surfactant-directed self-assembly,[7] self-assembly of block-copolymers,[8] self-assembly and polymerization of liquid crystals,[9,10,11] sol-gel methods,[12,13] dip-coating,[14] chemical vapor deposition,[15] and by templating silica colloidal crystals.[16,17]

For any emerging membrane preparation technology, commercial translation requires both precise control over membrane performance and scalability of the membrane preparation process. Successful membrane preparation processes should provide good control over the average pore diameter with a narrow pore diameter distribution to enable size exclusion separations. Presently, depending on the membrane material, pore size is controlled by preparation conditions, such as etching conditions in ion-track etched membranes and anodized alumina membranes, or predetermined by the size of the template used in membrane preparation.[16,17]

Inorganic membranes[18] are particularly attractive in the fields of high temperature

gas separation,[19,20] water treatment,[21] and as catalytic support and membrane reactors[22] due to their mechanical, chemical, and thermal stability. Most commonly, inorganic nanoporous membranes are prepared by anodization of aluminum[5] and by sol-gel methods.[12] These methods, however, are not very time- and cost-effective.

Assembly of silica colloidal spheres provides an alternative efficient approach to the preparation of inorganic nanoporous membranes with high thermal and chemical stability. Colloidal particles can be self-assembled into silica colloidal crystals with close-packed face-centered cubic (fcc) arrangement of silica spheres and ordered arrays of three-dimensional interconnected voids.[23] The void size in colloidal crystals can be easily controlled in the 5-100 nm range by changing the silica sphere diameter.[23] Earlier, we reported[24] the preparation of robust free-standing 200 μm-thick colloidal membranes with approximately 1×1 cm^2 dimensions and no mechanical defects by sintering silica colloidal crystals at 1050 °C. We also demonstrated[25] that molecular transport through these membranes is size-selective and the selectivity is enhanced by the tortuous path diffusing molecules take through the colloidal crystal. Our results suggested that sintered silica colloidal membranes have potential applications in size-selective separations. In addition, we showed that surface modification of colloidal nanopores leads to gated silica colloidal membranes.[26] However, ordered silica colloidal crystals used in the preparation of the above membranes are limited in size, which results in smaller area of the corresponding membranes. It is also difficult to obtain silica colloidal crystals of uniform thickness by vertical deposition from colloidal suspensions, yet uniform thickness would be important for practical applications of nanoporous colloidal membranes.[27]

To avoid these drawbacks, we decided to prepare silica colloidal membranes by

pressing silica spheres together in a die set. This would provide uniform membrane thickness, while the membrane area would be limited only by the die set dimensions. This process would be time-efficient compared to the vertical deposition, which requires hours. Surprisingly, despite these attractive features, to the best of our knowledge, such a method has not been described before. On the other hand, the resulting colloidal membranes would possess no crystalline order, thus not containing uniform pores and requiring verification of size exclusion behavior.

In this article, we report the preparation of nanoporous membranes by pressing silica spheres with a hydraulic press at 5000 lb followed by sintering at 1050 °C. We studied the diffusion of a dye-labeled dendrimer and of polystyrene nanospheres of various diameters through pressed silica colloidal membranes to determined the "cut-off" of the membranes and to demonstrate its tunability. We also performed pore-filling of these membranes with a proton-conducting polymer.

2.2 Experimental Section

2.2.1 Materials

Ammonium hydroxide (28-30% as NH_3, EMD Chemicals, Inc.), tetraethyl orthosilicate (99.999% metal basis, Alfa Aesar), Polyspherex™ Polystyrene spheres of 25 nm, 100 nm and 250 nm diameter (Phosphorex Inc), and 3-sulfopropylmethacrylate (Aldrich) were used as received. Deionized water with 18 MΩ resistivity used in all experiments was obtained from a Barnstead "E-pure" water purification system. All ethanol used was 200 proof.

2.2.2 Instruments

Scanning electron microscopy (SEM) images were obtained using a FEI Novanano 630 instrument. Optical microscopy images were obtained using a Nikon Eclipse ME600 instrument. A Branson 1510 sonicator was used for all sonications. UV/Vis measurements were performed using an Ocean Optics USB2000 or USB4000 instrument. A Clay Adams Compact II Centrifuge (3200 rpm, Becton Dickinson) was used for all centrifugations. A Fisher Scientific Isotemp Programmable Muffle Furnace (Model 650) was used for calcination and sintering.

2.2.3 Preparation of Silica Spheres

Silica spheres were prepared according to the previously reported procedure.[24,28] All glassware was cleaned with distilled water prior to use. A batch of silica spheres was made by mixing 500 mL of an ethanol solution containing TEOS (51.4 mL, 0.20 mol) with 500 mL of ethanol solution containing NH_4OH (70.0 mL, 1.1 mol) and water (257 g, 14.3 mol). These two solutions were poured simultaneously in a 2 L Erlenmeyer flask and vigorously stirred. The resulting mixture had final concentrations of 0.2 M TEOS, 1.1 M NH_3, and 17.0 M H_2O. After about 30 min of being stirred, the solution became cloudy, indicating silica sphere formation. After 24 h, the silica spheres were centrifuged in 15 mL centrifuge tubes (Corning) at 1163g for 15 min. After all of the spheres were collected as pellets at the bottom of the centrifuge tubes, the supernatant was decanted, and the silica spheres were purified by repetitive cycle of suspending the spheres in 10 mL of a solvent by sonication for 15 min, during which the tubes were periodically shaken by hand to free any pieces of the pellet stuck to the sides of the tubes, followed by centrifugation. Following solvents were used: water (twice), 25% ethanol in water, 50%

ethanol, 75% ethanol, and 100% ethanol (twice). After the final centrifugation, the supernatant was decanted, and the silica spheres were dried in a stream of nitrogen for 12 h. Dried spheres were later calcinated by placing them into a Petri dish, breaking all large aggregates with spatula, and placing the dish in the oven programmed to heat the spheres for 4 h at 600 °C. The heating rate in the oven was set to 20 °C/min. SEM images of the spheres were taken and the diameters determined from 100 individually measured silica spheres in each sample to be 390±10 nm after the calcination.

Silica spheres of 220 nm diameter were prepared following the procedure above but using different amounts of reagents. The final concentrations of the reagents were 0.2 M TEOS (51.4 mL, 0.20 mol), 0.4 M NH_3 (26.78 mL, 0.4 mol), and 16.0 M H_2O (288 g, 16.0 mol) in a 1.0 L ethanolic solution. The reaction mixture was stirred vigorously for 24 h at room temperature. SEM images of the spheres were taken and the diameters determined from 100 individually measured silica spheres in each sample to be 260±20 nm and 230±20 nm before and after calcination, respectively.

Silica spheres of 70 nm in diameter were prepared and calcinated following the reported procedure.[29] The spheres were synthesized using the following concentrations of the reagents TEOS (15.2 ml, 0.12 M final concentration), NH_4OH (24.2 mL, 0.80 M NH_4OH final concentration) in ethanol with total volume of solution being 500 mL. The reaction mixture was stirred vigorously overnight at room temperature. The spheres were collected and washed by ultracentrifugation for 20 min at 4 °C using a gradient series of 100% water, 50% ethanol, and absolute ethanol (twice). SEM images of the spheres were taken and the diameter determined from 100 individually measured silica spheres to be 70±10 nm after the calcination.

2.2.4 Preparation of Pressed Silica Colloidal Membranes

A stainless steel dry pressing die set (13 mm ID, supplied by iCL, Inc.) was loaded with dry silica spheres (all large aggregates were broken using spatula) and placed in Carver laboratory hydraulic press. A pressure of 5000 pounds was applied for 30 seconds, after which the pressed material was carefully removed from the die set and placed into the oven, covered with a small ceramic plate to create even distribution of heat and prevent curving, and heated at 1050 °C for 12 h. The membrane shrunk to 10.5 mm in diameter after the sintering. The thickness of the membrane could be varied from 0.9 to 1.5 mm by the amount of silica spheres used. Silica membranes of 30 mm diameter were prepared following the same procedure and using a 30 mm ID stainless steel dry pressing die set (Across International, NJ). Upon sintering at 1050 °C for 24 h, the diameter of the pressed membranes decreased to 25 mm. The photographs of silica colloidal membranes are shown in Figure 2.1.

2.2.5 Mechanical Testing of Pressed Silica Colloidal Membranes

We used the four-point bending test to determine the flexural strength of the membranes. This test uses a rectangular beam of the analyzed material supported at two points from below (the support span) and bearing a load that makes contact at two points above (the loading span). The load is increased until the beam fractures, and this rupture force is used to calculate the flexural strength. If the loading span is one third of the length of the support span, then the flexural strength is calculated as $\sigma = \frac{FL}{bd^2}$, where σ is flexural strength (Pa), F is rupture force (N), L is support length (m), b is beam width (m), and d is beam thickness (m). A test apparatus was constructed with 4 cm in its largest dimension (Figure 2.2). Copper rods 1 mm in diameter were used to form the

contact points of the loading and support spans and were mounted on acrylic sheets. The apparatus consisted of two pieces: a base containing the supporting rods and a top containing the load contact points. The base also had rods inserted vertically into the corners that aligned with holes in the top piece. We used a hanging weight that was attached to the two ends of the beam that rested across the top of the apparatus to apply pressure to the membrane samples. The membrane test samples were cut to a rectangular shape using a carbon dioxide laser.

2.2.6 Diffusion Measurements

Diffusion through the colloidal membranes was measured by placing the circular-shaped membrane 13 mm in diameter between two connected 1-cm quartz cuvettes. The feed cuvette contained 4.00 mL of diffusing species in water while the receiving cuvette contained 4.00 mL of deionized water. The membrane was placed between two PTFE o-rings (Small Parts Inc.) to guard against leaking, and the assembly is then secured with a clamp. Epoxy resin was used as an adhesive in this assembly. Each cuvette was covered with Parafilm to prevent solvent evaporation, and the contents of both cuvettes continually stirred with a magnetic stir bar to ensure even distribution of diffusing species through the cuvette. The concentration of PS beads in feed cuvette was approximately 10^{13} particles/ml for each PS size. The receiving cuvette was placed between two fiber optic cables and initially blanked. The flux was monitored by recording the absorbance at 546 nm for dye-labeled dendrimers and at 250 nm for polystyrene spheres in the receiving cuvette for at least 12 h. Data points were acquired every 150 s with an initial delay of 150 s. Prior to using a membrane for a new trial, it was immersed in deionized water for at least two days and water was replaced occasionally to ensure removal of any

remaining probe molecule or particles from the membrane.

2.3 Results and Discussion

2.3.1 Preparation and Structure of Pressed Membranes

In order to prepare the pressed silica colloidal membranes, we generated Stöber silica spheres and calcinated them at 600 °C for 4 h. Calcination is commonly used to prevent crack formation in large-area silica colloidal crystals.[30] It removes solvents (water and ethanol) trapped inside the silica spheres, which causes shrinking of silica spheres and increases their density (ca. 2.17 g/cm^3 compared to ca. 1.97 g/cm^3 for as-made silica spheres).[30]

Calcinated silica spheres were pressed and sintered at 1050 °C, as described in the Materials and Methods section above. The resulting membranes (Figure 2.1) are robust and durable, having uniform thickness and fixed circular shape. The thickness was measured with digital caliper with 0.01 mm increment. For approximately 1mm thick membranes, the thickness in different spots of the membrane was uniform within the caliper resolution. The uniform thickness of the pressed membranes comes from the used method – pressing in a circular press die set, where pressure is distributed evenly. The overall thickness is precisely controlled by amount of silica spheres loaded into the press die set. The membranes could be manipulated, sonicated, sandwiched between plastic or metal gaskets, and even dropped from 1 m height without breaking or cracking. Optical microscopy at 50× magnification (Figure 2.3) showed minor cracks on the surface of the membranes, which are not seen at the 200× magnification (Figure 2.3). However, as will be discussed below, based on the diffusion measurements, we concluded that the cracks do not penetrate the entire thickness of the membrane.

We tested the flexural strength of silica colloidal membranes using the apparatus described above, and found it to be 19±6 MPa (2700±800 psi). This value is ca. 17% of the flexural strength of acrylic (17,000 psi) and is about 40% of flexural strength of ordered silica colloidal membranes prepared by vertical deposition (49±9 MPa, 7000±1200 psi). The latter result is expected as ordered silica colloidal membranes contain a close-packed structure with a maximum number of contacts between the silica spheres, while pressed membranes are disordered with silica spheres having fewer contacts with neighboring spheres, i.e., fewer connection points after sintering, which reduces the mechanical strength of the membrane.

This disordered structure can be seen in the SEM image of the pressed membrane (Figure 2.3). The SEM images of pressed membranes show no visible long- or short-range order of silica particles in the assembly, thus nanopore size cannot be established from silica sphere diameter, unlike in ordered silica colloidal crystal membranes, where nanopore size can be calculated using simple geometrical considerations.[31] For example, because the molecular transport through such ordered membranes occurs normal to the (111) plane of the fcc-packed structure and diffusing species enter the membrane through the concave triangular openings between the adjacent silica spheres, the distance from the center of their projection to the surface of the nearest sphere, which is ca. 15% of the sphere radius, can be assigned as the "radius" of colloidal nanopores. In contrast, for pressed colloidal membranes, the voids in several locations in SEM image appear to be larger than the silica sphere diameter.

To further characterize the geometry of pressed silica colloidal membranes, we studied the diffusion of the generation-1 dye-labeled PAMAM dendrimer[25] through the

membrane comprised of silica spheres 390 nm in diameter. We measured the diffusion rate (R_D) through the membrane of a known thickness (L) and area (S) driven by a known concentration gradient (ΔC). R_D was determined by recording the number of moles of the dendrimer that diffused through the membrane as a function of time. Knowing the value of R_D allowed for the calculation of the molecular flux J_{membr} through the membrane according to eq 2.1.

$$R_D = J_{membr} \times S \tag{2.1}$$

Fick's law for diffusion is shown in eq 2.2.

$$J_{membr} = \frac{\Delta C}{L} \times D_{membr} \tag{2.2}$$

It was used to determine the diffusion coefficient D_{membr} of a diffusing dendrimer species as it traversed the pressed silica colloidal membrane.

We found the diffusion coefficient of $1.4\pm0.4 \times 10^{-10}$ m^2/s for the dendrimer. This value is 2.7 times smaller than the diffusion coefficient of this dendrimer in solution ($3.8\pm0.1 \times 10^{-10}$ m^2/s) determined by diffusion NMR.[32] This D_{membr} value reflects the effect of the membrane geometry described by void fraction (ε) and tortuosity (τ) and related to the diffusion coefficient in solution D_{sol} as shown in eq 2.3.

$$D_{membr} = \frac{\varepsilon}{\tau} \times D_{sol} \tag{2.3}$$

Therefore, a smaller D_{membr} for pressed membranes compared to D_{sol} results from void fraction for the membrane that is less than unity and its tortuosity that may be more than unity. For the ordered closed-packed colloidal crystal, the void fraction ε_{fcc} is 0.26

and tortuousity τ_{fcc} is 3.0, reducing the D_{fcc} by the factor of 11.5 compared to D_{sol}. In contrast, D_{membr} for the disordered pressed colloidal membrane is only 2.7 smaller than D_{sol}, which suggests the void fraction is larger than 0.26 and tortuosity is smaller than 3.0. Because both values affect D_{membr}, it is impossible to calculate them using this value alone. Thus, we calculated the void fraction of the pressed membrane independently, based on its volume displacement. Assuming the pressed silica membrane to be a perfect cylinder of known diameter and thickness, we calculated the total volume of the membrane. Using the weight of the membrane and density of silica (2.17 g/cm^3) and of air (1.20×10^{-3} g/cm^3) inside the membrane, we then calculated the void fraction of the membrane. We estimated ε_{membr} to be 0.37, significantly higher than that of the fcc-packed colloidal crystals. Based on this value and D_{membr}, tortuousity τ_{membr} of the pressed membrane is 1.0. In other words, the transport through the pressed colloidal membranes proceeds in a linear path as opposed to the fcc-packed colloidal crystals.

2.3.2 Size-exclusion of Pressed Silica Colloidal Membranes

In order to determine the size cut-off for the transport through pressed colloidal membranes, and to establish if the cut-off can be controlled by varying the silica spheres diameter, we measured the diffusion of the polystyrene spheres through the pressed membranes comprised of silica spheres with different sizes. A representative plot of flux for polystyrene (PS) spheres 25, 100, and 250 nm in diameter through the pressed membrane comprised of 390 nm silica spheres (membrane-390) is shown in Figure 2.4A. Polystyrene spheres of all three sizes diffuse through the pressed membrane. The flux of 25 nm PS spheres is ca. 10 times greater than that for 250 nm PS spheres and ca. 4 times greater than that of 100 nm PS, which results from both membrane geometry and the

difference in diffusion coefficients of the PS spheres. The fact that all PS particles diffuse through this membrane indicates that membrane-390 possesses the size cut-off greater than 250 nm. This is more than half of the diameter of silica spheres used to prepare the membrane. In contrast, ordered silica colloidal crystals, which possess uniform pores with pore "diameter" of ~15% of silica sphere diameter,[25] would provide a size cut-off of 59 nm in the case of 390 silica spheres.

Next, we tested the cut-off of pressed silica membranes made of 220 and 70 nm silica spheres (membrane-220 and membrane-70, respectively). The plot of the flux of PS spheres through membrane-220 is shown in Figure 2.4B. No significant diffusion of 250 nm PS spheres through this membrane was observed, thus 220 nm silica spheres upon pressing form colloidal membranes with cut-off of at least 250 nm; however, membrane-220 is permeable for both 25 nm and 100 nm PS spheres. The flux of 25 nm PS spheres through the membrane-220 is ca. 5 times greater than flux of 100 nm PS spheres, which, taking into account the difference between diffusion coefficients of 25 nm PS and 100 nm PS (D_{sol} inversely proportional to particle size), makes the diffusion coefficient of 25 nm PS through membrane-220 ca. 25% greater compared to 100 nm PS. The flux of 25 nm PS through membrane-220 is almost the same as that through membrane-390. The flux of 100 nm PS spheres through membrane-220 is about 2.5 times smaller than that for membrane-390. Membrane-70 is also not permeable for 250 nm PS spheres, but permeable for 25 nm and 100 nm PS beads (data not shown). Flux values for 25 and 100 nm PS through membrane-70 are almost identical (with flux of 25 nm PS being 20% greater than that for 100 nm PS) to each other, presumably due to sterics rather than diffusion coefficients of PS spheres. Both values are smaller than

those for membrane-220 by the factor of ca. 7 and 1.5, respectively. Based on these observations, we conclude that the cut-off for membrane-70 is greater than 100 nm; however, there is a smaller number of pores of that size available than in the other two membranes.

Thus, pore size in pressed membranes could be larger than actual silica sphere size; however, overall pore size still depends on silica sphere size and can be controlled by varying the diameter of silica particles. Pressed membranes can block the diffusion of certain particles if smaller silica spheres are used for the preparation of the membranes.

2.4 Conclusions

We demonstrated that robust nanoporous membranes with uniform thickness can be prepared by pressing calcinated silica spheres followed by sintering at 1050 °C. The diameter and thickness of the pressed membranes can be controlled by the size of the press die and amount of loaded silica spheres, respectively. The developed procedure is easy, fast, and reliable. Comparison of the pressed membranes with the vertically deposited membranes is shown in Table 2.1.

Although the sphere arrangement in the resulting membranes is disordered and their pore size is not uniform, pressed membranes are capable of size-selective transport, which was shown by diffusion experiments for polystyrene spheres of different size. The largest polystyrene spheres (250 nm) did not diffuse through the pressed membranes comprised of smaller size silica spheres (220 and 70 nm), while 100 nm polystyrene spheres showed very small flux through the latter. We also demonstrated that pressed silica colloidal membranes can be used as a scaffold for the preparation of pore-filled fuel cell membranes. We filled the pores with sulfonated polymer brushes and measured the

proton conductivity of the resulting fuel cell membranes, which was high and comparable to that of Nafion™.

Our present work on pressed sintered colloidal membranes includes the modification of the silica surface inside the membrane with organic moieties and polymer brushes to improve size-selectivity and introduce other modes of selectivity. Size- and charge-selective separations of biomacromolecules using pressed silica colloidal membranes are to be studied as well.

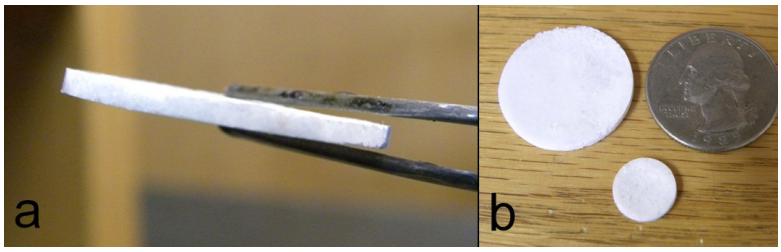

Figure 2.1. The photographs of pressed silica colloidal membranes (a) side view of pressed sinteres silica colloidal membrane 25 mm in diameter and ~1 mm in thickness; (b) front view of 25- and 11 mm-diameter membranes in comparison with a ¢25 coin.

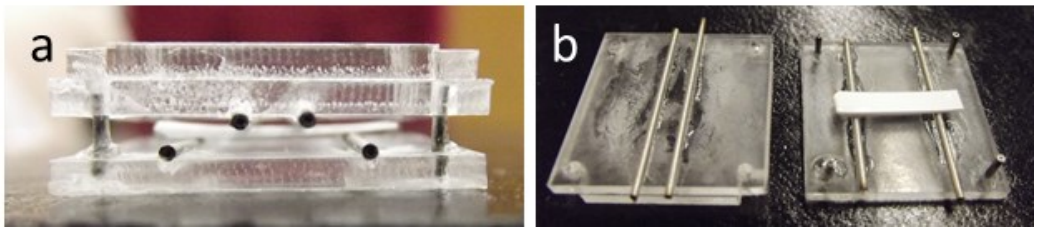

Figure 2.2. 4-Point bending test apparatus (a) assembled and (b) disassembled.

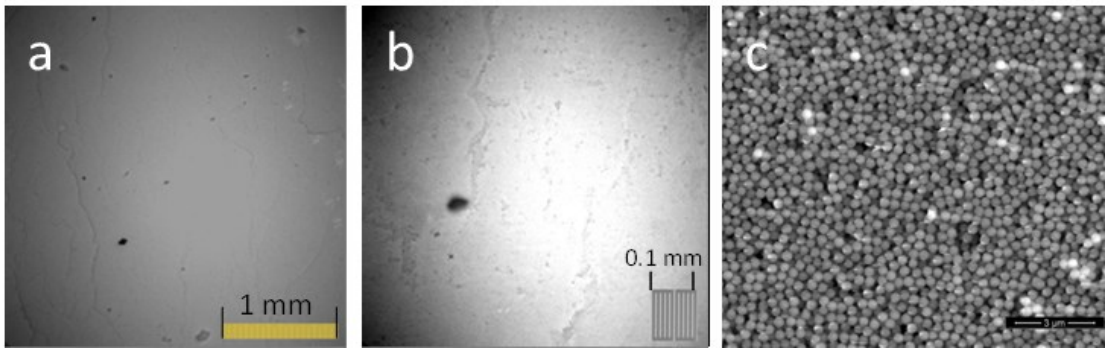

Figure 2.3. Images of pressed and sintered membrane comprised of 390 nm silica spheres. (a) optical microscopy image with 50× magnification; (b) optical microscopy image with 200× magnification; (c) SEM image, scale bar is 3 μm.

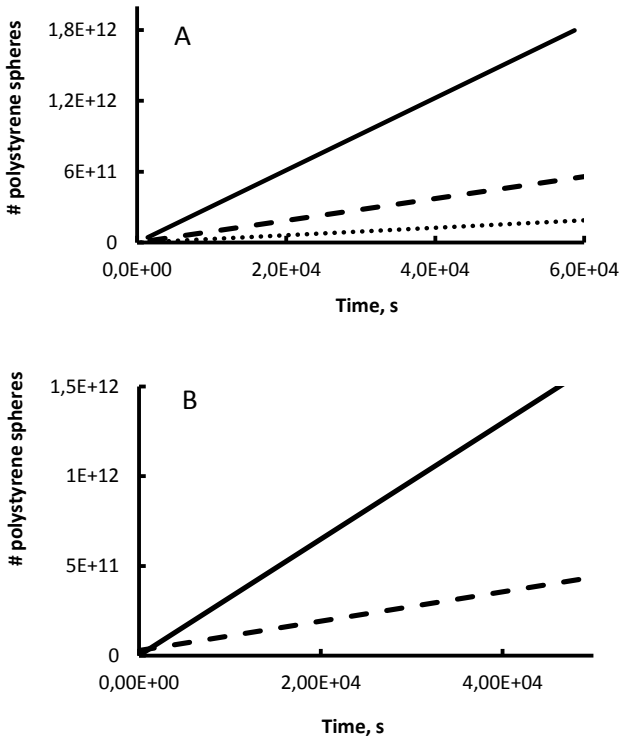

Figure 2.4. Representative flux plots of PS particles (25 nm PS (-), 100 nm PS (- -), 250 nm PS (•••)) through pressed silica colloidal membranes comprised of (a) 390 nm silica spheres, (b) 220 nm silica spheres.

Table 2.1. Comparison of silica colloidal membranes prepared by vertical deposition and by pressing.

Parameter\Membrane	Vertical deposition	Pressing
Controlled thickness	No	Yes
Controlled area	No	Yes
Capable of size-selective separation	Yes	Yes
Capable of surface modification	Yes	Yes
Porosity	26%	37%
Preparation time, h	>24	12

2.5 References

[1] Gin, D. L.; Noble, R. D. Designing the Next Generation of Chemical Separation Membranes. *Science* **2011**, *332*, 674−676.

[2] Hotta, K.; Yamaguchi, A.; Teramae, N. Deposition of Polyelectrolyte Multilayer Film on a Nanoporous Alumina Membrane for Stable Label-Free Optical Biosensing. *J. Phys. Chem. C* **2012**, *116*, 23533−23539.

[3] Deng, J.; Toh, C.-S. Impedimetric DNA Biosensor Based on a Nanoporous Alumina Membrane for the Detection of the Specific Oligonucleotide Sequence of Dengue Virus. *Sensors* **2013**, *13*, 7774–7785.

[4] Tong, H. D.; Jansen, H. V.; Gadgil, V. J.; Bostan, C. G.; Berenschot, C. G. E.; van Rijn, C. J. M.; Elwenspoek, M. Silicon Nitride Nanosieve Membrane. *Nano Lett*. **2004**, *4*, 283-287.

[5] Toh, C.-S.; Kayes, B. M.; Nemanick, E. J.; Lewis, N. S. Fabrication of Free-Standing Nanoscale Alumina Membranes with Controllable Pore Aspect Ratios. *Nano Lett*. **2004**, *4*, 767–770.

[6] Yoshida, M.; Asano, M.; Suwa, T.; Reber, N.; Spohr, R.; Katakai, R. Creation of Thermo-responsive Ion-track Membranes. *Adv. Mater*. **1997**, *9*, 757–758.

[7] Liu, N. G.; Dunphy, D. R.; Atanassov, P.; Bunge, S. D.; Chen, Z.; Lopez, G. P.; Boyle, T. J.; Brinker, C. J. Photoregulation of Mass Transport through a Photoresponsive Azobenzene-Modified Nanoporous Membrane. *Nano Lett*. **2004**, *4*, 551–554.

[8] Nunes, S. P.; Behzad, A. R.; Peinemann, K.-V. Self-Assembled Block Copolymer Membranes: From Basic Research to Large-Scale Manufacturing. *J. Mater. Res*. **2013**, *28*, 2661–2665.

[9] Kato, T., Yasuda, T., Kamikawa, Y., Yoshio, M. Self-Assembly of Functional Columnar Liquid Crystals. *Chem.Commun.*, **2009**, *7*, 729–739.

[10] Gin, D.L., Bara, J.E., Noble, R.D., Elliott, B.J. Polymerized Lyotropic Liquid Crystal Assemblies for Membrane Applications. *Macromol. Rapid Commun.* **2008**, *29*, 367–389.

[11] Kato, T., Mizoshita, N., Kishimoto, K. Functional Liquid-Crystalline Assemblies: Self-Organized Soft Materials. *Angew. Chem. Int. Ed.* **2006**, *45*, 38–68.

[12] Sakka, S. *Handbook of Sol-Gel Science and Technology*, Kluwer Academic Publishers: Norwell, MA, 2005.

[13] Gestel, T. V.; Hauler, F.; Bram, M.; Meulenberg, W. A.; Buchkremer, H. P. Synthesis and Characterization of Hydrogen-Selective Sol-Gel SiO_2 Membranes Supported on Ceramic and Stainless Steel Supports. *Sep. Purif. Technol.* **2014**, *121*, 20–29.

[14] Park, J.; Jung, M. Hydrogen Permeation of SiC-CeO_2 Composite Membrane by Dip-coating Process. *J. Korean Ceram. Soc.* **2013**, *50*, 485-488.

[15] Miyajima, K.; Eda, T.; Nair, B. N.; Honda, S.; Iwamoto, Y. Hydrothermal Stability of Hydrogen Permselective Amorphous Silica Membrane Synthesized by Counter Diffusion Chemical Vapor Deposition Method. *J. Ceram. Soc. Jpn* **2013**, *121,* 992–998.

[16] Xu, H.; Goedel, W. A. From Particle-Assisted Wetting to Thin Free-Standing Porous Membranes. *Angew. Chem. Int. Ed*. **2003**, *42*, 4694-4696.

[17] Xu, H.; Goedel, W. A. Polymer-Silica Hybrid Monolayers as Precursors for Ultrathin Free-Standing Porous Membranes. *Langmuir* **2002**, *18*, 2363–2367.

[18] Stroeve, P.; Ileri, N. Biotechnical and Other Applications of Nanoporous Membranes. *Trends Biotechnol.* **2011**, *29*, 259–266.

[19] Kanezashi, M.; Sasaki, T.; Tawarayama, H.; Yoshioka, T.; Tsuru, T. Hydrogen Permeation Properties and Hydrothermal Stability of Sol–Gel-Derived Amorphous Silica Membranes Fabricated at High Temperatures. *J. Am. Ceram. Soc*. **2013**, *96*, 2950–2957.

[20] Ghosh, D.; Sinha, M. K.; Purkait, M. K. A Comparative Analysis of Low-Cost Ceramic Membrane Preparation for Effective Fluoride Removal Using Hybrid Technique. *Desalination* **2013**, *327*, 2–13.

[21] Zhu, Y.; Chen, S.; Quan, X.; Zhang, Y.; Gao, C.; Feng, Y. Hierarchical Porous Ceramic Membrane with Energetic Ozonation Capability for Enhancing Water Treatment. *J. Membr. Sci.* **2013**, *431*, 197–204.

[22] Jiang, H.; Meng, L.; Chen, R.; Jin, W.; Xing, W.; Xu, N. Progress on Porous Ceramic Membrane Reactors for Heterogeneous Catalysis over Ultrafine and Nano-sized Catalysts. *Chin. J. Chem. Eng.* **2013**, *21*, 205–215.

[23] Wong, S.; Kitaev, V.; Ozin, G. A. Colloidal Crystal Films: Advances in Universality and Perfection. *J. Am. Chem. Soc.* **2003**, *125*, 15589–15598.

[24] Bohaty, A. K.; Smith, J. J.; Zharov, I. Free-Standing Silica Colloidal Nanoporous Membranes. *Langmuir* **2009**, *25*, 3096–3101.

[25] Ignacio-de Leon, P. A.; Zharov. I. Size-Selective Transport in Colloidal Nano-Frits. *Chem. Commun.* **2011***, 47*, 553–555.

[26] Zharov, I.; Khabibullin, A. Surface-Modified Silica Colloidal Crystals: Nanoporous Materials with Controlled Molecular Transport. *Acc. Chem. Res.* **2014**, *47*, 440–449.

[27] Birnbaum, A. J.; Zalalutdinov, M. K.; Wahl, K. J.; Pique, A. Fabrication and Response of Laser-Printed Cavity-Sealing Membranes. *J. Microelectromech. Syst.* **2011**, *20*, 436-440.

[28] Stöber, W.; Fink, A.; Bohn, E. Controlled Growth of Monodispersed Spheres in the Micron Size Range. *J. Colloid Interface Sci.* **1968**, *26*, 62–69.

[29] Hiramatsu, H.; Osterloh, F. pH-Controlled Assembly and Disassembly of Electrostatically Linked CdSe−SiO_2 and Au−SiO_2 Nanoparticle Clusters. *Langmuir* **2003**, *19*, 7003–7011.

[30] Chabanov, A. A.; Jun, Y.; Norris, D. Avoiding Cracks in Self-Assembled Photonic Band-Gap Crystals. *J. Appl. Phys. Lett*. **2004**, *84*, 3573–3575.

[31] Schepelina, O.; Zharov, I. Polymer-Modified Opal Nanopores. *Langmuir* **2006**, *22*, 10523–10527.

[32] Fritzinger, B.; Scheler, U. Scaling Behaviour of PAMAM Dendrimers Determined by Diffusion NMR. *Macromol. Chem. Phys.* **2005**, *206*, 1288–1291.

CHAPTER 3

EFFECT OF SULFONIC GROUP CONTENT IN PORE-FILLED SILICA COLLOIDAL MEMBRANES ON THEIR PROTON CONDUCTIVITY AND DIRECT METHANOL FUEL CELL PERFORMANCE

3.1 Introduction

Polymer electrolyte fuel cells are attractive alternative power sources for stationary, automobile, and portable applications because they provide high energy density, low operational temperature, and do not contribute to pollution.[1,2] The proton exchange membrane is the key component of the fuel cell,[3] as it allows for proton transport and separates the fuel and the oxidant.[4,5] In addition to possessing high proton conductivity, it is crucial for a fuel cell membrane to be nonswelling upon exposure to methanol and water, to be mechanically and thermally stable, and to remain hydrated at elevated temperatures.[6] Polymer electrolyte membranes (PEMs) that are the most commonly separators used in fuel cells do not fully satisfy the above requirements.[7] Thus, several alternative approaches to PEMs have been developed in the recent years. Often, these approached are based on developing new polymer electrolytes, such as sulfonated polystyrenes, polyarylene ethers and thioethers, polyimides and polyphosphazenes.[8] Regardless of the composition, these polymer electrolytes contain microphase-separated hydrophilic channels that allow for the proton transport.[5]

Another emerging approach to fuel cell membranes is to prepare materials

containing robust porous scaffolds filled with proton carriers such as polymer electrolytes, which together constitute proton-conducting channels.[9] The resulting pore-filled hybrid organic-inorganic membranes meet and exceed many performance requirements due to their better mechanical stability and nonswelling properties.[2,10,11]

The porous scaffolds in pore-filled membranes have been made of cross-linked track-etched polyethylene,[12,13,14] track-etched polycarbonate,[15] silica,[16] photo-electrochemically etched silicon,[17] 3D-ordered polyimide prepared by colloidal crystal templating method,[18] polysulfone prepared by phase-inversion,[19] and other materials.[20] The porous substrate can be filled by impregnation with ion-conductive polymers, such as Asahi polysulfone,[12,14] sulfonated poly(styrene-vinyl pyrrolidone-divinyl benzene),[13] poly(vinyl alcohol),[15] or poly(acrylamid) containing sulfonic groups.[16,18,19] However, this method may lead to leaching of the polymer and thus membrane instability. To stabilize the pore-filled structures, polymers can be cross-linked,[20] but grafting them on the pore surface appears to be a superior approach. We used this approach in the preparation of novel pore-filled membranes, where the rigid ordered silica colloidal crystal containing a continuous network of interconnected mesopores provides mechanical and thermal stability, nonswelling, and water retaining properties, while poly(3-sulfopropylmethacrylate) or poly(stryrenesulfonic acid) brushes grown from the surface of silica and filling the pores provide proton conductivity.[21] We found that the proton conductivity of pore-filled silica colloidal membranes is comparable to that of Nafion™ and increases with increasing temperature and relative humidity.[21] Others also utilized the surface-grafting approach, for example, in poly(sulfopropylmethacryrlate-oligo(ethyleneglycol)methacryrlate)-filled porous etched silicon[9,17] or in poly(2-

acrylamide-2-methylpropane sulfonic acid)-filled track-etched polycarbonate membranes.[22]

One of the important questions in this area, answering which is essential for the fundamental understanding of proton conductivity in polymer electrolyte membranes and for their optimization in general, and for pore-filled membranes in particular, is studying the dependence of proton conductivity of the membrane and the fuel cell performance on the amount of sulfonic groups in the polymer filling the pores.

The influence of sulfonation degree on proton conductivity, methanol permeability, water uptake, and mechanical properties of proton conductive membranes was studied earlier for a few membranes, such as sulfonated poly(ether ketone ketone),[23] sulfonated poly(styrene-isobutylene-styrene),[24] cross-linked fluorinated aromatic polyethers containing sulfonic groups,[25] sulfonated polyimide,[26] and sulfonated poly(styrene-indene-polyvinylidene fluoride).[27] It was demonstrated[24,26] that the proton conductivity generally increases with increasing degree of sulfonation (DS) and reaches its maximum at 75-90%. One study[25] showed that the current density of a fuel cell also increased with increasing sulfonic group content. However, high sulfonation degrees of the polymer membranes cause high water uptake and methanol permeability, leading to swelling and creating difficulties in using such membranes in fuel cells.

Pore-filled silica membranes do not swell in water, thus allowing systematic studies of proton conductivity and fuel cell performance in the entire (0-100%) range of sulfonic group content. Moreover, the preparation of pore-filled silica colloidal membranes[21] by surface-initiated atom transfer radical polymerization (SI-ATRP) allows for precise control of the polymer composition and results in unique membrane structures

with low molecular weight polymer chains inside the mesopores.

To the best of our knowledge, the dependence of their proton conductivity and the fuel cell performance on the amount of sulfonic acid groups in the polymer filling the pores was only studied by Choi et al.[28] They used polyolefine porous substrate pore-filled with cross-linked polymer containing sulfonic acid groups. It was shown that proton conductivity increases linearly with increasing amount of proton conductive polymer. However, the studied material is still prone to swelling in water due to the nature of the substrate or fuel and the pore-filling cross-linked polymer can leach out of the pores with time. Also, more systematic stufy of conductivity as a function of sulfonation degree is needed.

In this work, the sulfonic group content in the membranes was varied by copolymerizing 3-sulfopropylmethacrylate (SPM) and 2-ethoxy-ethylmethacrylate (EEMA) in different ratios using SI-ATRP (Figure 3.1) inside the mesopores of silica colloidal membranes. Proton conductivity measurements for the PSPM/PEEMA brush-filled membranes and open circuit voltage (OCV) and linear polarization measurements for the corresponding membrane-electrode assemblies (MEAs) were carried out in order to determine their dependence on the sulfonic group content. To the best of our knowledge, this is the first example of an investigation for the dependence of OCV on the sulfonic group content in proton conductive membrane. Methanol uptake for the PSPM/PEEMA brush-filled membranes was also measured in order to explain the OCV dependence on the sulfonic group content.

3.2 Experimental Section

3.2.1 Instrumentation

Dynamic light scattering (NICOMP 380 ZLS) was used to determine the size of polymer-modified silica particles. Scanning electron microscope (Hitachi S300N) and tunneling electron microscope (FEI Techna G2 T-12) were used to image unmodified and polymer-modified silica particles and pore-filled membranes. Nuclear magnetic resonance NMR (Varian I-500) was used to determine the structure and composition of copolymers in solution. Gel permeation chromatography (AKTA FPLC) was used to determine the molecular weight of copolymers in solution. Thermogravimetric analysis of polymer-modified silica particles was performed using TGA Q500 (TA Instruments). OCV and linear polarization measurements were carried out using DY-2023 bipotentiostat (Digi-IVY). The electrochemical impedance of the samples was measured using Princeton Applied Research VersaSTAT.

3.2.2 Materials

3-Sulfopropylmethacrylate, 2,2'-dipyridyl, 2-bromoisobutyryl bromide, 3-aminopropyl-triethoxysilane were purchased from Sigma-Aldrich and used as received. 2-Ethoxyethylmethacrylate was purchased from Sigma-Aldrich and passed through Al_2O_3 column before use to remove the inhibitor. Tetraorthosilicate (TEOS) was purchased from Alfa Aesar and used as received. 18 MΩ·cm water was obtained from a Barnsted "E-pure" water purification system.

3.2.3 Copolymerization of EEMA and SPM in Solution

Copolymerization of EEMA and SPM (Figure 3.1) was carried out in 12 mL of a 2:1 (by weight) mixture of degassed methanol and water, containing 2,2'-dipyridyl (1.6

mmol, 0,2496 g), $CuCl_2$ (0.12 mmol, 16 mg), CuCl (0.4 mmol, 40 mg), and 2-bromoisobutyryl bromide (0.1 mmol, 12.3 μL) at room temperature. The molar ratio of the monomers was varied, while the total amount of the monomers was 20 mmol. After 24 h, the samples were quenched by exposing it to air and adding cold water, then samples were precipitated by excess of DMF or ethanol and repeatedly washed with appropriate solvent for removing excess of initial monomers and initiator. For gel permeation chromatography (GPC) analysis, copolymer samples were dissolved in water and passed through PD-10 column (SEPHADEX-25) in order to remove low molecular weight impurities.

3.2.4 Preparation of Silica Spheres

Silica spheres were prepared according to the previously reported procedure.[29] All glassware was cleaned with deionized water prior to use. A batch of silica spheres was made by mixing 500 mL of ethanol solution containing TEOS (51.4 mL, 0.20 mol) with 500 mL of ethanol solution containing NH_4OH (70.0 mL, 1.1 mol) and water (257 g, 14.3 mol). These two solutions were poured simultaneously into a 2 L Erlenmeyer flask and vigorously stirred. The resulting mixture had final concentrations of 0.2 M TEOS, 1.1 M NH_3, and 17.0 M H_2O. After ca. 30 min of stirring, the solution became turbid, indicating silica sphere formation. After 24 h, the silica spheres were centrifuged in 15 mL centrifuge tubes (Corning) at 1163 g for 15 min. After all of the spheres were collected as pellets at the bottom of the centrifuge tubes, the supernatant was decanted, and the silica spheres were purified by repetitive cycle of suspending the spheres in 10 mL of solvent by sonication for 15 min, during which the tubes were periodically shaken by hand to free any pieces of the pellet stuck to the sides of the tubes, followed by

centrifugation. The following solvents were used: deionized water (twice), 25% ethanol in water, 50% ethanol, 75% ethanol, and pure ethanol (twice). After the final centrifugation, the supernatant was decanted, and the silica spheres were dried in a stream of nitrogen for 12 h. These spheres were calcinated in the oven programmed to heat the spheres for 4 h at 600 °C. The heating rate in the oven was 20 °C/min. SEM images of the spheres were obtained and the diameters determined from 100 individually measured silica spheres in each sample to be 394±13 nm after calcination. A second batch of the spheres was prepared using the same precursor concentrations, the silica spheres after drying, and calcination for 4 h at 600 °C were 391±37 nm in diameter.

3.2.5 Modification of Silica Particles with Copolymers

Silica spheres were modified with initiator moieties in two steps. First, silica spheres (2 g) were stirred in 20 mL of dry acetonitrile containing 1 mL (4.3 mmol) of 3-aminopropyltriethoxysilane for 17 h at room temperature. Amine-modified silica particles were collected and rinsed with acetonitrile 4 times by centrifugation. Next, amine-modified spheres were stirred in 100 mL of dichloromethane solution containing 2 mL of triethylamine (0.15 M solution), 1.6 mL of 2-bromoisobutyrylbromide (0.13 M solution), and a catalytic amount of DMAP for 12 h at room temperature. Initiator-modified spheres were isolated and rinsed 4 times with dichloromethane by centrifugation.

The formation of PSPM/PEEMA brushes on the initiator-modified silica spheres (1.0 g) was carried out in 12 mL of a 2:1 (by weight) mixture of degassed methanol and water, containing 2,2'-dipyridyl (1.6 mmol, 0.25 g), $CuCl_2$ (0.12 mmol, 16 mg), CuCl (0.4 mmol, 40 mg), and varying amounts of monomers EEMA and SPM (combined

amount of monomers was 20 mmol) at room temperature for 12 h. After the polymerization reaction was quenched with water, the sample was rinsed with water and soaked in 1 M HCl for 12 h in order to exchange potassium cations for protons. Next, the sample was rinsed with water to remove excess acid. A transmission electron microscopy (TEM) image of PSPM/PEEMA-modified silica spheres is shown in Figure 3.2.

3.2.6 Preparation of Silica Colloidal Membranes

Silica colloidal membranes were prepared by vertical deposition of 15 wt% ethanol colloidal solutions of calcinated silica spheres onto a glass substrate.[30] The resulting colloidal crystals were 450-700 μm thick and were sintered in a furnace at 1050 °C for 12 h, becoming very robust and durable after that. An SEM image of such membrane is shown in Figure 3.3. Colloidal membranes were also prepared in a stainless steel dry pressing die set (13 mm ID, supplied by ICL), as was described in Chapter 2 of this dissertation.

3.2.7 Pore-filling of Silica Colloidal Membranes

Sintered colloidal membranes were rehydroxylated in solution of tetrabutylammonium hydroxide of pH=10 at 60 °C for 12 h, then rinsed with large excess of water (2×), 1 M nitric acid, methanol (2×), water (2×), and acetonitrile. Rehydroxylated membranes were modified with amine groups by placing them into 20 mL of solution of APTES (4.3 mmol) in dry acetonitrile at room temperature under nitrogen atmosphere for 17 h. After the surface modification, the membranes were repeatedly rinsed with acetonitrile and air-dried. Amine-modified membranes were placed in 100 mL of dichloromethane solution containing 2 mL of triethylamine (0.15 M

solution), 1.6 mL of 2-bromoisobutyrylbromide (0.13 M solution), and a catalytic amount of DMAP for 12 h at room temperature. Initiator-modified membranes were repeatedly rinsed with dichloromethane and air-dried. Copolymer brushes with various molar ratios of monomers were grown inside the initiator-modified silica membranes via ATRP by placing the membranes in 12 mL of a 2:1 by mass mixture of degassed methanol and water, containing 2,2'-dipyridyl (1.6 mmol, 0.2496 g), $CuCl_2$ (0.12 mmol, 16 mg), CuCl (0.4 mmol, 40 mg), and varying amounts of monomers (with total amount being 20 mmol) at room temperature for 12 h. After quenching the polymerization reaction, the membranes were rinsed with water and placed in 1 M HCl solution overnight, and then rinsed with water. SEM images of pore-filled silica colloidal membranes are shown in Figure 3.4.

3.2.8 Electrochemical Impedance Spectroscopy Measurements

Electrochemical impedance spectroscopy measurements were carried out for pore-filled ordered silica colloidal membranes. Silver paint was coated on both sides of the membranes to serve as electrodes. The impedance was measured using a two-probe testing device placed in humidity- and temperature-controlled chamber according to the previously reported procedure.[21] The relative humidity was controlled by injecting deionized water through a heated inlet tube and was kept 98% during the experiments. The complex impedance of the samples was measured and the proton conductivity was calculated using $\sigma = l/RA$, where σ is the ionic conductivity, l is the distance between the two electrodes, R is the ohmic resistance of the membrane, and A is the cross-sectional area of the material.

3.2.9 Open-circuit Voltage and Linear Polarization Measurements

OCV and linear polarization were measured using a home-made static membrane-electrode assembly (MEA) with pore-filled silica colloidal membranes (Figure 3.5). The 10×10 mm square platinized carbon (ELAT GDE 5 gpm) cloth was used as the cathode. The anode was prepared as following: the catalyst powder (20% HP Pt:Ru alloy (1:1 atomic ratio) on Vulcan XC-72R Carbon suspended in a water-ethanol mixture (4 mg of powder alloy in 50 μL water and 100 μL ethanol) was evenly applied using a paint brush onto 4 square (10×10 mm) pieces of Toray carbon paper. The resulting pieces were air dried for 12 h and were ready to use. The anode and cathode were placed inside custom-made 21×15 mm graphite plates, which had 4 loops of serpentine channel of 0.8 mm width and 11 mm length for each loop and were modified with slits to inject fuel. The plates were attached to the pore-filled silica membranes using double-sided tape. To achieve better connection between silica membrane and anode or cathode, a drop of Nafion perfluorinated resin solution in an alcohol-water mixture was applied on membrane surface. The aluminum foil strips were clamped to graphite plates using a plastic clamp and connected to potentiostat with alligator clips. 3 M methanol solution in water was used as fuel, which was supplied drop wise to the anode using a syringe through the slits in graphite plates. The cathode was exposed to the air, which served as a source of oxygen. After a drop of methanol was applied, the open-curciut voltage (OCV) of the system was measured until equilibrium was reached. Since no constant fuel flow existed in the system, OCV decreased after the cell consumed the fuel. Thus, the equilibrium value of OCV was recorded and polarization was measured starting from that OCV in 1 mV steps (hold time at each step was 1 sec) until the potential decreased to 1

mV.

3.2.10 Methanol Uptake Measurements

First, the weight was determined for the pore-filled membranes after drying under vacuum at 80 °C at 4. Next, the weight of the membranes was determined after soaking them in methanol at room temperature for 24 h, then wiping the samples with filter paper. The methanol uptake of the pore-filled membranes was calculated as shown in eq 3.1.

$$methanol\ uptake\ (\%) = \frac{W_{MeOH} - W_{dry}}{W_{dry}} \times 100\% \quad (3.1)$$

where W_{dry} is the dry weight of the membrane and W_{MeOH} is the weight of the membrane after soaking in methanol.

3.3 Results and Discussion

3.3.1 Copolymerization of EEMA and SPM in Solution

In order to control the sulfonic group content in the polymer filling the pores in silica colloidal membranes, we chose 2-ethoxyethyl-methacrylate as a copolymerizing monomer because it does not contribute to proton conductivity while having the size similar to SPM, which is important for preventing any undesired steric effects. Both EEMA and SPM copolymerize successfully with other methacrylate derivatives,[31-33] but to the best of our knowledge, copolymerization of EEMA and SPM has not been reported.

Thus, we investigated the EEMA and SPM copolymerization in solution in order to establish the relative rates of polymerization of both monomers. This information was necessary to be able to control the copolymer composition by varying the monomer ratio. The solution copolymerization was also performed to measure the molecular weight of

the copolymers. First, equal amounts of SPM and EEMA monomers were copolymerized. Aliquots were taken after 1, 2, and 24 h of polymerization and copolymer samples were isolated. According to the GPC analysis, molecular weights of the samples after 1, 2, and 24 h of copolymerization were 25, 41, and 45 kDa, respectively. The ^{1}H NMR spectra of the copolymers showed characteristic peaks at 2.9 ppm (-O-CH_2- in SPM fragment) and 3.6–3.7 ppm (-CH_2-O-CH_2- in EEMA fragment). Integration of these peaks gave the molar ratio of SPM/EEMA monomers in copolymer of 1.02, closely matching the initial monomer ratio. We prepared two more copolymers using 75 mol% and 25 mol% SPM, and found the peak integration for PSPM/PEEMA copolymers to be 3.15:1 and 1:3.07, respectively. Based on these results, we concluded that the polymerization rates of SPM and EEMA monomers are similar, which makes it possible to control the content of SPM monomers in the copolymers and thus the sulfonic group content by varying the ratio of the monomers participation in the polymerization.

3.3.2 Preparation of PSPM/PEEMA Brushes on Silica Surface

Next, PSPM/PEEMA copolymer brushes of various compositions were grown on the silica surface in order to model their growth inside the colloidal mesopores. The silica spheres surface-modified with initiator moieties were placed in methanol/water solution containing equal amounts of SPM and EEMA and ATRP catalyst, and the polymerization was carried out for 12 h. To confirm that the PSPM/PEEMA brushes grow successfully on the silica surface, TEM images of the polymer-modified silica spheres were obtained (Figure 3.2) and showed a polymer layer on the silica surface. According to dynamic light scattering (DLS) measurements, the hydrodynamic diameter of the polymer-modified spheres in water was 1100±400 nm, which corresponds to ca.

350 nm length of swollen polymer brush in solution.

In addition, we performed thermogravimetric (TGA) analysis of PSPM/PEEMA-modified silica spheres, which showed the weight loss of ~24 wt%, which corresponds to ca. 230 monomers in each polymer brush, assuming that the grafting density of the polymer is ~0.6 polymer brush per 1 nm^2 of silica surface.[34] This corresponds to the length of the single expanded dry polymer brush of ca. 60 nm.

3.3.3 Membrane Pore-filling with PSPM/PEEMA Brushes

Sintered silica colloidal membranes were rehydroxylated in the presence of a base in order to restore the hydroxyl groups on silica surface. The silica surface was then modified with amino groups followed by ATRP initiator 2-bromoisobutyrylbromide. PSPM/PEEMA brushes of various monomer ratios were grown on silica surface inside the membrane mesopores via surface-initiated ATRP. Polymer-modified membranes were characterized using TGA and SEM. SEM images (Figure 3.4) confirmed that filling the colloidal mesopores with the polymer brushes does not alter the geometry of the membrane, as silica spheres remained close-packed.

The TGA weight loss for PSPM/PEEMA-filled silica colloidal membrane was ca. 4%, which, assuming a similar behavior of the polymer brush on silica surface inside the mesopores and that on silica spheres suspended in solution, corresponds to ca. 13 nm dry or ca. 70 nm swollen polymer brush. In silica colloidal crystals containing close-packed face-centered cubic arrangements of silica spheres, the distance from the center of the tetrahedral voids, which form the mesopores, to the silica sphere surface is 22.5% of the sphere radius (calculated by elementary trigonometry). For a membrane comprised of silica spheres 400 nm in diameter, this distance is 45 nm. Since all the conductivity and

fuel cell performance experiments were carried out at 98% RH, we assume that polymer brushes inside the mesopores prepared by ATRP are fully hydrated and swollen and thus fill the colloidal mesopores completely.

3.3.4 Proton Conductivity as a Function of Sulfonic Group Content

Proton exchange membranes (PEMs) are often prepared by treating polymeric materials with sulfonating agents,[23,24] with the degree of sulfonation controlled by varying the sulfonation time and sulfonating agent. The amount of sulfonic groups in PEMs can be also controlled by varying the sulfonated monomer ratio during the polymerization.[25-26] This method allows for a wider range of sulfonic group content and for precise control of this content. ATRP lends itself naturally to this approach, which we utilized in our work.

We varied the amount of SPM monomer in copolymers filling the colloidal mesopores from 0% to 100% by changing the SPM/EEMA monomer ratio. Proton conductivities measured for the membranes with various SPM content at 98% RH are shown in Table 3.1. As expected, the highest value of the proton conductivity was obtained for the membrane filled with pure SPM brushes. It is 0.011±0.007 S cm^{-1}, and is comparable to that of Nafion™ reported in the literature[35] and measured using our experimental setup (0.010±0.004 S cm^{-1}). At the same time, the proton conductivity of the membrane modified with pure EEMA was negligibly small. This is also expected, as EEMA monomer does not contain an acidic group.

The plot of the proton conductivity of the pore-filled membranes as the function of mol% of SPM monomer in copolymer brushes (Figure 3.6) is sigmoidal with three distinct regions. First, there is a low conductivity region corresponding to the 20-40%

sulfonic group content. Increasing the sulfonic group content to 50% leads to a four-fold increase in proton conductivity. In the narrow range of 50-75% sulfonic group content, the proton conductivity grows sharply. Finally, the third region is characterized as saturation in proton conductivity, where increasing sulfonic group content from 75 to 100% causes the proton conductivity growth by only ~20%.

The proton transport in acidic polyelectrolytes involves a combination of two processes: (1) vehicle diffusion involving translation of solvated protons (e.g., hydronium ions) and (2) structure diffusion involving solvent-assisted proton hopping.[36] The latter mechanism is thought to be dominant in humidified polymer electrolyte membranes. In most PEMs, acidic groups form ion-rich clusters that must be connected with each other to provide proton conductivity. This is facilitated by water uptake, which increases with increasing amount of sulfonic groups and eases the formation of hydrophilic ionic pathways.[24,26] It can be concluded from our proton conductivity measurements that ion-rich clusters become connected to each other when sulfonated monomers constitute 50-60% of the copolymer. This observation is similar to the previously reported results, where a rapid increase in proton conductivity of was observed for poly(styrene-isobutylene-styrene) membranes at 63% sulfonation and reached its maximum at 84%.[24] That membrane showed a slight decrease in proton conductivity at 92%, which was explained by the formation of random ionic pathways at high sulfonation levels.[24] We do not observe the decrease in ionic conductivity at high sulfonic group content levels (90-100%), which suggests that that the formation of random ionic pathways is suppressed in rigid hydrophilic silica matrix with interconnected mesopores.

3.3.5 Fuel Cell Performance as a Function of Sulfonic Group Content

Ordered silica colloidal membranes serve as a good system for proton conductivity measurements. However, they are limited in size, since it is challenging to obtain uniform and evenly thick large area colloidal membranes by self-assembly. OCV and polarization measurements of fuel cell require the attachment of 21 × 15 mm graphite plates to the membrane, so that nonuniform thickness and area of ordered silica colloidal membranes make this assembly hard to prepare. To avoid these drawbacks, we prepared silica colloidal membranes by pressing silica spheres together using hydraulic press followed by sintering as was described in Chapter 2 of this thesis. This provides an even distribution of particles throughout the membrane, resulting in membranes with uniform thickness. The size of the membrane is only limited by the dimensions of the die set. This preparation of nanoporous silica membranes is also time-efficient. Despite the fact that pressing the silica spheres provides membranes that are less ordered compared to the self-assembled membranes, their overall structure and pore dimensions remain the same.

In order to prepare the MEA and to test fuel cell performance, we filled the pores of the colloidal membranes as described above and measured the open circuit voltage (OCV) values for fuel cells made with membranes with varying sulfonic group content (Table 3.1). Figure 3.6 shows the dependence of OCV on the sulfonic group content. The observed OCV dependence at low and medium sulfonic group content (up to 60%) is similar to that of the proton conductivity. However, unlike the proton conductivity, OCV does not increase at the higher sulfonic group content. In the case of 100% sulfonated monomer content, the voltage is smaller compared to that for 75% and 60% content. The OCV plot suggests that modification of silica surface with copolymer having 65% of

SPM monomer is optimal for the fuel cell performance. This is likely due to the interplay between the proton conductivity and methanol permeability of the membrane.[37] Indeed, while the non-acidic EEMA monomer in the copolymer lowers the proton conductivity of the pore-filled membranes, it should also lower the methanol permeability of the membrane as the result of the lower polarity of the ethoxyethyl functional group. Our methanol uptake measurements confirmed this suggestion.

It has been shown that methanol permeability is directly related to the methanol uptake for hybrid membranes,[38] which should be true for our pore-filled membranes in particular due to their nonswelling structure. Thus, we measure methanol uptake for the pore-filled membranes. The average methanol uptake for the membrane with 50-60% SPM monomer content is 5%, while for 75% and 100% SPM content the methanol uptake is 13% and 17%, respectively. The proton conductivity does not change significantly above 75% SPM monomer content, while methanol permeability increases significantly. This, in turn, reduces the performance of the fuel cell using membranes pore-filled with 75-100% PSPM.

For comparison, we prepared a similar model fuel cell using Nafion 117 as proton conductive membrane. This fuel cell showed an OCV of ca. 400 mV. Thus, the OCV of fuel cells using pore-filled silica colloidal membranes with 60 and 75% sulfonic group content exceeded the potential of our Nafion 117 fuel cell and was comparable to that for Nafion and other PEM-based DMFCs reported earlier.[39,40] It is important to note that this potential is significantly smaller than the standard electromotive force for the ideal DMFC (1.2 V).[41] We speculate that this to be due to using a model fuel cell, which required a redesign for a thicker membrane and did not allow for good connection

between the anode and cathode and the membrane separator.

Representative polarization curves for the model fuel cells using pore-filled colloidal membranes are shown in Figure 3.7. Since the active surface area was 1 cm^2, the current density ($\mu A/cm^2$) matches the current values (μA). The plots represent single experiments, which were reproducible for each sample with different sulfonic group content. The membranes with sulfonic group content above 60% showed similar current values, with the highest value corresponding to the membrane with 75% content (above 450 μA), which is in good agreement with the OCV measurements. This current is significantly higher than that measured for the same fuel cell design but using a Nafion 117 membrane separator (ca. 25 μA).

3.4 Conclusions

We prepared pore-filled proton conducting membranes with various sulfonic group content by surface-initiated polymerization of EEMA and SPM monomers in different ratios. We demonstrated that there is a sigmoidal dependence of the proton conductivity in copolymer-filled silica colloidal membranes on the amount of sulfonic groups in the copolymer and that there is no significant increase of the proton conductivity with increasing sulfonic group content above 75%. We built MEAs using these membranes and studied their performance in a direct methanol fuel cell. We found that OCV for these MEAs reached its maximum at 65% sulfonic group, and decreases after that. We attribute this effect to the increased methanol cross-over, which was confirmed by methanol uptake measurements for the membranes.

The pore-filled silica colloidal membranes are a promising material for fuel cell fabrication, with characteristics that are comparable or exceeding Nafion 117 in the same

fuel cell design. Presently, we are studying the dependence of fuel cell performance on the pore geometry and structure and on the composition of the polymer brushes in order to further improve the performance of the pore-filled colloidal membranes. We are also developing a new fuel cell design to enable an efficient use of this type of membranes.

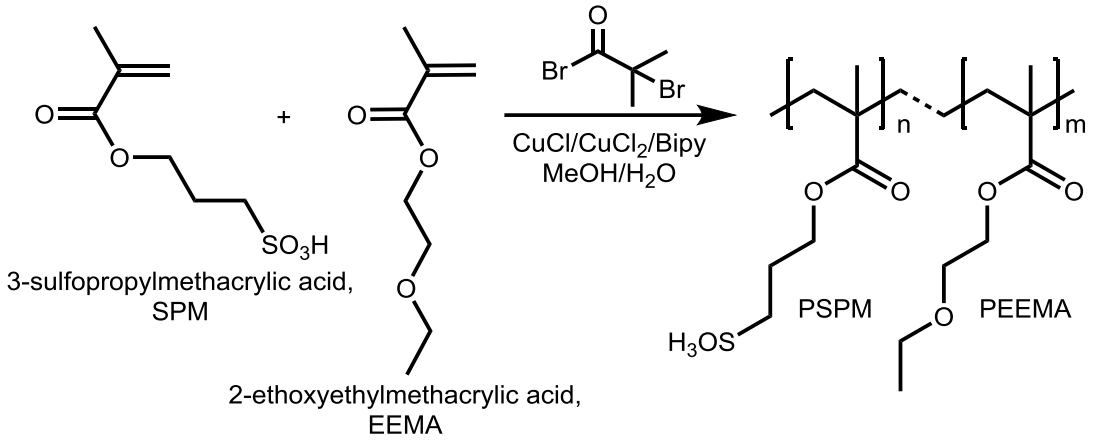

Figure 3.1. Structures of SPM and EEMA and their copolymerization reaction.

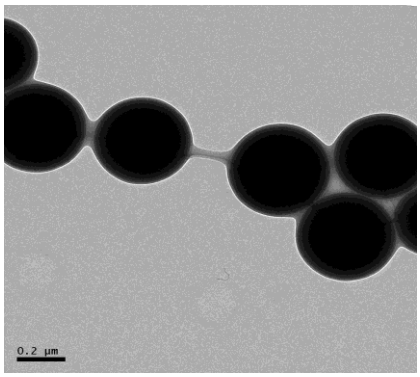

Figure 3.2. TEM image of PSMP/PEEMA modified silica spheres. Scale bar is 0.2 µm.

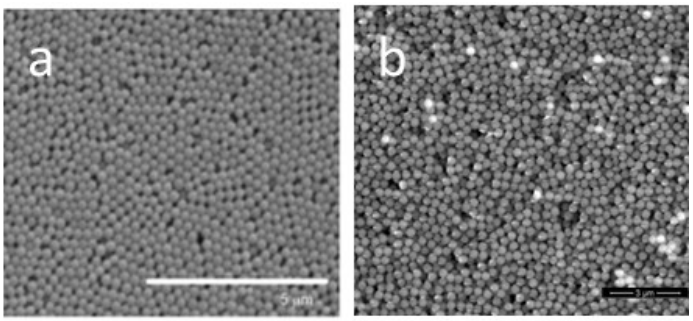

Figure 3.3. SEM images of sintered silica colloidal membranes comprised of 400 nm silica spheres: (a) self-assembled membrane, scale bar = 5 µm; (b) pressed membrane, scale bar = 3 µm.

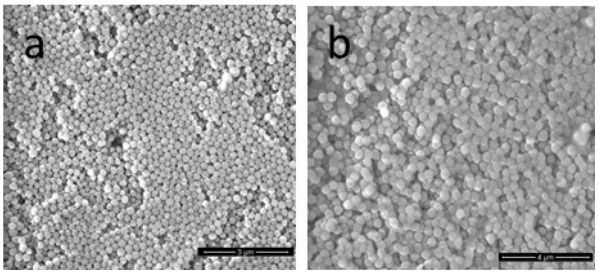

Figure 3.4. SEM images of (a) self-assembled (scale bar = 3 μm) and (b) pressed (scale bar = 4 μm) sintered silica colloidal membranes pore-filled with PSPM/PEEMA brushes (50 mol% SPM).

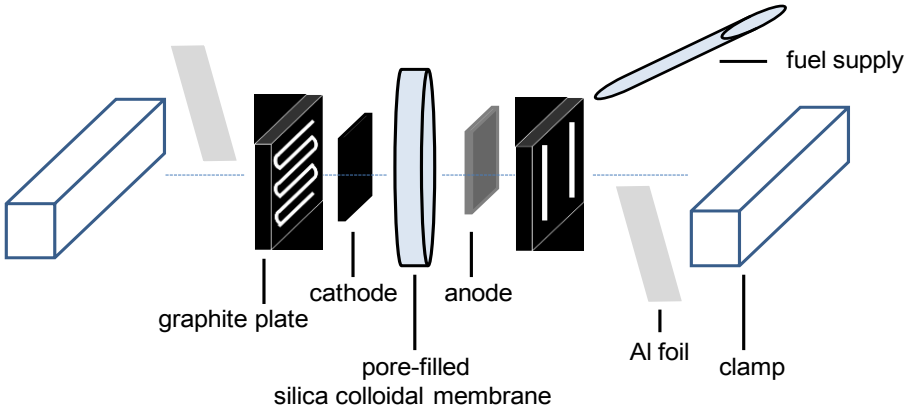

Figure 3.5. The schematic representation of model MEA prepared using pore-filled proton conducting silica colloidal membrane.

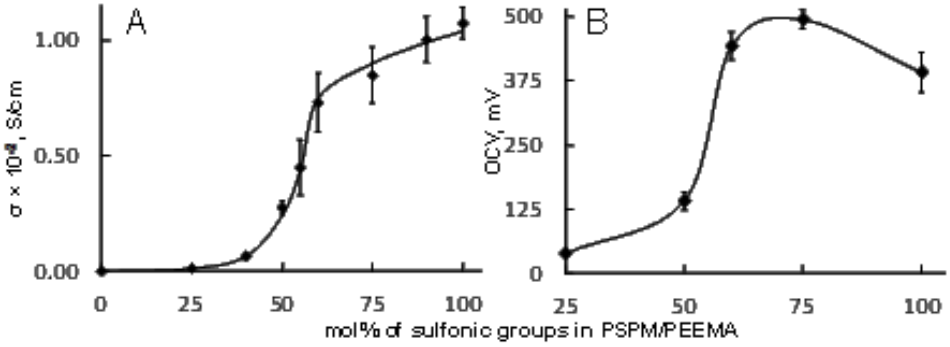

Figure 3.6. Plot of room temperature proton conductivity for vertically deposited membranes (A) and room temperature open circuit voltage for pressed membranes (B) as a function of SPM content in the pore-filling copolymer.

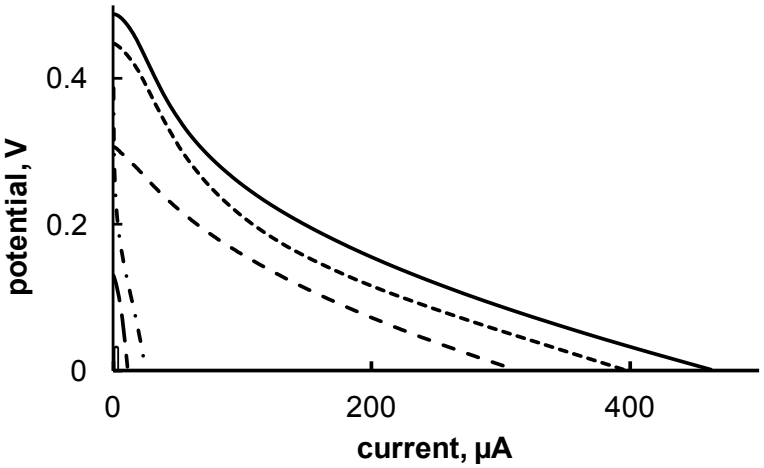

Figure 3.7. Polarization curves for fuel cells using PSMP/PEEMA-filled membranes containing 75% (–), 60% (--), 100% (- -), 50% (– –), 25% (=) SPM, and using Nafion 117 (- • -) at room temperature.

Table 3.1. Dependence of pore-filled membrane proton conductivity, methanol uptake, and open circuit voltage of the corresponding fuel cell on SPM content in the pore-filling copolymer at room temperature and 98% R.H.

Sulfonic group content, mol%	$\sigma \times 10^{-2}$, S cm^{-1}	Methanol uptake, %	OCV, mV
0	negligible	-	-
25	0.012±0.001	-	40±5
40	0.064±0.012	-	-
50	0.27±0.03	3	140±20
55	0.45±0.12	-	-
60	0.73±0.13	5	440±30
75	0.85±0.12	13	495±20
90	1.00±0.10	-	-
100	1.07±0.07	17	390±40

3.5 References

[1] Vielstich, W.; Lamm, A.; Gasteiger, H. A. *Handbook of Fuel Cells - Fundamentals, Technology, and Applications*; John Wiley & Sons Ltd.: Chichester, U.K., 2003.

[2] Tripathi, B.; Shahi, K. Recent Progress on Organic-Inorganic Nanocomposite Polymer Electrolyte Membranes for Fuel Cell Applications. *Prog. Polym. Sci.*, **2011**, 36, 945–979.

[3] Steele, B. C.; Heinzel, A. Materials for Fuel-Cell Technologies. *Nature*, **2001**, *414*, 345–352.

[4] Winter, M.; Brodd, R.J. What Are Batteries, Fuel Cells, and Supercapacitors? *Chem. Rev*. **2004**, *104*, 4245–4269.

[5] Hickner, M. A.; Pivovar, B. S. The Chemical and Structural Nature of Proton Exchange Membrane Fuel Cell Properties. *Fuel Cells* **2005**, *5*, 213–229.

[6] Mauritz, K. A.; Moore, R. B. State of Understanding of Nafion. *Chem. Rev.*, **2004**, *104*, 4535–4586.

[7] Gary, F. M. *Polymer Electrolytes*; Royal Society of Chemistry: Cambridge, UK, 1997.

[8] Hickner, M. A.; Ghassemi, H.; Kim, Y. S.; Einsla, B. R.; McGrath, J. E. Alternative Polymer Systems for Proton Exchange Membranes (PEMs). *Chem. Re*v. **2004**, *104*, 4587–4611.

[9] Soler-Illia, G. J. A. A.; Azzaroni, O. Multifunctional Hybrids by Combining Ordered Mesoporous Materials and Macromolecular Building Blocks. *Chem. Soc. Rev.*, **2011**, *40*, 1107–1150.

[10] Valle, K.; Belleville, P.; Pereira, F.; Sanchez, C. Hierarchically Structured Transparent Hybrid Membranes by in Situ Growth of Mesostructured Organosilica in Host Polymer. *Nat. Mater*. **2006**, *5*, 107–111.

[11] Bhattacharyya, A. J.; Maier, J. Second Phase Effects on the Conductivity of Non-Aqueous Salt Solutions: "Soggy Sand Electrolytes". *Adv. Mater.* **2004**, *16*, 811–814.

[12] Zhang, H.; Ohashi, H.; Tamaki, T.; Yamaguchi, T. Water Movement in a Solid-State Alkaline Fuel Cell Affected by the Anion-Exchange Pore-Filling Membrane Properties. *J. Phys. Chem. C*, **2013**, *117*, 16791−16801.

[13] Park, S.-H.; Choi, Y.-W.; Park, J.-S. Characterization of Sulfonated Poly(Styrene-Co-Pyrrolidone) Pore-Filling Membranes for Fuel Cell Applications. *J. Appl. Electrochem.*, **2011**, *41*, 849–857.

[14] Jung, H.; Ohashi, H.; Tamak, T.; Yamaguchi, T. Improvement of Thermal-Stability of Anion Exchange Membranes for Fuel Cell Applications by Controlling Water State. *Chem. Lett.*, **2013**, *42*, 14–16.

[15] Gohil, J. M.; Karamanev, D. G. Novel Pore-Filled Polyelectrolyte Composite Membranes for Cathodic Microbial Fuel Cell Application. *J. Power Sources*, **2013**, *243*, 603–610.

[16] Kanamura, K.; Mitsui, T.; Munakata, H. Preparation of Composite Membrane between a Uniform Porous Silica Matrix and Injected Proton Conductive Gel Polymer. *Chem. Mater.*, **2005**, *17*, 4845–4851.

[17] Yameen, B.; Kaltbeitzel, A.; Langer, A.; Müller, F.; Gösele, U.; Knoll, W.; Azzaroni, O. Highly Proton-Conducting Self-Humidifying Microchannels Generated by Copolymer Brushes on a Scaffold. *Angew. Chem. Int. Ed.*, **2009**, *48*, 3124–3128.

[18] Yamamoto, D.; Munakata, H.; Kanamura, K. Synthesis and Characterization of Composite Membrane with Three-Dimensionally Ordered Macroporous Polyimide Matrix for DMFC. *J. Electrochem. Soc.*, **2008**, *155*, B303–B308.

[19] Tay, S. W.; Liu, Z.; Hong, L. Proton Exchange Membrane Synthesized by Pore-Filling Polymerization Technique. *Mater. Res. Soc. Symp. Proc.*, **2012**, *1410*.

[20] Yang, Q.; Adrus, N.; Tomicki, F.; Ulbricht, M. Composites of Functional Polymeric Hydrogels and Porous Membranes. *J. Mater. Chem*., **2011**, *21*, 2783–2811.

[21] Smith, J. J.; Zharov, I. Preparation and Proton Conductivity of Self-Assembled Sulfonated Polymer-Modified Silica Colloidal Crystals. *Chem. Mater.* **2009**, *21*, 2013–2019.

[22] Chen, H.; Palmese, G. R.; Elabd, Y. A. Electrosensitive Permeability of Membranes with Oriented Polyelectrolyte Nanodomains. *Macromolecules*, **2007**, *40*, 781–782.

[23] Swier, S.; Chun, Y.-S.; Gasa, J.; Shaw, M. T.; Weiss, R. A. Sulfonated Poly(Ether Ketone Ketone) Ionomers as Proton Exchange Membranes. *Polym. Eng. Sci.*, **2005**, *45*, 1081–1091.

[24] Aviles-Barreto; S. L.; Suleiman, D. Transport Properties of Sulfonated Poly (Styrene-Isobutylene-Styrene) Membranes with Counter-Ion Substitution. *J. App. Polym. Sci.*, **2013**, *129*, 2294–2304.

[25] Lee, K.-S.; Jeong, M.-H.; Kim, Y.-J.; Lee, S.-B.; Lee, J.-S. Fluorinated Aromatic Polyether Ionomers Containing Perfluorocyclobutyl as Cross-Link Groups for Fuel Cell Applications. *Chem. Mater.*, **2012**, *24*, 1443−1453.

[26] Mistri, E. A.; Mohanty, A. K.; Banerjee, S. Synthesis and Characterization of New Fluorinated Poly(Ether Imide) Copolymers with Controlled Degree of Sulfonation for Proton Exchange Membranes. *J. Membr. Sci.*, **2012**, *411–412*, 117–129.

[27] Becker, C. M.; Biagini, A. B.; Forte, M. M. C.; Amico, S. C.; Vargas, J. V. C.; Azambuja, D. S. Sulfonation and Characterization of Styrene-Indene Copolymers for the Development of Proton Conducting Polymer Membranes. *Polímeros*, **2012**, *22*, 395–400.

[28] Park, J.S., Choi, Y.W., Highly Crosslinkable and Proton-conducting Polyelectrolytes of Pore-filling Membranes for Proton Exchange Membrane Fuel Cells. *Chem. Lett.* **2013**, *42*, 998–1000.

[29] Stöber, W.; Fink, A.; Bohn, E. Controlled Growth of Monodispersed Spheres in the Micron Size Range. *J. Colloid Interface Sci.* **1968**, *26*, 62–69.

[30] Bohaty, A. K.; Smith, J. J.; Zharov, I. Free-Standing Silica Colloidal Nanoporous Membranes. *Langmuir* **2009**, *25*, 3096–3101.

[31] Hill, D. J. T.; O'Donnell, J. H.; Pomery, P. J.; Whittaker, M. R. A High Resolution NMR Investigation into the Microstructure of HEMA and EEMA Copolymers. *Polym. Gels Networks*, **1995**, *3*, 85–97.

[32] Hachawee, K.; Lerdwijitjarud, W.; Sittattrakul, A.; Sirivat, A. Structural Effect of Ferrocenecarboxymethylated Polymers on Their Electrical Behavior under the Exposure to Methanol and Acetone Vapors. *Mat. Sci. Eng. B*, **2008**, *153*, 10–20.

[33] Lukas, J.; Smetana, K.; Petrovicky, P.; Paleckova, V.; Vacik, J.; Dvorankova, B.; Broz, L.; Pospisilova, D.; Holikova, Z.; Bartunkova, J. Biological Properties of Copolymer of 2-Hydroxyethyl Methacrylate with Sulfopropyl Methacrylate. *J. Mater. Sci. Mater. Med.*, **2001**, *12*, 639–646.

[34] Choi, J., Hui, C. M., Pietrasik, J., Dong, H., Matyjaszewski, K., Bockstaller, M. R. Toughening Fragile Matter: Mechanical Properties of Particle Solids Assembled from Polymer-Grafted Hybrid Particles Synthesized by ATRP *Soft Matter*, **2012**, *8*, 4072–4082.

[35] Zhang, X. J. Porous Organic-Inorganic Hybrid Electrolytes for High-Temperature Proton Exchange Membrane Fuel Cells. *J. Electrochem. Soc.*, **2007**, *154*, B322–B326.

[36] Kreuer, K.; Paddison, S.; Spohr, E.; Schuster, M. Transport in Proton Conductors for Fuel Cell Applications: Simulations, Elementary Reactions, and Phenomenology. *Chem. Rev.*, **2004**, *104*, 4637–4678.

[37] Li, X.; Roberts, E. P. L.; Holmes, S. M. Evaluation of Composite Membranes for Direct Methanol Fuel Cells. *J. Power Sources*, **2006**, *154*, 115–123.

[38] Miyake, N.; Wainright, J. S.; Savinell, R. F. Evaluation of a Sol-Gel Derived Nafion/Silica Hybrid Membrane for Polymer Electrolyte Membrane Fuel Cell Applications: II. Methanol Uptake and Methanol Permeability. *J. Electrochem. Soc.*, **2001**, *148*, A905–A909.

[39] Hudak, N.; Barton, S. Mediated Biocatalytic Cathode for Direct Methanol Membrane-Electrode Assemblies. *J. Electrochem. Soc.*, **2005**, *152*, A876–A881.

[40] Iulianelli, A.; Basile, A. Sulfonated PEEK-based polymers in PEMFC and DMFC applications: A review. *Int. J. Hydrogen Energy*, **2012**, *37*, 15241–15255.

[41] Scott, K.; Xing, L. In *Advances in Chemical Engineering, Volume 41*; Sundmacher, K. Ed.; Academic Press: San Diego, CA, USA, Waltham, MA, USA, London, UK, Oxford, UK, Amsterdam, the Netherlands, 2012; Chapter 3, pp. 145–196.

CHAPTER 4

REVERSIBLE ASSEMBLY OF TUNABLE ULTRAFILTRATION MEMBRANES FROM "HAIRY" SILICA NANOPARTICLES

4.1 Introduction

Ultrafiltration is a type of filtration through the semipermeable membrane, which is used on industrial scale for purification of water and in food industry[1,2,3] and in research laboratories for separations of inorganic and biological nanoparticles and synthetic and biological macromolecules.[4] Ultrafiltration membranes contain nanopores in the 1-100 nm range[3] and are typically made of porous polymeric or ceramic materials. These membranes are prone to blockage and fouling, and given the importance of ultrafiltration, novel membrane materials, particularly those prepared using alternative approaches, are desired.[1,2] Nanoporous membranes reversibly assembled from colloidal particles constitute such a novel approach. They can be disassembled back to the building blocks and may be advantageous due to recyclability, cleaning, and reuseability, as well as ability to easily control the pore size. Here, we report the preparation and characterization of durable nanoporous membranes with controlled thickness, area, and pore size via reversible assembly of polymer brush-grafted ("hairy") silica nanospheres. We describe two types of reversible ultrafiltration membranes: (1) membranes made of silica particles grafted with polymer brushes carrying acidic and basic groups, and (2) membranes in which the grafted polymer brushes have neutral groups. The former are

stable in most organic solvents and easily disassemble in water, while the latter are water-stable and disassemble in organic solvents. Both types of membranes are capable of size-selective transport and ultrafiltration.[1]

Nanoporous membranes are widely used in ultrafiltration[5] and attract increasing attention due to their potential applications in molecular separations,[6] biosensing,[7,8] drug-delivery,[9] catalysis,[10,11] optics,[12] etc. Many of these applications require control over the nanopore size, a narrow pore size distribution,[13,14] and a functional membrane surface.[15,16] Additional requirements include good mechanical, chemical and thermal stability,[17] and simple and economical preparation processes.[17]

The typical materials used for nanoporous membrane preparation are polymers,[18] ceramics,[19] zeolites,[20,21] and metal oxides.[22] Polymer ultrafiltration membranes are usually made using track-etching or phase separation method with further cross-linking.[23] Ceramic ultrafiltration membranes are usually made of anodized alumina,[24] mesoporous silica, zeolites, etc.[17] Regardless of the material, these membranes are formed via irreversible covalent bonds[25] and often suffer from pore blocking and surface fouling during operation. Therefore, membranes formed by noncovalent reversible assembly of molecular or nanoscale building blocks could provide a useful alternative in terms of fabrication, processing, cleaning, recycling, and reuseability.[25]

Using molecular building blocks to assemble nanoporous membranes allows for the preparation of thin supported materials suitable for utrafiltration of nanoparticles, as has been recently reported.[25] Such membranes, made by reversible self-assembly of perylene diimide-based organic molecules that contained a continuous three-dimensional network, formed in water/THF, could be dissolved in water/ethanol and possessed a cut-

off of 5 nm. While their formation was reversible and simple, the pore size of such membranes if defined by the structure of the molecular building block and thus cannot be easily varied in a broad range.

Self-assembly of colloidal particles into nanoporous membranes would allow combining the advantages of the reversible assembly with easy pore size tunability and cheap building blocks. The challenge in this case is to develop a system that is held together by noncovalent interactions strong enough to provide materials that can withstand the ultrafiltration conditions.

So far, only gold nanoparticles were used to form self-assembled nanoporous membranes, either by chemically directed assembly of AuNPs and polyamidoamine dendrimers (PAMAM), in which the pore size was controlled by varying the dendrimer generation,[26] or by self-assembly of dodecanethiol-ligated Au nanocrystals,[27,28] where the pore size was controlled by the gold nanoparticles size. The free-standing AuNP/dendrimer membranes are relatively easy to prepare, are durable, and are capable of size-selective separations and filtration; however, the small size of the gold nanoparticles and their high cost limit scaling up and achieving a broader pore size range. Other colloidal particles have been self-assembled into loops using topological interaction by entangled DNA single strands[29] and host-guest interactions and the mutual molecular recognition of the cyclodextrins and hydrocarbon groups,[30] while high affinity binding of surface-attached “host” cucurbituril and “guest” ferrocene molecules was used for surface adhesion.[31]

Assembling silica colloidal spheres into ultrafiltration membranes would provide a cheap alternative to gold nanoparticles while allowing for flexibility in the pore size.

Recently, we demonstrated that covalently-bound silica colloidal membranes[32] are capable of size-selective transport[33] that can be tuned by varying the silica sphere diameter, as well as charge-[32] and enantioselective transport after the suitable silica surface modification. The covalently formed silica colloidal membranes are mechanically, thermally, and chemically stable, but have to be prepared by sintering above 1000 °C.[32]

In this work, we report the reversible formation of two types of nanoporous membranes via the self-assembly of silica nanospheres. To introduce relatively strong but reversible interactions between the spheres, we modified the surface of the spheres with polymer brushes through atom transfer radical polymerization (ATRP). The first type of nanoporous membranes was prepared using silica spheres carrying acidic poly(3-sulfopropylmethacrylate), PSPM, and basic poly(N-dimethylaminoethylmethacrylate) (PDMAEMA), brushes. The membrane preparation process involves mixing two colloidal solutions of silica spheres and air-drying to let the solvent evaporate. We called the resulting material "*acid-base membranes.*" In the second type of nanoporous membranes, poly(hydroxyethylmethacrylate) (PHEMA), brushes were formed on the silica sphere surface and the membranes were prepared by the deposition of PHEMA-modified silica spheres from ethanol. These were called "*neutral membranes.*"

4.2 Experimental Section

4.2.1 Preparation of Silica Colloidal Spheres

All silica spheres were prepared according to previously reported procedure from solution with final concentrations of 0.2 M TEOS, 0.6 M NH_4OH, and 17 M H_2O.[34] The spheres were purified by repetitive cycle of suspending the spheres in ethanol and water

by sonication followed by centrifugation. Then the silica spheres were dried in a stream of nitrogen for 12 h and calcinated in an oven at 600°C for 4 h. SEM images of the spheres were taken and the diameters determined to be 330 ± 30 nm after preshrinking. The second batch was prepared following the same procedure with same concentrations, resulting in the formation of 390±20 nm silica spheres. The other two batches of spheres were prepared following the same procedure with 0.6 M and 1.2 M as the final concentrations of ammonia, resulting in the formation of 290±30 nm and 480±50 nm silica spheres, respectively; after preshrinking, the sizes reduced to 280±20 nm and 460±30 nm, respectively.

4.2.2 Preparation of Polymer-modified Silica Spheres

The calcinated silica spheres were first rehydroxylated and modified with 2-bromoisobutyrylbromide (ATRP initiator) as reported earlier.[35] The PSPM-r-PEEMA and PDMAEMA-r-pMMA brushes were grown on the surface of silica spheres via ATRP according to previously reported procedures.[36] The grafting of PSPM and PSPM-r-PEEMA brushes onto initiator-modified silica spheres (1 g) was carried out in of a 2:1 by mass mixture of degassed methanol and water, containing 2,2'-dipyridyl, $CuCl_2$, CuCl as well as equal amounts of monomers EEMA and SPM (0.01 mol of each) at room temperature for 12 h in a nitrogen atmosphere. Polymerization was quenched by exposing the reaction mixture to open air and the addition of cold water. Polymer-modified silica spheres were repeatedly rinsed with water and methanol, soaked in 1 M HCl for 12 h to exchange potassium ions with protons, then the sample was rinsed with water again to remove excess acid. The grafting of PDMAEMA and PDMAEMA-r-pMMA brushes onto initiator-modified silica spheres (1 g) was carried in degassed acetone/water mixture

(9:1 ratio by mass respectively) containing 2,2'-dipyridyl, $CuCl_2$, CuCl, as well as equal amounts of monomers DMAEMA and MMA (0.01 mol each) at 50 ºC in nitrogen atmosphere for 12 h. Then polymerization was quenched by exposing the reaction mixture to open air and addition of cold water. Polymer-modified silica spheres were repeatedly rinsed with water and acetone and placed in a flask containing degassed acetonitrile with 0.5 mL of bromoethane for 12 h in order to quarternize the amine group. The sample was finally rinsed with acetonitrile and ethanol to remove excess bromoethane. The grafting of pHEMA brushes onto initiator-modified silica spheres (1 g) was carried out in of degassed methanol, containing PMDETA, $CuBr_2$, CuBr, as well as HEMA (5.7×10^{-3} mol) at 70 ºC for 12 h in nitrogen atmosphere. The resulting modified particles were washed in methanol and water.

4.2.3 Assembly of the Membranes

The separate colloidal solutions of "acid-polymer" and "base-polymer"-modified silica spheres (1 g each) were prepared in 10 mL of ethanol. The solutions were mixed together in 25 mL beaker or 4 inch Petri dish and air-dried. p(HEMA) modified particles were dispersed in an ethanol solution and left to air-dry.

4.2.4 Diffusion Measurements through Nanoporous Membranes

Diffusion experiments through the colloidal membranes were performed by placing a piece of membrane between two connected 1 cm quartz cuvettes. The feed cell contained 4.00 mL of a ferrocene-carboxaldehyde solution in ethanol or polystyrene or dansyl-labeled silica spheres dispersed in ethanol, while the reservoir cell contained 4.00 mL of ethanol. The flux was monitored by recording the absorbance at 555 nm for dye-labeled dendrimers, 250 nm for polystyrene spheres, 323 nm for dansyl-labeled silica

spheres, and 200 nm for gold nanospheres in the reservoir cell for at least 12 h. Prior to using a membrane for a new trial, the membranes were immersed in ethanol for at least 24 h and the solvent replaced occasionally to ensure the removal of any previous probe molecule or particle from within the membranes.

4.2.5 Pressure-driven Filtration of Nanoparticles

A UHP-25 pressure filtration system was used for this procedure. A membrane was quantitatively deposited on the support by driving 10 mL of silica solution (total amount of polymer-modified silica spheres in 80% ethanol and 20% water is 1g, but can be varied depending on desired membrane thickness) under constant 21 psi air stream. The support was 25 mm in diameter disc made of nylon and celullose filter membranes having 0.1 μm and 0.2 μm pores. Silica spheres of 280 nm and 460 nm in diameter were modified with pHEMA brushes, and the 390nm silica spheres were modified with "acid" and "base" polymer brushes. The membrane was air-dried for 15 min. Aqueous solutions, containing G5 PAMAM dendrimer and 20 nm and 40 nm gold nanospheres, were driven through the "neutral" membrane separately. The solutions of G5 PAMAM dendrimer and 25nm and 39 nm polystyrene spheres in ethanol were driven through the "acid-base" membranes separately. The filtrates were analyzed using DLS, IR, and UV-vis spectroscopy. Between the runs, the membrane was cleaned by driving ethanol through it and left to air-dry for 15 min.

4.2.6 Flux Measurements

A "neutral" membrane was prepared as above with silica spheres that were 460 nm in diameter and a regenerated cellulose filter disc support (pore size 0.2 μm, disc diameter 25 mm). Distilled water was driven once through the naked filter first and then

twice through the supported membrane (the membrane was dried for 15 min between experiments) under constant driving pressure of ~0.35 bar (5 psi) and ~1.45 bar (21 psi). Time taken to expel 4 mL of water was recorded after 1 mL of liquid had already been pushed through. The flux through "acid-base" membrane was measured following the same procedure and using 390 nm silica spheres modified with "acid" and "base" polymer brushes.

4.2.7 Mechanical Testing of Pressed Silica Colloidal Membranes

The flexural strength of free-standing "neutral" membranes was estimated using the 4-point bending test. The membrane test samples were cut to rectangular shape using a carbon dioxide laser. The rectangular beam of the free-standing membrane was supported at two points from below (the support span) and bearing a load that makes contact at two points above (the loading span). The load was increased until the beam fractures, and this rupture force was used to calculate the flexural strength. If the loading span is one third the length of the support span, then the flexural strength is calculated using the eq 4.1:

$$\sigma = \frac{FL}{bd^2} \tag{4.1}$$

where σ is flexural strength (Pa), F is rupture force (N), L is support length (m), b is beam width (m), and d is beam thickness (m).

4.3 Results and Discussion

4.3.1 Acid-base Membranes

To form these membranes, we prepared "hairy" silica spheres using surface-initiated ATRP of SPM and DMAEMA (Figure 4.1A) and varied the length of the

polymer brushes using the polymerization time to find the optimal ratio of this length to the silica sphere diameter. We discovered that when the polymer brush length is larger or equal to the silica sphere diameter, smooth nonporous films are formed after casting from colloidal solution. In contrast, upon mixing two ethanol colloidal solutions containing 390 nm silica spheres modified with short PSPM and PDMAEMA brushes (in average, 10 and 40 nm, respectively, according to TGA data), we observed the formation of a porous material. Initially, a gel formed within several seconds and after complete evaporation of ethanol, irregular cracked pieces of a porous material formed, which were not suitable for ultrafiltration. We believe that the cracking resulted from capillary stress generated during drying,[37] from rigidity of the resulting polymer-polymer aggregates. To improve the membrane properties, additional monomers, 2-ethoxyethyl methacrylate (EEMA), and methyl methacrylate (MMA), were added to PSPM and PDMAEMA brushes, respectively. The suitable molar ratios for copolymer brushes were found experimentally. The EEMA:SPM and MMA:DMAEMA molar 0.3:0.7 and 0.7:0.3 ratios did not lead to the desired properties of the material. On the other hand, molar ratios of 1:1 were optimal for the formation of durable, flexible, and large area (~1.5 cm^2) crack-free membranes. We speculate that crack reduction is caused by slower solvent drying due to higher "affinity" of neutral PMMA and PEEMA towards ethanol compared to charged PSPM and PDMAEMA.

The thickness of the membrane can be controlled by the concentration of the "hairy" particles in solution. For example, it changed from 0.5 to 1 mm with a concentration change from 6 to 12 wt%. The flexibility of the membrane depends on the thickness and the length/thickness ratio, for instance, a piece of the membrane prepared

from 4 wt% solution that is 10 mm long and 0.2 mm thick shows significant flexibility (Figure 4.1 D). The SEM image in Figure 4.1C shows close-packed, yet disordered silica spheres in the membrane with clearly visible connecting polymers.

The particle-particle interactions in particle brush systems are mainly caused by polymer brush entanglement, responsible for holding the particles in the membrane together.[38,27] These interactions depend on the polymer brushes' length and grafting density. With increasing degree of polymerization, the material's fracture toughness increases and transition from particle-like deformation to polymer-like deformation occurs.[38] However, the particle brush system with too long polymer brushes will not remain porous, due to complete filling of voids by polymer brushes. Thus, a balance between the material's mechanical properties and porosity should be found by adjusting the polymer brush length.

We believe that due to different solvation of polymers by different solvents,[39] the polymer brush interactions can be tuned by solvent variation. Indeed, the membranes remain relatively strong in organic solvents, such as ethanol, acetonitrile, acetone, DMF, and benzene, where the membranes are stable and durable for days. The membranes also remain stable in organic solvents for at least 2 h under sonication. However, these interactions are disrupted in water, where the membranes soften in 5-10 min and completely disperse within ~ 5 min of sonication. Within ~10 s after sonication, the membrane re-assembles from solution into a gel at the bottom of the vial (Figure 4.1 B). The membranes re-assemble after complete water evaporation and remain durable and pliable. They can withstand multiple cycles of assembly-disassembly without losing their properties. SEM images confirmed that the membranes disassemble into single silica

spheres and that the packing of silica spheres in re-assembled membranes is similar to the initially deposited membrane. Thus, the assembly of the "acid-base" membranes is completely reversible.

We speculate that this reversible assembly behavior in different solvents is due to the different solvation of polymer brushes on the silica surface.[39] Acidic and basic polymer brushes interact strongly in organic solvents, while water effectively solvates sulfonic and quaternized amino groups and disrupts these interactions more effectively than organic solvents, so the polymer brushes swell and cause weaker interactions between polymer brushes and therefore between spheres. Presence of both positive and negative charges holds the silica spheres together and prevents complete dissolution of the membrane.

To demonstrate that "acid-base" membranes made of "hairy" 390 nm silica spheres are porous and capable of size-selective transport, we performed diffusion experiments using Rhodamine B-labeled PAMAM dendrimers, dansyl-labeled silica particles, and polystyrene (PS) particles in ethanol. We found that G5 PAMAM dendrimer (ca. 6 nm in diameter) diffuses quickly through these membranes, while no diffusion was observed for 100 and 250 nm dansyl labeled silica particles. Furthermore, we found that 54 nm PS particles diffused through this membrane, while 84 nm PS particles did not diffuse. Thus, the size cut-off for these "acid-base" membranes is between 54 and 84 nm. The pore "diameter" for a close-packed colloidal crystal can be estimated as ca. 15% of the silica sphere diameter.[33] For the colloidal crystal made of 390 nm silica spheres, this "diameter" is 59 nm, suggesting that randomly packed "hairy" silica spheres produce a reasonably close-packed arrangement as well.

Next, we deposited 390 nm silica spheres modified with PSPM/PEEMA and PDMAEMA/PMMA brushes on top of a regenerated cellulose filter with 0.2 μm pore size. The thickness of deposited membranes can be varied from a few micrometers to ca. 0.5 mm by changing the concentration of silica in colloidal solution. Just as for free-standing "acid-base" membranes, the fast formation of gel is observed due to strong affinity of "acid" and "base" polymer brushes to each other. Once all of the solvent is pushed through the device, the membrane is left on top of the support. The solvent behavior of dry supported membranes remained same as that of free-standing "acid-base" membranes: they can be completely dispersed in water in minutes of sonication and redeposited on the same or new support.

The supported "acid-base" membranes were tested for ultrafiltration performance. We measured the flux of ethanol through the 0.5 mm-thick membrane using the driving pressure of 1.45 bar (21 psi). The average flux through the regenerated cellulose filter under this pressure was 7600 l/m^2hr^1 (33 gpm). The average flux of ethanol through the "acid-base" membrane under the same pressure was 380 l/m^2hr^1 (1.6 gpm). This flux is comparable or exceeds the flux of commercially available ultrafiltration drinking water membranes (Neo-Pure TL3 Ultrafiltration system - 1 gpm for 25 nm cutoff size).[40]

We used ethanol solutions of G5 PAMAM dendrimer and polystyrene nanoparticles to determine the membrane cut-off. The 6 nm dendrimer molecules passed through the membrane, while 39 nm polystyrene nanoparticles were retained, which was confirmed by dynamic light scattering (DLS) and UV-Vis spectroscopy of the permeate. In addition, we found that 25% of 25 nm polystyrene particles passed through the membrane. Thus the cut-off of the membrane is between 25 and 39 nm. This is

significantly smaller compared to the cut-off (between 54 and 84 nm) found in diffusion experiments for the same membrane. We believe that this difference in cut-off is due to the time factor, i.e., in the case of the pressure-driven ultrafiltration, nanoparticles have much shorter time (seconds) to make their tortuous way across the membrane and thus retain more efficiently, while the same nanoparticles can travel across the membrane during the slow (hours) diffusion experiments.

4.3.2 "Neutral" Membranes

Ultrafiltration in organic solvents can have some interesting applications;[41] however, aqueous ultrafiltration is more widely used in various areas such as water purification,[5] protein concentration and food industry,[24] etc. We discovered that nanoporous membranes can be prepared by deposition of "hairy" silica spheres carrying poly(2-hydroxyethyl methacrylate), PHEMA, brushes from their ethanol solutions (Figure 4.2 A). The length of PHEMA brushes on 330 silica spheres required to prepare the membranes was ~15 nm (determined by DLS) with the average molecular weight of ~3000 g/mol (approximately 24 HEMA monomers per brush), as determined by thermogravimetric analysis (TGA). After ethanol evaporation, membranes material formed as smooth and evenly thick flat pieces of ~ 2 cm^2. Their thickness can be controlled in the range from 0.4 to 0.7 mm by the concentration of the "hairy" spheres in colloidal solution in the 6 to 10 wt%. Generally, there were significantly fewer cracks observed compared to the "acid-base" membranes. We believe this is also caused by drying the membrane slowly and by the larger interconnection of the polymer brushes of HEMA compared to the PSPM and PDMAEMA brushes. SEM images of the membranes (Figure 4.2 B) showed close-packed silica spheres.

We measured the flexural strength of the "neutral" membranes using the 4-point bending test, and found it to be 0.5±0.1 MPa (73±15 psi). This value is significantly smaller than the flexural strength of sintered silica colloidal membranes (49±8.5 MPa, 7,000±1,200 psi), which were prepared earlier.[32] This is expected as silica spheres in sintered membranes are connected to each other by strong Si-O-Si covalent bonds, while self-assembled "neutral" membranes form via noncovalent interactions of PHEMA brushes. Despite the low flexural strength, the "neutral" membranes can be handled, sonicated, sandwiched between two plastic or two metal plates, and even dropped from 1 m height without breaking or cracking.

We found that "neutral" membranes are stable in water for at least 72 h, but soften in ethanol and acetonitrile within ~ 30 min and completely disperse in 24 h. The sonication speeds up this process and the membranes disperse completely after 15 min of sonication. Unlike "acid-base" membranes where silica spheres carrying oppositely charged polymer brushes attract each other, this solvent behavior of "neutral" membranes should arise from different solvation of PHEMA brushes by different solvents. The PHEMA brushes swell more in organic solvents such as ethanol and methanol,[42] which causes the membranes to complete disassemble, while water solvates PHEMA to a smaller extent.[42] However, as will be discuss below, we believe that water salvation of PHEMA brushes leads to some swelling, which affects the membrane pore size.

We measured the flux of water through the 1.3 mm thick "neutral" membrane made of 460 nm PHEMA-modified silica spheres deposited on 0.2 μm regenerated cellulose support. The driving pressure was ~0.35 bar (5 psi) and ~1.45 bar (21 psi). The average water flux through the bare support was 1700 l/m^2hr^1 (7.5 gpm) with driving

pressure of 0.35 bar. The average flux of water through the "neutral" membrane under the same pressure was 18 l/m^2hr^1 (0.08 gpm). This result is comparable to other nanoporous ultrafiltration membranes with similar porosity (ca. 25%).[40,43] However, such polymer membranes are much thinner. Thus, taking thickness into account, the "neutral" membrane shows high flux. As expected, applying higher driving pressure resulted in higher flux. The average water flux under 1.45 bar was 103 l/m^2hr^1 (0.45 gpm), thus the flux increases by a factor of 5.7 when pressure is 4.2 times higher. This flux is comparable or exceeds the flux of commercially available ultrafiltration drinking water membranes (Watts WQCFU-T-13KIT 3 Stage Kwik-change Ultrafiltration system – 0.5 gpm for 0.2 μm cut-off size[40]). The flux through the "neutral" membranes was ca. 4 times smaller than that for "acid-base" membranes while the "neutral" membranes were ca. 2.6 times thicker than "acid-base" membranes. Thus, "neutral"membranes show high flux of water and can be potentially applied in filtration and water purification systems.

According to the diffusion experiments in water, the cut-off of the "neutral" membrane made of 330 nm silica spheres was 20 nm, as determined using G5 PAMAM dendrimer (6 nm in diameter), which showed high diffusion rate and 20 nm gold nanoparticles, which were retained by the membrane. We believe that the much lower cut-off of the "neutral" membranes compared to the "acid-base" membranes comprised of comparably sized silica spheres results from swelling of PHEMA polymer brushes in water, which partially blocks the pores, reducing the effective pore size.[28]

Silica spheres of two different diameters (280 and 460 nm) modified with PHEMA brushes were deposited from ethanol solution on top of a nylon filter with 0.2 μm pore size (Figure 4.3 A-C). Supported "neutral" membranes could be redispersed in

ethanol and deposited again. Due to the weaker interaction between PHEMA brushes compared to the interactions of the brushes carrying charged sulfonic and quaternized amino groups, the supported "neutral" membranes needed to be thicker (ca. 1.3 mm) than "acid-base" membranes.

The 6 nm dendrimer molecules passed through the membranes made of 280 nm "hairy" silica spheres, while 20 nm gold nanoparticles were retained (Figure 4.3 D), which was confirmed by DLS and UV-Vis spectroscopy of the permeate. This cut-off is similar to that observed in diffusion experiments. As expected, the membrane made of PHEMA-modified 460 nm silica spheres had a higher cut-off: they were permeable for 20 nm gold nanoparticles while 40 nm gold nanoparticles were retained. The cut-off is smaller than calculated for close-packed silica colloidal crystals made of 280 and 460 nm spheres (44 and 70 nm, respectively), which we attribute to the swelling of PHEMA brushes in water. These results demonstrate that reversible "neutral" membranes are capable of size-selective ultrafiltration and that their pore size can be varied by changing the silica spheres size.

The deposited "neutral" membrane with trapped gold nanoparticles can be dissolved in by sonication, forming colloidal solution containing "hairy" silica spheres and gold nanoparticles. After quick sonication, heavy silica particles sediment, while gold nanoparticles remain in solution and thus can be separated. Depending on size of silica and gold, the complete separation may require several sonication-centrifugation cycles. The purified silica spheres can be dissolved and deposited into nanoporous membrane again (Figure 4.3 E,F). This separation process and membrane reusing are illustrated in Figure 4.4.

4.4 Conclusions

In conclusion, in this work we introduced a novel concept of reversible assembly of nanoporous membranes from polymer-modified colloidal nanoparticles. The membranes can be deposited from solution and dispersed by changing the solvent. This creates advantages in terms of recycling, cleaning, and reusing the membrane without performance loss. Membranes made of silica spheres modified with polymer brushes carrying acidic and basic functional groups remain stable in organic solvents and disassemble in water, while membranes made of PHEMA-modified silica spheres are stable in water and disassemble in organic solvents. The membranes can withstand multiple cycles of assembly-disassembly. The membrane cut-off can be controlled by varying the silica sphere diameter and also depends on polymer brush structure. The membranes can be prepared as both free-standing materials and as supported films. The control over the pore size, high flux, durability, time- and cost-efficiency of membrane preparation, and the ability to recover the retentate and clean the membranes by disassembly makes these membranes a promising material for ultrafiltration and size-selective separations.

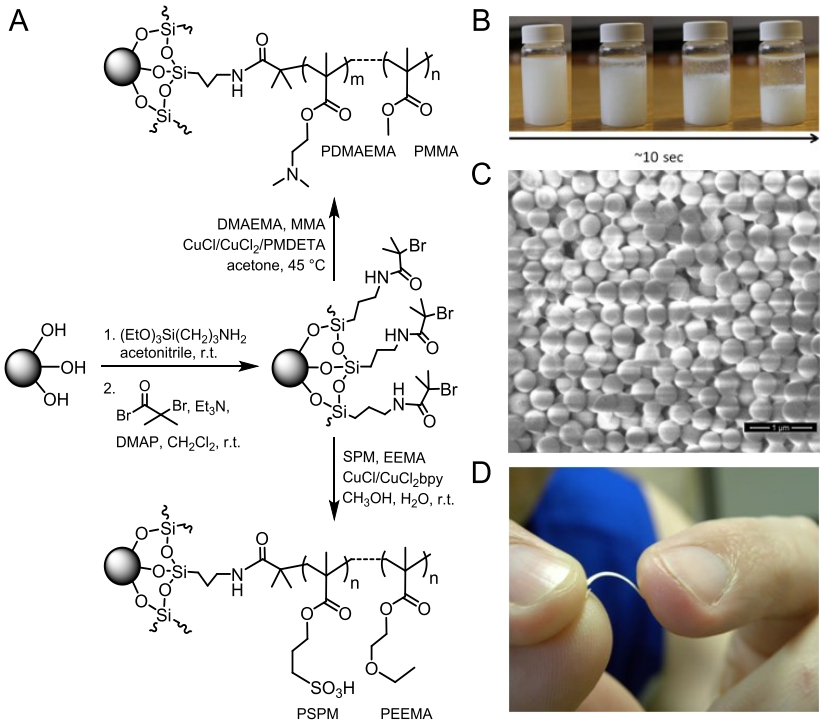

Figure 4.1. Preparation and properties of "acid-base" membranes. (A) Preparation of copolymer brushes in the surface of silica spheres. (B) Dispersion of "acid-base" membranes in ethanol and gel formation. (C) Flexible "acid-base" membrane. (D) Representative SEM image of "acid-base" membrane. Scale bar is 1 μm.

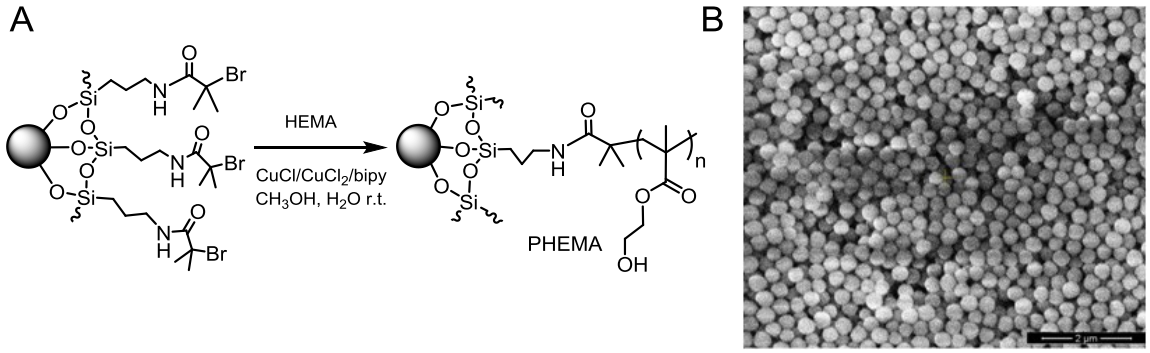

Figure 4.2. "Neutral" membrane: (A) Preparation of PHEMA brushes on the surface of silica spheres; (B) Representative SEM image of the "neutral" membrane. Scale bar is 2 μm.

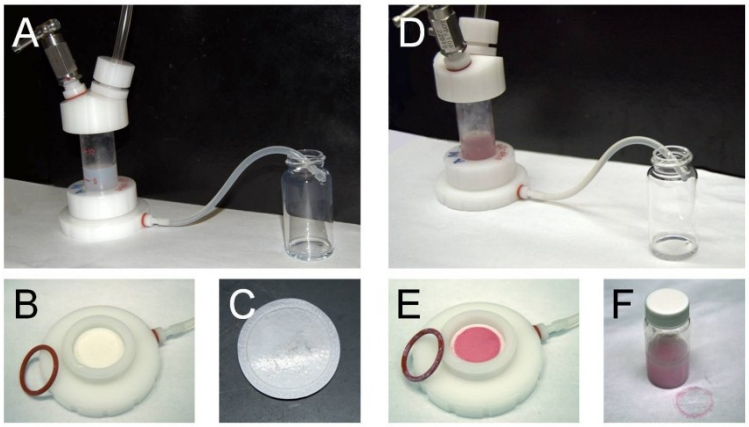

Figure 4.3. Preparation of supported "neutral" membrane and isolation of Au nanoparticles. (A) Formation of "neutral" membrane on cellulose support inside stirred cell. (B) Disassembled stirred cell with "neutral" membrane on support. (C) Supported membrane. (D) Ultrafiltration of 20 nm Au nanoparticles through "neutral" membrane made of 280 nm "hairy" silica spheres. (E) Disassembled stirred cell with Au nanoparticles trapped inside the "neutral" membrane. (F) Dispersed "neutral" membrane with Au nanoparticles in solution.

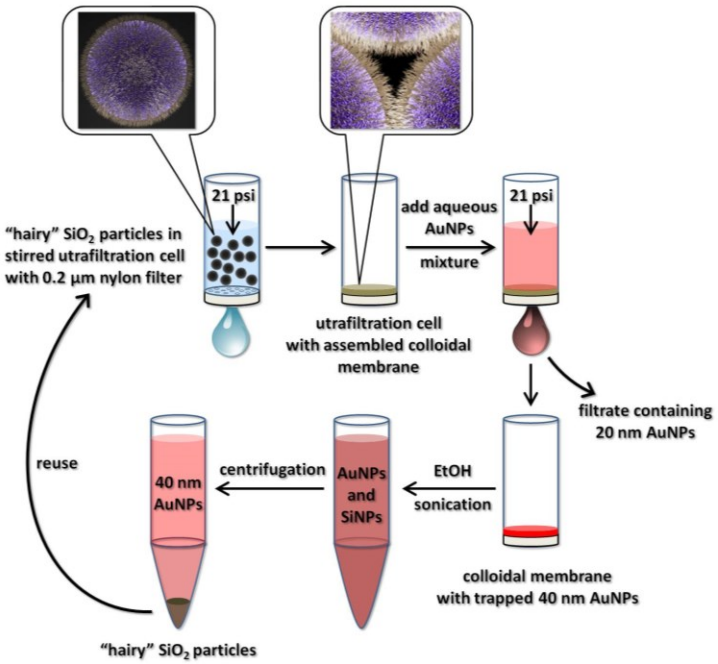

Figure 4.4. Schematic representation of the separation of 20 and 40 nm Au nanoparticles using the "neutral" ultrafiltration membrane and membrane recycling.

4.5 References

[1] Ma, H.; Burger, C.; Hsiao, B. S.; Chu, B. Fabrication and Characterization of Cellulose Nanofiber Based Thin-Film Nano Fibrous Composite Membranes. *J. Membr. Sci.* **2014**, *454*, 272–282.

[2] Miao, J.; Lin, H.; Wang, W.; Zhang, L.-C. Amphoteric Composite Membranes for Nanofiltration Prepared from Sulfated Chitosan Crosslinked with Hexamethylene Diisocyanate. *Chem. Eng. J.* **2013**, *234***,** 132–139.

[3] Cheryan, M. *Ultrafiltration and microfiltration handbook*, CRC Press: Boca Raton, FL, 1998, Chapter 1, pp. 1–28.

[4] Vandezande, P.; Gevers, L. E. M.; Vankelecom, I. F. J. Solvent Resistant Nanofiltration: Separating on a Molecular Level. *Chem. Soc. Rev*. **2008**, *37*, 365–405.

[5] Querelle, S. E.; Jackson, E. A.; Cussler, E. A.; Hillmyer, M. A. Ultrafiltration Membranes with a Thin Poly(Styrene)‑B‑Poly(Isoprene) Selective Layer. *ACS Appl. Mater. Interfaces* **2013**, *5*, 5044−5050.

[6] Krieg, E.; Albeck, S.; Weissman, H.; Shimoni, E.; Rybtchinski, B. Separation, Immobilization, and Biocatalytic Utilization of Proteins by a Supramolecular Membrane. *PLoS ONE* **2013**, *8*, e63188.

[7] Deng, J.; Toh C.-S. Impedimetric DNA Biosensor Based on a Nanoporous Alumina Membrane for the Detection of the Specific Oligonucleotide Sequence of Dengue Virus. *Sensors* **2013**, *13*, 7774–7785.

[8] Hotta, K.; Yamaguchi, A.; Teramae, N. Deposition of Polyelectrolyte Multilayer Film on a Nanoporous Alumina Membrane for Stable Label-Free Optical Biosensing. *J. Phys. Chem. C* **2012**, *116*, 23533−23539.

[9] Jeon, G.; Yang, S. Y. Kim, J. K. Functional Nanoporous Membranes for Drug Delivery. *J. Mater. Chem.* **2012**, *22*, 14814−14834.

[10] Wei, L.; Kawamoto, K. Upgrading of Simulated Syngas by Using a Nanoporous Silica Membrane Reactor. *Chem. Eng. Technol*. **2013**, *36*, 650–656.

[11] Li, Q.; Cui, S.; Yan, X. Electrocatalytic Oxidation of Glucose on Nanoporous Gold Membranes. *J. of Solid State Electrochem*. **2012**, *16*, 1099–1104.

[12] Zhao, Q.; Yin, M.; Zhang, A.; Prescher, S.; Antonietti, M.; Yuan, J. Hierarchically Structured Nanoporous Poly(Ionic Liquid) Membranes:Facile Preparation and Application in Fiber-Optic pH Sensing. *J. Am. Chem. Soc*. **2013**, *135*, 5549 −5552.

[13] Sershen, S.; West, J. Implantable, Polymeric Systems for Modulated Drug Delivery. *Adv. Drug Delivery Rev.* **2002**, *54*, 1225–1235.

[14] Adiga, S. P.; Jin, C.; Curtiss, L. A.; Monteiro-Riviere, N. A.; Narayan, R. J. Nanoporous Membranes for Medical and Biological Applications. *Wiley Interdiscip. Rev.: Nanomed. Nanobiotechnol.* **2009**, *1*, 568–581.

[15] Nishizawa, M.; Menon, V. P.; Martin, C. R. Metal Nanotubule Membranes with Electrochemically Switchable Ion-Transport Selectivity. *Science* **1995**, *268*, 700–702.

[16] Smuleac, V.; Butterfield, D. A.; Bhattacharyya, D. Permeability and Separation Characteristics of Polypeptide-Functionalized Polycarbonate Track-Etched Membranes. *Chem. Mater*. **2004**, *16*, 2762–2771.

[17] Stroeve, P.; Ileri, N. Biotechnical and Other Applications of Nanoporous Membranes. *Trends Biotechnol.* **2011**, *29*, 259–266.

[18] Mansourpanah, Y.; Gheshlaghi, A. Effects of Adding Different Ethanol Amines During Membrane Preparation on the Performance and Morphology of Nanoporous PES Membranes. *J Polym Res*. **2012**, *19*, 1–7.

[19] Chang, Y.; Ling, Z.; Liu, Y.; Hu, X.; Li, Y. A Simple Method for Fabrication of Highly Ordered Porous α-Alumina Ceramic Membranes. *J. Mater. Chem.* **2012**, *22*, 7445–7448.

[20] Chiang, A. S. T.; Chao, K.-J. Membranes and Films of Zeolite and Zeolite-Like Materials. *J. Phys. Chem. Solids* **2001**, *62*, 1899–1910.

[21] Chong Lua. A.; Shen, Y. Influence of Inorganic Fillers on the Structural and Transport Properties of Mixed Matrix Membranes. *J. Appl. Polym. Sci.* **2013**, *128*, 4058–4066.

[22] Chaudret, B.; Philippot, K. Organometallic Nanoparticles of Metals or Metal Oxides. *Oil Gas Sci. Technol.* **2007**, *62*, 799–817.

[23] Ulbricht, M. Advanced Functional Polymer Membranes. *Polymer* **2006**, *47*, 2217–2262.

[24] Peng Lee, K.; Mattia, D. Monolithic Nanoporous Alumina Membranes for Ultrafiltration Applications: Characterization, Selectivity–Permeability Analysis and Fouling Studies. *J. Membr. Sci.* **2013**, *435*, 52–61.

[25] Krieg, E.; Weissman, H.; Shirman, E.; Shimoni, E.; Rybtchinski B. A Recyclable Supramolecular Membrane for Size-Selective Separation of Nanoparticles. *Nat. Nanotechnol.* **2011**, *6*, 141–146.

[26] Park, M.-H.; Subramani, C.; Rana, S.; Rotello, V. M. Chemoselective Nanoporous Membranes via Chemically Directed Assembly of Nanoparticles and Dendrimers. *Adv. Mater*. **2012**, *24*, 5862–5866.

[27] Mueggenburg, K. E.; Lin, X.-M.; Goldsmith, R. H.; Jaeger, H. M. Elastic Membranes of Close-Packed Nanoparticle Arrays. *Nat. Mater.,* **2007***, 6*, 656–660.

[28] He, J.; Lin, X.-M.; Chan, H.; Vukovic, L.; Kral, P.; Jaeger H. M. Diffusion and Filtration Properties of Self-Assembled Gold Nanocrystal Membranes. *Nano Lett.* **2011**, *11*, 2430–2435.

[29] Feng, L., Sha, R., Seeman, N. C. Chaikin, P. M. Topological Interaction by Entangled DNA Loops. *Phys. Rev.* **2012**, *109*, *188301*, 1–5.

[30] Harada, A.; Kobayashi, R.; Takashima, Y.; Hashidzume, A.; Yamaguchi, H. Macroscopic Self-Assembly through Molecular Recognition. *Nat. Chem.* **2011**, *3*, 34–37.

[31] Ahn, Y.; Jang, Y.; Selvapalam, N.; Yun, G.; Kim, K. Supramolecular Velcro for Reversible Underwater Adhesion. *Angew. Chem. Int. Ed.* **2013**, *52*, 3140–3144.

[32] Bohaty, A. K.; Smith, J. J.; Zharov, I. Free-Standing Silica Colloidal Nanoporous Membranes. *Langmuir* **2009**, *25*, 3096–3101.

[33] Ignacio-de Leon, P. A.; Zharov. I. Size-Selective Transport in Colloidal Nano-Frits. *Chem. Commun.* **2011***, 47*, 553–555.

[34] Stöber, W.; Fink, A.; Bohn, E. Controlled Growth of Monodispersed Spheres in the Micron Size Range. *J. Colloid Interface Sci.* **1968**, *26*, 62–69.

[35] Schepelina, O.; Poth, N.; Zharov, I. pH-Responsive Nanoporous Silica Colloidal Membranes. *Adv. Funct. Mater.* **2010**, *20*, 1962–1969.

[36] Smith, J. J.; Zharov, I. Preparation and Proton Conductivity of Self-Assembled Sulfonated Polymer-Modified Silica Colloidal Crystals. *Chem. Mater.* **2009**, *21*, 2013–2019.

[37] Singh, K.; Tirumkudulu, M. Cracking in Drying Colloidal Films. *Phys. Rev.* **2007**, *98*, *218302*, 1–4.

[38] Choi, J.; Hui, C. M.; Pietrasik, J.; Dong, H.; Matyjaszewski, K.; Bockstaller, M. R. Toughening Fragile Matter: Mechanical Properties of Particle Solids Assembled from Polymer-Grafted Hybrid Particles Synthesized by ATRP. *Soft Matter*, **2012**, *8*, 4072–4082.

[39] Malavolta, L.; Oliveira, E.; Cilli, E. M.; Nakaie, C. R. Solvation of Polymers as Model for Solvent Effect Investigation: Proposition of a Novel Polarity Scale. *Tetrahedron*, **2002**, *58*, 4383–4394.

[40] FreshWaterSystems.com Ultrafiltration Systems Catalog http://www.freshwatersystems.com/c-761-ultrafiltration-systems.aspx, accessed March 7, 2014

[41] Cai, W.; Sun, Y.; Piao, X.; Li, J.; Zhu, S. Solvent Recovery from Soybean Oil/Hexane Miscella by PDMS Composite Membrane. *Chin. J. Chem. Eng.* **2011**, 19, 575–580.

[42] Campan, R.; Cazaux, F.; Coqueret, X. Controlled Swelling of Poly(Hydroxyethyl Methacrylate) Hydrogels by Photochemical Grafting of Hydrophobic Acrylates. *Macromol. Mater. Eng.* **2002**, *287*, 924–930.

[43] Yang, S. Y.; Ryu, I.; Kim, H. Y.; Kim, J. K.; Jang, S. K.; Russell, T. P. Nanoporous Membranes with Ultrahigh Selectivity and Flux for the Filtration of Viruses. *Adv. Mater*. **2006**, *18*, 709–712.

CHAPTER 5

NOVEL SOLID POLYMER ELECTROLYTE HYBRID MATERIALS FOR LITHIUM RECHARGEABLE BATTERIES

5.1 Introduction

Lithium rechargeable batteries are used in a wide variety of applications; such as electric vehicles, portable electronics, personal communication, etc.[1] Presently used liquid electrolyte batteries have a number of serious disadvantages. The liquid electrolytes are not entirely stable chemically or electrochemically, and the always-possible leakage makes liquid electrolyte batteries both unreliable and environmentally unsafe.[2] Thus, the solid polymer electrolyte (SPE) has been recognized as a promising material for the production of lithium batteries.[3,4] Performance parameters that are common to all lithium polymer electrolytes and that will be required to ensure technological success in any application include high lithium conductivity at room temperature, high transport number for the lithium cation, and good mechanical stability.[5] Most commonly used SPEs are based on complexes formed between polyethylene oxide (PEO, also known as polyethylene glycol, PEG) and various lithium salts, usually having large noncoordinating anions.[6,7] These systems have good mechanical properties, large redox stability windows, good compatibility with cathodes and lithium anode, a very high solvating power, and chain flexibility at elevated temperatures.[8] However, they possess low conductivity at ambient temperature, very low cation transference numbers, and high

crystallinity.[9] A few approaches to improve lithium conductivity and transport number of the cation at room temperature were reported: random copolymers,[10] block copolymers,[11] comb-branched block copolymers,[12] networks,[13] and single lithium conductors[14] were applied. Another fundamentally different approach is to prepare composite electrolytes,[15] in which lithium conductivity is enhanced by the addition of an insoluble second phase, such as aluminum oxide or silica. Other methods include preparation of gel-polymer electrolytes,[16,17] molten conducting salts,[18] addition of aluminum oxide,[19] or chloride.[20] However, the need to optimize simultaneously the lithium conductivity and mechanical properties of SPEs limits suitable polymer architectures. At the same time, fundamental understanding of lithium ionic conductivity as a function of polymer structure and composition is needed to optimize lithium rechargeable batteries.

In this work, we develop novel hybrid SPE materials, where silica colloidal membranes provide rigid and durable matrix and pore-filling surface-grafted polymer brushes provide lithium ion conductivity. To the best of our knowledge, this approach is applied for the first time for SPE preparation. The architecture of the proposed materials makes them particularly suitable for systematic studies needed to understand the lithium transport through polymer brushes inside the nanopores. We use PEG-containing polymers to enable lithium ion conductivity in silica-based SPEs. Since pure PEG chains cannot be surface-grafted to silica via ATRP, we use commercially available methacrylate-based monomers that contain PEG chains, such as (polyethyleneglycol)methacrylate (PEGMA), which has been reported to provide lithium conducting SPEs[21-23] (Figure 5.1). The PEGMA monomers are available with various lengths of attached PEG chains, which allows studying ionic conductivity as a function of

PEG length. This approach allows the preparation of durable solid material with short enough PEG chains to prevent PEG crystallization and ensure high ionic conductivity.

We apply two different approaches to the preparation of ion-conductive materials, each of them having their own advantages and limits. In the first method, close-packed silica colloidal membranes were prepared via vertical deposition and then sintered in the oven, as was described in previous chapters. The resulting durable membranes were then modified with pore-filling surface-grafted PEGMA brushes with desired chain length inside the pores and impregnated with $LiPF_6$ to introduce ionic conductivity. The pore size can be controlled by varying silica spheres' size. This method allows for the preparation of stable and durable free-standing SPE material with controlled pore size. However, the amount of PEG chains introduced inside the pores is limited by the void fraction of highly-ordered silica colloidal membranes (26%) and the detailed study of ionic conductivity as a function of number of PEG chains is challenging. This method is good as proof of concept for Li^+-conductive hybrid pore-filled colloidal membranes.

In the second approach, we grafted poly(hydroxyethyl) methacrylate brushes to silica colloidal spheres via ATRP. Next, PHEMA brushes were modified with an initiator and PEGMA brushes were grown on the PHEMA backbone (Scheme 5.1). Silica colloidal spheres modified with the resulting comb-polymer brushes were then assembled into colloidal membranes via horizontal deposition and impregnated with $LiPF_6$. It is known that when a lithium salt-solvating polymer is chosen as one block component in block copolymer SPEs, continuous, nanoscopic, ion-conducting pathways can form.[24] Thus, by varying the PEG side-chain size, the distance between the PEO-containing blocks and their length, we will be able to affect the lithium transport and study the

structure-conductivity relationships.

We measured ionic conductivity of resulting SPEs using electrochemical impedance spectroscopy to estimate the potential of the material as part of lithium rechargeable battery. The experiments are similar to those described in Chapter 3.

5.2 Experimental Section

5.2.1 Materials

Ammonium hydroxide (28-30% as NH_3, EMD Chemicals, Inc.), tetraethyl orthosilicate (99.999% metal basis, Alfa Aesar), *N*,*N*,*N*′,*N*′,*N*″-pentamethyldiethylenetriamine (PMDETA), 2-bromoisobutyryl bromide (2-BIB), 3-aminopropyltriethoxysilane, and lithium hexafluorophosphate (all from Sigma-Aldrich) were used as received. HEMA and two types of PEGMA monomers (average M_n 500 g/mol and 950 g/mol) (Sigma Aldrich) were passed through Al_2O_3 column to remove inhibitor prior to use. Deionized water with 18 MΩ resistivity used in all experiments was obtained from a Barnstead "E-pure" water purification system. All ethanol used was 200 proof. Dimethylformamide (DMF) and tetrahydrofuran (THF), dichloromethane (DCM) were reagent grade.

5.2.2 Instruments

Scanning electron microscopy (SEM) images were obtained using a FEI Novanano 630 instrument. A Branson 1510 sonicator was used for all sonications. A Clay Adams Compact II Centrifuge (3200 rpm, Becton Dickinson) was used for all centrifugations. A Fisher Scientific Isotemp Programmable Muffle Furnace (Model 650) was used for calcination and sintering. The complex impedance of the samples was measured using Princeton Applied Research VersaSTAT. Thermogravimetric analysis of

polymer-modified silica particles was performed using TGA Q500 (TA Instruments).

5.2.3 Preparation of Silica Spheres and Silica Colloidal Membranes

Silica spheres were prepared according to the previously reported procedure.[25,26] All glassware was cleaned with distilled water prior to use. A batch of silica spheres was made by mixing 500 mL of an ethanol solution containing TEOS (51.4 mL, 0.20 mol) with 500 mL of ethanol solution containing NH_4OH (27.0 mL, 0.4 mol) and water (287 g, 16 mol). These two solutions were poured simultaneously in a 2 L Erlenmeyer flask and vigorously stirred. The resulting mixture had final concentrations of 0.2 M TEOS, 0.4 M NH_3 and 17.0 M H_2O. After about 30 min of being stirred, the solution became cloudy, indicating silica sphere formation. After 24 h, the silica spheres were centrifuged in 15 mL centrifuge tubes (Corning) at 1163g for 15 min. After all of the spheres were collected as pellets at the bottom of the centrifuge tubes, the supernatant was decanted and the silica spheres were purified by repetitive cycle of suspending the spheres in 10 mL of a solvent by sonication for 15 min, during which the tubes were periodically shaken by hand to free any pieces of the pellet stuck to the sides of the tubes, followed by centrifugation. Following solvents were used: water (twice), 25% ethanol in water, 50% ethanol, 75% ethanol, and 100% ethanol (twice). After the final centrifugation, the supernatant was decanted and the silica spheres were dried in a stream of nitrogen for 12 h. Dried spheres were later calcinated by placing them into a Petri dish, breaking all large aggregates with spatula, and placing the dish in the oven programmed to heat the spheres for 4 h at 600 °C. The heating rate in the oven was set to 10 °C/min. SEM images of the spheres were taken and the diameters determined from 100 individually measured silica spheres in each sample to be 240±10 nm after the calcination.

Silica colloidal membranes were prepared by vertical deposition. Four glass microscope slides were placed into a 100ml beaker containing silica suspended in ethanol. The suspension was 12% silica by mass. Each suspension used 42 mL of ethanol. These were left overnight to deposit the membranes as the ethanol evaporated. The resulting membranes were 400-1000 μm thick and were sintered in a furnace at 1050 °C for 12 h (10 ºC/min ramp), becoming very robust and durable after that.

5.2.4 Pore-filling of Silica Colloidal Membranes

Sintered colloidal membranes were rehydroxylated in solution of tetrabutylammonium hydroxide of pH=10 at 60 °C for 12 h, then rinsed with large excess of water (2×), 1 M nitric acid, methanol (2×), water (2×), and acetonitrile. Rehydroxylated membranes were modified with amine groups by placing them into 20 mL of solution of APTES (4.3 mmol) in dry acetonitrile at room temperature under nitrogen atmosphere for 17 h. After the surface modification, the membranes were repeatedly rinsed with acetonitrile and air-dried. Amine-modified membranes were placed in 100 mL of dichloromethane solution containing 2 mL of triethylamine (0.15 M solution), 1.6 mL of 2-bromoisobutyrylbromide (0.13 M solution), and a catalytic amount of DMAP for 12 h at room temperature. Initiator-modified membranes were repeatedly rinsed with dichloromethane and air-dried. PEGMA brushes were grown inside the initiator-modified silica membranes via ATRP by placing the membranes in 15 mL of DMF, containing PMDETA (0.5 mmol, 100 μm), $CuCl_2$ (0.12 mmol, 16 mg), CuCl (0.4 mmol, 40 mg), and large excess of PEGMA monomer (30-50 mmol passed through alumina column) at 40 ºC for 12 h. After quenching the polymerization reaction by exposing the reaction mixture to air, the membranes were repeatedly rinsed with DMF

and ethanol and dried under constant air flow. The resulting pore-filled membranes were then impregnated by $LiPF_6$ using following procedure: 0.1g of dry $LiPF_6$ was dissolved in 1 ml of ethanol, the resulting solution was added drop by drop evenly distributed over the membrane surface, letting the membrane dry between drops.

5.2.5 Preparation of Comb-polymer Modified Silica Spheres and Membranes

First, silica spheres were modified with amine groups by suspending them into 20 mL of solution of APTES (4.3 mmol) in dry acetonitrile at room temperature under nitrogen atmosphere for 17 h. After the surface modification, the membranes were repeatedly rinsed with acetonitrile and air-dried. Amine-modified membranes were placed in 100 mL of dichloromethane solution containing 2 mL of triethylamine (0.15 M solution), 1.6 mL of 2-bromoisobutyrylbromide (0.13 M solution), and a catalytic amount of DMAP for 12 h at room temperature. Initiator-modified spheres were repeatedly washed with dichloromethane via centrifugation-sonication cycles and air-dried. The grafting of PHEMA brushes onto initiator-modified silica spheres (1 g) was carried out in of degassed methanol, containing PMDETA (0.5 mmol, 100 μm), $CuCl_2$ (0.12 mmol, 16 mg), CuCl (0.4 mmol, 40 mg), as well as HEMA (2ml passed through alumina column) at 70 ºC for 12 h in nitrogen atmosphere. The resulting modified particles were washed in methanol and water. Then PHEMA-modified spheres were modified with 2-bromoisobutyrylbromide again, the reaction was carried out in 30 ml of anhydrous pyridine in presence of 0.1 ml of 2-BIB. The reaction mixture was stirred at 0 ºC for 3 h and then at room temperature for 24 h. The spheres were washed with THF, acetone and DCM and air-dried. Then PEGMA brushes were grafted onto initiator-modified PHEMA backbone. The reaction was carried out according to reported procedure,[27] in 10ml of

DMF, in presence of PMDETA (0.5 mmol, 100 μm), $CuCl_2$ (0.12 mmol, 16 mg), CuCl (0.4 mmol, 40 mg), and large excess of PEGMA monomer (30-50 mmol) at 40 ºC for 12 h. The resulting comb-polymer modified spheres were washed with DMF and ethanol.

The lithium ion-conducting membranes were prepared using comb-polymer modified spheres by horizontal deposition. 0.5g of polymer-modified silica and 0.1g of $LiPF_6$ were dissolved in 5 ml of ethanol in 10ml beaker and let the solvent evaporate overnight. After complete solvent evaporation the smooth and crack-free membrane self-assembled at the bottom of the beaker as single piece.

5.2.6 Ionic Conductivity Measurements

Electrochemical impedance spectroscopy measurements were carried out for both pore-filled ordered silica colloidal membranes and for self-assembled comb-polymer modified silica membranes. Silver paint was coated on both sides of the membranes to serve as electrodes. Then the membranes were dried in vacuum at 80°C for at least 4 h to remove water and other solvent residues.

The impedance was measured using a two-probe testing device placed in humidity- and temperature-controlled chamber according to the previously reported procedure.[28] The relative humidity was kept ~25% during all experiments. The measurements were carried out at room temperature. The complex impedance of the samples was measured and the ionic conductivity was calculated using $\sigma=l/RA$, where σ is the ionic conductivity, l is the distance between the two electrodes, R is the ohmic resistance of the membrane, and A is the cross-sectional area of the material.

5.3 Results and Discussion

The PEGMA-500 and PEGMA-950 polymer brushes were grown on silica surface inside the pores of silica colloidal membranes. The resulting pore-filled membranes are robust and durable, easy to handle, and easy to modify with electrodes. To confirm successful polymerization, the resulting material was characterized by TGA. According to TGA results, the average PEGMA-500 brush is comprised of only ~ 2 PEGMA monomer fragment, assuming the grafting density is 0.5 brush per nm^2 of silica surface. We explain such a low molecular weight of grown polymer brushes by large PEGMA monomer's size. The monomer with average M_n = 500g/mol is bulky and the ATRP rate is limited by monomer diffusion inside the pores to the silica surface. These polymer brushes are significantly shorter than those grown using smaller monomers, such as polysulfopropyl methacrylate, polydimethylaminoethoxymethacrylate, or PHEMA (in which average polymer brushes consist of 20-40 monomer fragments), that were previously discussed in Chapters 3 and 4.

Pore-filled silica membranes were then impregnated with $LiPF_6$ and ionic conductivity was measured. The average ionic conductivity values measured at room temperature are shown in Table 5.1. As expected, the average conductivity of the membranes modified with shorter PEG chains is higher than of those with longer chains. It can be explained by higher mobility of shorter PEG chains compared to longer chains. Both membranes show good ionic conductivity, comparable or exceeding similar membranes with ion conductive PEG chains.[29] We believe that good conductivity arises from formation of ion-conductive pathways inside the pores through the membrane, where Li^+ ions coordinate with flexible PEG chains. These SPE materials provides a

good proof of concept for our approach; however, a further study of ionic conducitivity as a function of PEG chain length, temperature, humidity, as well as pore size and geometry in pore-filled silica-based SPEs is clearly needed.

In our second approach, silica spheres were first modified with PHEMA brushes. According to the TGA data, the average PHEMA brush contained ~72 HEMA monomer fragments, assuming the grafting density is 0.5 brush per 1 nm^2 of silica surface. Later PEGMA brushes were grafted onto PHEMA backbone. According to TGA results, in average 0.4 PEGMA-500 fragments were grafted onto each HEMA fragment, i.e., average PHEMA brush comprised of 36 HEMA fragments contained ~14 PEGMA units. The comb-polymer modified silica spheres were dispersed in ethanol with $LiPF_6$ and horizontally deposited from solution. Upon solvent evaporation, silica spheres self-assembled into smooth and solid film. The resulting material was pliable and crack-free; however, it was significantly less durable than sintered silica membranes and could easily break upon little pressure. Similar to the membranes described in Chapter 4, this membrane is held together via noncovalent van der Waals interactions, which are significantly weaker than covalent bonds. This could possibly limit the applications of the resulting SPEs.

However, this material has several significant advantages over pore-filled sintered silica membranes. In the pore-filled sintered silica membranes, the growth of polymer brushes is limited by void fraction of the membrane. The polymerization rate is also limited by diffusion of monomers to the silica surface inside the pores. Self-assembled silica membranes do not have these limitations, since polymerization is done on loose silica spheres in solution before assembling the membrane. Also, different parameters of

SPE, such as polymer brush length, geometry and composition are easier to control in self-assembled membranes, compared to sintered silica membranes.

The average conductivity of self-assembled SPE is $2.7\pm0.3 \times 10^{-4}$ S/cm, which is significantly lower, than that for sintered silica membranes. We predicted that the conductivity of self-assembled membranes will be higher than for sintered membranes due to the larger amount of PEG chains present. In addition, the PEG chains in self-assembled SPE should have higher flexibility, since they are attached to another flexible polymer backbone instead of silica surface. We explain the lower conductivity of self-assembled SPE by the lower amount of loaded $LiPF_6$ in the membrane. Further investigation of ionic conductivity as a function of lithium salt load is needed for both sintered and self-assembled SPEs.

5.4. Conclusions and Future Directions

In this work, we introduced new SPE materials for lithium rechargeable batteries. In the first approach, we prepared highly-ordered sintered silica membranes with pores filled with PEGMA chains and impregnated with lithium salt. The membrane showed good ionic conductivity and mechanical properties. We found that the membrane modified with shorter PEG chains possesses higher conductivity presumably due to higher mobility of polymer brushes. We showed good proof of concept for this method. In the second approach, we prepared self-assembled membrane comprised of comb-polymer modified silica spheres impregnated with lithium salt. The resulting SPE is not as durable as the sintered membrane, but is easier to prepare. It also shows good ionic conductivity and could be a perspective material for SPE for lithium batteries.

Clearly, a more detailed study is needed for both developed models. Ionic

conductivity in both systems needs to be studied as a function of polymer chain length, geometry, composition, as well as lithium salt load, temperature, etc. Both approaches have their advantages and disadvantages. Different lithium battery applications require different parameters and thus both methods might be useful in developing SPEs for lithium batteries.

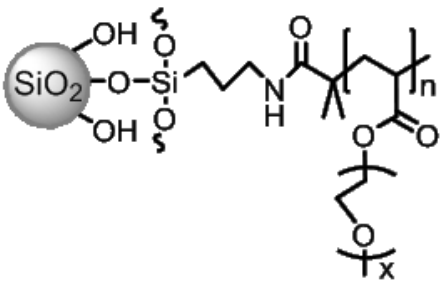

Figure 5.1 PEGMA brush grafted to the surface of silica sphere.

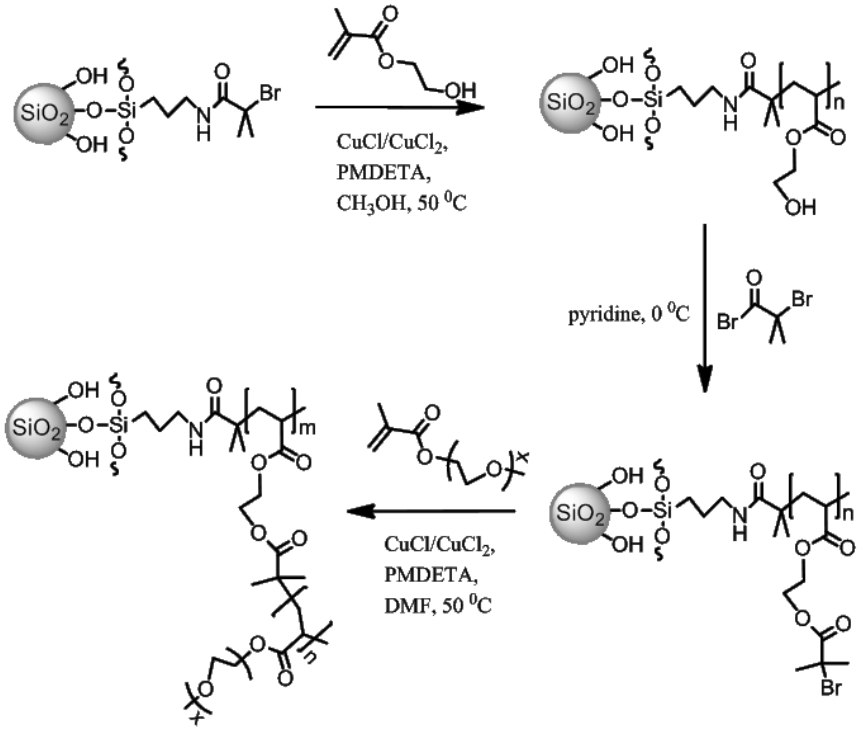

Scheme 5.1 Preparation of comb-polymer modified silica spheres.

Table 5.1. Li^+ ionic conductivites of silica colloidal membranes modified with different PEGMA monomers.

Mw PEG, g/mol	σ_{avg}, S/cm $\times 10^{-3}$
500	1.3
950	0.84

5.5. References

[1] Julien, C. Solid State Batteries. In *CRC Handbook of Solid State Electrochemistry*; Gellings, P. J.; Bouwmeester, H. J. M., Eds.; CRC: Boca Raton, 1997; Chapter 11, pp. 371–406.

[2] Wakihara, M.; Yamamoto, O., Eds. *Lithium Batteries*, Wiley-VCH: Berlin, New York, Chichester, Brisbane, Singapore, Toronto, 1998.

[3] Einset, A. G.; Wnek, G. E. Polymer Electrolyte Review. In *Handbook of Solid State Batteries & Capacitors*; Munshi, M. Z. A., Ed.; World Scientific: Singapore, New Jersey, London, Hong Kong, 1995; Chapter 15, pp. 289–310.

[4] Wright, P. V. Polymer Electrolytes - the Early Days. *Electrochim. Acta* **1998**, *43*, 1137–1143.

[5] Fauteux, D.; Massucco, A.; McLin, M.; van Buren, M.; Shi, J. Lithium Polymer Electrolyte Rechargeable Battery. *Electrochim. Acta* **1995**, *40*, 2185–2190.

[6] Fenton, B. E.; Parker, J. M.; Wright, P. V. Complexes of Alkali Metal Ions with Poly(Ethylene Oxide). *Polymer* **1973**, *14*, 589.

[7] Armand, M. B. Polymer Electrolytes. *Annu. Rev. Mater. Sci.* **1986**, *16*, 245–261.

[8] Stainer, M.; Hardy, L. C.; Whitmore, D. H.; Schriver, D. F. Stoichiometry of Formation and Conductivity Response of Amorphous and Crystalline Complexes Formed Between Poly(ethylene oxide) and Ammonium Salts: PEO_x• NH_4SCN and PEO_x• $NH_4SO_3CF_3$. *J. Electrochem. Soc.* **1984**, *131*, 784–790

[9] Quartarone, E.; Mustarelli, P.; Magistris, A. PEO-Based Composite Polymer Electrolytes. *Solid State Ionics* **1998**, *110*, 1–14.

[10] Giles, J. R. M. Electrolytic Conduction in Amorphous Salt Complexed Polyethers. *Solid State Ionics* **1987**, *24*, 155–167.

[11] Giles, J. R. M.; Gray, F. M.; McCallum, J. R.; Vincent, C. A. Synthesis and Characterization of ABA Block Copolymer-Based Polymer Electrolytes. *Polymer* **1987**, *28*, 1977–1981.

[12] Sun, J.; McFarlane, D. R.; Forsyth, M. Mechanical Properties of Polyether-Plasticiser-Salt Systems as Polymer Electrolytes. *Solid State Ionics* **1996**, *85*, 137–141.

[13] Giles, J. R. M.; Greenhall, M. P. Ionic Conduction in Phosphate Ester-Crosslinked

Polyethylene Glycols Complexed with Lithium Trifluoromethanesulfonate. *Polymer Comm.* **1986**, *27*, 360.

[14] Rawsky, G. C.; Fujinami, T.; Shriver, D. F. Aluminosilicate/Polyethylene Glycol Copolymers: a New Class of Polyelectrolytes *Polym. Mater. Sci. Eng.* **1994**, *71*, 523.

[15] Dudney, N. J. Composite Electrolytes. In *Handbook of Solid State Batteries & Capacitors*; Munshi, M. Z. A., Ed.; World Scientific: Singapore, New Jersey, London, Hong Kong, 1995; Chapter 12, pp. 231–246.

[16] Meyer, W. H. Polymer Electrolytes for Lithium-Ion Batteries. *Adv. Mater.* **1998**, *10*, 439–448.

[17] Scrosati, B. Conducting Polymers: Advanced Materials for New Design, Rechargeable Lithium Batteries. *Polym. Int.* **1998**, *47*, 50–55.

[18] Angell, C. A.; Xu, K.; Zhang, S.-S.; Videa, M. Variations on the Salt-Polymer Electrolyte Theme for Flexible Solid Electrolytes. *Solid State Ionics* **1996**, *86-88*, 17–28.

[19] Ogata, N.; Sanui, K.; Rikukawa, M.; Yamada, W.; Watanabe, M. Super Ion Conducting Polymers For Solid Polymer Electrolytes. *Synth. Met.* **1995**, *69*, 521–524.

[20] Ardel, G.; Golodnitsky, D.; Peled, E.; Wang, Y.; Bajue, S.; Greenbaum, S. Bulk and Interfacial Ionic Conduction in LiI/Al_2O_3 Mixtures. *Solid State Ionics* **1998**, *113-115*, 477–485.

[21] Lee, J.-T.; Wu, M.-S.; Wang, F.-M.; Liao, H.-W.; Li, C.-C.; Chang, S.-M.; Yang, C.-R. Gel Polymer Electrolytes Prepared by In Situ Atom Transfer Radical Polymerization at Ambient Temperature. *Electrochem. Solid-State Lett.* **2007**, *10*, A97–A100.

[22] Gerbaldi, C.; Nair, J. R.; Meligrana, G.; Bongiovanni, R.; Bodoardo, S.; Penazzi, N. Highly ionic conducting methacrylic-based gel-polymer electrolytes by UV-curing technique. *J. Appl Electrochem.* **2009**, *39*, 2199–2207.

[23] Luo, D.; Li, Y.; Yang, M. Preparation and Characterization of Novel Crosslinked Poly[Glycidyl Methacrylate–Poly(Ethylene Glycol) Methyl Ether Methacrylate] as Gel Polymer Electrolytes. *J. Appl. Polym. Sci.* **2011**, *120*, 2979–2984.

[24] Trapa, P. E.; Huang, B.; Won, Y.-Y.; Sadoway, D. R.; Mayes, A. M. Block Copolymer Electrolytes Synthesized by Atom Transfer Radical Polymerization for Solid-State, Thin-Film Lithium Batteries. *Electrochem. Solid-State Lett.* **2002**, *5*,

A85–A88.

[25] Stöber, W.; Fink, A.; Bohn, E. Controlled Growth of Monodispersed Spheres in the Micron Size Range. *J. Colloid Interface Sci.* **1968**, *26*, 62–69.

[26] Bohaty, A. K.; Smith, J. J.; Zharov, I. Free-Standing Silica Colloidal Nanoporous Membranes. *Langmuir* **2009**, *25*, 3096–3101.

[27] Di, C.; Jiang, X.; Yin, J. Synthesis of Stimuli-Responsive Star-Like Copolymer H20-PNIPAm-r-PEGMA via the ATRP Copolymerization. Technique and its Micellization in Aqueous Solution. *J. Appl. Polym. Sci.* **2010**, *115*, 1831–1840.

[28] Smith, J. J.; Zharov, I. Preparation and Proton Conductivity of Self-Assembled Sulfonated Polymer-Modified Silica Colloidal Crystals. *Chem. Mater.* **2009**, *21*, 2013–2019.

[29] Luo D., Li Y., Yang M. Preparation and Characterization of Novel Crosslinked Poly[Glycidyl Methacrylate–Poly(Ethylene Glycol) Methyl Ether Methacrylate] as Gel Polymer Electrolytes. *J. Appl. Polym. Sci.*, **2011**, *120*, 2979–2984.

CHAPTER 6

CONCLUSIONS AND FUTURE DIRECTIONS

Silica-based nanoporous membranes are a promising material for various applications, including energy applications, bioseparations, drug delivery, and water purification, due to their mechanical and chemical stability, easy preparation, and well-defined surface chemistry. In this dissertation, we described the development of novel silica and hybrid nanoporous membranes and their applications in fields of fuel cells, lithium batteries, ultrafiltration, and separations. We also used different approaches to make membrane preparation process faster and easier and more environmentally friendly.

We described the preparation of novel silica nanoporous membranes by pressing silica colloidal spheres followed by sintering in the oven. The preparation is very time- and cost-effective and easy to scale up, which makes it successfully comparable to commercial methods, such as electrochemical and deposition methods. The resulting membranes were mechanically durable, crack-free, and possessed uniform thickness and area. We controlled the pore size of the membranes by varying the silica spheres' size used for membrane preparation. Studying the diffusion of polystyrene beads through the pores, we showed that developed membranes are capable of size-selective transport. Due to fast and easy preparation process, these membranes are promising in the area of separations and filtration, as well as controlled ion and molecular transport. With further modification of silica surface with functional organic moieties and polymer brushes,

these membranes will be capable of not only size- but also charge- and chiral-selective separations. Introducing ion-exchange moieties will allow preparation of cheap ion-exchange membranes using our approach. Future directions in this project include these studies.

To demonstrate the utility of the pressed membranes, we developed proton conductive pore-filled silica colloidal membranes prepared by both pressing and vertical deposition and we evaluated the fuel cells prepared using pressed membranes. We modified these membranes by filling the membrane pores with surface-attached proton conductive polymer brushes and prepared membrane-electrode assembly to test fuel cell performance. We studied how the proton conductivity and fuel cell performance depends on the number of sulfonic groups in the pore-filling polymer brushes. We found that the proton conductivity and fuel cell voltage and current generally increase with increasing degree of sulfonation; however, the dependence is not linear. Our approach in which silica membrane provides rigid matrix and functional polymer brushes provide proton conductivity is very convenient for fundamental studying of proton conductivity, because the silica-based membranes do not swell or dissolve in water and methanol. In our membranes, every parameter of the membrane, such as polymer brush length, geometry, and composition, as well as pore size, can be tuned in order to achieve better performance of the device. Future directions here include a further study of proton conductivity and fuel cell performance as a function of various membrane parameters listed above. These studies will be beneficial for both fundamental research and optimization of fuel cell design.

We described the preparation and characterization of reversible nanoporous

membranes, comprised of polymer-modified silica colloidal spheres. The reversible assembly of nanoporous membranes provides advantages in recycling, cleaning, and reusing of the material. We developed two types of reversible membranes. The first type was assembled using silica spheres modified with polymer brushes containing acidic and basic functional groups. These membranes showed size-selective transport in organic solvents, but dissolved in water. The second type was prepared from silica spheres modified with PHEMA brushes; they were stable in water and also showed size-selective transport, while they could be dissolved in ethanol. This approach is promising in the area of reusable membranes for water purification, bioseparations, and ultrafiltration due to its cost- and material-efficiency. The PHEMA-modified silica reversible membranes have a potential in separation and trapping of biological species, such as proteins. The conditions of separations can be tuned by using various buffers as media instead of water, as well as PHEMA brush length. The polymer brushes can also be prepared from PHEMA copolymerized with functional polymers to introduce other interactions with separated molecules, such as chiral or charge interactions. This is the next step and promising direction for this material. Other directions include research on charge-selective separations through acid-base membranes in organic solvents and on size-selective separations through both acid-base and neutral membranes as function of polymer brush length.

We applied our approach for the preparation of both pore-filled and self-assembled silica membranes to develop a new SPE material for lithium rechargeable batteries. We successfully prepared ion conductive SPE from each of the materials and demonstrated the proof of concept for these approaches. Both approaches are promising

for the preparation of SPEs for lithium batteries; however, intensive research is still needed to complete this project. A systematic study of ionic conductivity as a function of polymer brush composition and geometry, PEG chain length and lithium salt load is needed in order to achieve high ionic conductivity and to demonstrate the efficiency of our material as lithium battery SPE.

In conclusion, we applied several approaches to prepare novel nanoporous membranes using such convenient material as silica colloidal spheres. We combined the well-known advantages of silica spheres, such as low cost, easy preparation, size control, mechanical and thermal stability, and well-established surface chemistry, with advantages of our approaches: time- and cost-effective methods, reversibility, and control of every parameter of the material, in order to develop new promising silica-based materials for various applications.